



HAL
open science

Seafloor classification with a multi-swath multi-beam echo sounder

Trung Kiên Nguyen

► **To cite this version:**

Trung Kiên Nguyen. Seafloor classification with a multi-swath multi-beam echo sounder. Signal and Image processing. Ecole nationale supérieure Mines-Télécom Atlantique, 2017. English. NNT : 2017IMTA0035 . tel-01825173

HAL Id: tel-01825173

<https://theses.hal.science/tel-01825173>

Submitted on 28 Jun 2018

HAL is a multi-disciplinary open access archive for the deposit and dissemination of scientific research documents, whether they are published or not. The documents may come from teaching and research institutions in France or abroad, or from public or private research centers.

L'archive ouverte pluridisciplinaire **HAL**, est destinée au dépôt et à la diffusion de documents scientifiques de niveau recherche, publiés ou non, émanant des établissements d'enseignement et de recherche français ou étrangers, des laboratoires publics ou privés.



IMT Atlantique
Bretagne-Pays de la Loire
École Mines-Télécom

**UNIVERSITE
BRETAGNE
LOIRE**

THÈSE / IMT Atlantique

sous le sceau de l'Université Bretagne Loire

pour obtenir le grade de

DOCTEUR D'IMT Atlantique

Spécialité : Signal, Image, Vision

École Doctorale Mathématiques et STIC

Présentée par

Trung Kiên Nguyen

Préparée dans le département Signal & communications

Laboratoire Labsticc

Seafloor classification with a Multi-swath Multi-beam Echo sounder

Thèse soutenue le 19 décembre 2017

devant le jury composé de :

Christophe Collet

Professeur des universités, Université de Strasbourg / rapporteur et président

Pierre Cervenka

Directeur de recherche, Institut Jean le Rond d'Alembert / rapporteur

Samantha Dugelay

Chercheur, CMRE NATO - La Spezia (Italie) / examinateur

Didier Charlot

Ingénieur, Ixblue - Brest / examinateur

Xavier Lurton

Chercheur, Ifremer- Brest / examinateur

Gilles Le Chenadec

Maître de conférences, ENSTA Bretagne / examinateur

Jean-Marc Boucher

Professeur émérite, IMT Atlantique / examinateur

Ronan Fablet

Professeur, IMT Atlantique / directeur de thèse

Michel Legris

Enseignant-chercheur, ENSTA Bretagne / invité

Sous le sceau de l'Université Bretagne Loire
IMT Atlantique
Bretagne-Pays de la Loire
En accréditation conjointe avec l'École Doctorale – SICMA

Seafloor classification with a Multi-swath Multi-beam Echo Sounder

Thèse de Doctorat

Mention : *STIC – Sciences et Technologies de l'Information et des Communications*

présentée par

Trung-Kien NGUYEN

Département : **IMT Atlantique** – Signal et Communication
Laboratoire : **Lab-STICC**, Pôle CID, Équipe TOMS
Directeurs de thèse : **Jean-Marc Boucher et Ronan Fablet**
Soutenue le **19 décembre 2017**

Jury :

M. Christophe Collet - Professeur; Université de Strasbourg; iCube (Rapporteur)
M. Pierre Cervenka - Chercheur; l'Institut Jean le Rond d'Alembert; MPIA (Rapporteur)
M. Jean-Marc Boucher - Professeur émérite; IMT Atlantique; Lab-STICC (Directeur de thèse)
M. Ronan Fablet - Professeur; IMT Atlantique; Lab-STICC (Directeur de thèse)
Mme. Samantha Dugelay - Ingénieur; CMRE (Examineur)
M. Gilles Le Chenadec - Enseignant-chercheur; ENSTA Bretagne; Lab-STICC (Examineur)
M. Didier Charlot - Ingénieur expert; iXblue; (Examineur)
M. Xavier Lurton - Chercheur, IFREMER (Examineur)
M. Michel Legris - Enseignant-chercheur; ENSTA Bretagne; Lab-STICC (Invité).

Remerciements

J'adresse mes plus sincères remerciements à Jean-Marc et Ronan, mes directeurs de thèse, pour m'avoir proposé cette aventure scientifique. Vous m'avez été d'une aide précieuse, non seulement pour les questions scientifiques, mais aussi vous m'avez aidé à m'intégrer dans la communauté scientifique de mon domaine de recherche.

Je voudrais également remercier Didier, mon tuteur de l'entreprise, pour toutes les explications sur le SONAR et ses applications dont je n'avais avant aucune expérience. Je tiens aussi à remercier Gilles et Michel, mes encadrants, pour m'avoir suivi durant ma thèse.

Merci à Pierre, Christophe, Samantha et Xavier pour avoir accepté de faire partie de mon jury. Vos remarques m'ont permis d'améliorer mes capacités à transmettre mon travail et à améliorer les points faibles de mes raisonnements et de mes arguments.

En espérant n'oublier personne, je remercie chaleureusement mes collègues de l'entreprise iXBLUE, du département SC de IMT Atlantique ainsi que mes amis de Brest pour leur soutien durant ces 4 années de thèse. Merci pour tout, spécialement pour votre présence pendant ma période de maladie.

Contents

Remerciements	i
Abstract	vii
Résumé	ix
Résumé étendu	1
1 Introduction	5
2 Seafloor mapping sonar system	7
2.1 Seafloor Scattering	7
2.2 Classical systems	9
2.2.1 Single-Beam Echo Sounder	9
2.2.2 Side-Scan Sonar	9
2.2.3 Multi-Beam Echo Sounder	10
2.3 Multi-Swath Multi-Beam Echo Sounder	10
2.3.1 Historical	10
2.3.2 Current system	12
2.4 Conclusion	14
I Raw Data Processing	15
3 Backscatter data acquisition and processing	17
3.1 Sonar principle	17
3.1.1 Beam-Forming	18
3.1.2 Emission	19
3.1.3 Transmission	20
3.1.4 Reception	20
3.1.5 Bathymetry detection	21
3.1.6 Target strength	22
3.1.7 Backscatter strength	23
3.2 SEAPIX Backscatter Processing	23
3.2.1 Emission	23
3.2.2 Reception	24
3.2.3 Information extraction	25
3.3 Backscatter Imagery Processing	28
3.3.1 Backscatter imaging methods on the classical bathymetry mode	28
3.3.2 Multiswath Backscatter Imaging with Seapix	30

3.4	Acquisition campaign	31
3.4.1	Selection of the reference area	31
3.4.2	Survey parameters and dataset	33
3.5	Data collection for seafloor classification	35
3.5.1	Data collection for the bathymetry mode	35
3.5.2	Data collection for the longitudinal mode	36
3.6	Conclusion	36
4	SEAPIX backscatter data analysis	37
4.1	Statistical analysis for SEAPIX operating modes	37
4.1.1	Bathymetry mode distribution analysis	40
4.1.2	Longitudinal mode distribution analysis	44
4.2	Inter-mode statistical analysis	51
4.2.1	Visualization of <i>BS</i> distribution features	51
4.2.2	Distributions comparison	52
4.3	Pulse modulation consistency	54
4.4	Conclusion	54
II	Seafloor classification	57
5	State of the art of seafloor classification and application to SEAPIX	59
5.1	Level-based classification	60
5.2	Profile-based classification	62
5.3	Texture-based classification	69
5.4	Conclusion	70
6	Feature extraction for seafloor classification from Multi-swath MBES system	73
6.1	Introduction	73
6.2	Problem statement and related work	74
6.3	Multi-swath MBES and survey data	76
6.3.1	Multi-swath MBES	76
6.3.2	Survey Data	78
6.4	Feature extraction	81
6.4.1	Point-wise statistical features	82
6.4.2	Histogram of Oriented Gradients	82
6.4.3	Covariance feature	84
6.5	Evaluation	84
6.5.1	Experimental setup	84
6.5.2	Seafloor classification performance	85
6.5.3	Seafloor segmentation	88
6.6	Conclusion and perspectives	89
7	Fusion of MS MBES system data for seafloor classification	91
7.1	Introduction	91
7.2	Problem statement and related work	92
7.3	Proposed approach	94
7.3.1	Elementary classification models	94
7.3.2	Intra-mode fusion	96

7.3.3	Inter-mode fusion	98
7.4	Results and Discussion	102
7.4.1	Considered dataset	102
7.4.2	Single-mode classification results	102
7.4.3	Intra-mode fusion	104
7.5	Conclusion & Future works	116
8	Conclusions and Perspectives	123
	Bibliography	133

Abstract

Abstract: This thesis, co-directed by Jean-Marc Boucher and Ronan Fablet (IMT Atlantique) and co-supervised by Didier Charlot (iXBlue), Gilles Le Chenadec and Michel Legris (ENSTA Bretagne), was realized in the context of a convention CIFRE with the company iXBlue.

iXblue develops and commercializes a multibeam echosounder (MBES) SEAPIX primarily dedicated to the fishery market. The system is optimized to offer the best compromise between performances capabilities and cost. In addition to the classical characteristics of an MBES, it offers the unique feature of scanning the seafloor (and the water column volume) by electronical beamform multiple the emission swaths from port to starboard, as well as from forward to backward. The objective of the thesis is to study the contribution of these new multi-swath capacities in the analysis and classification of the seafloor.

The first part of the work consisted in carrying out a detailed analysis of the measurement chain. This study evaluated the consistency in acquiring the backscattering strength from different insonification modes. The second part investigated the discriminant characteristics of the backscattered signal while taking into account the acquisition geometry of each insonification mode. The last stage of the work involved to methods of fusing the acquired data. This study was carried out in two approaches; the first considers data from the same insonification mode (intra-mode) and the second from different modes (inter-mode), for the seafloor classification. The obtained experimental results highlight the interest of the proposed processing chain and a multi-mode architecture on the real datasets.

Keywords: *Multibeam echosounder, multiswath MBES, backscattering strength, seafloor classification, point-wise feature, information fusion.*

Résumé

Cette thèse, co-dirigée par Jean-Marc Boucher et Ronan Fablet (IMT Atlantique) et co-encadrée par Didier Charlot (iXBlue), Gilles Le Chenadec et Michel Legris (ENSTA Bretagne), a été réalisée dans le cadre d'une convention CIFRE au sein de la société iXBlue.

iXblue développe et commercialise un sondeur multifaisceaux (MBES) SEAPIX principalement dédié au marché de la pêche. Ce système a été développé pour offrir le meilleur compromis entre performances de détection et son coût de revient. Outre les caractéristiques classiques d'un MBES, il propose la particularité unique de pouvoir insonifier des fauchées différentes sous le navire par dépointage électronique du faisceau d'émission de bâbord à tribord et d'avant en arrière. Le travail de thèse a pour objectif d'étudier l'apport de ces nouvelles capacités multi-fauchées dans l'analyse et la classification des fonds marins.

La première partie du travail a consisté à réaliser une analyse détaillée de la chaîne de mesure. Cette étude a permis d'évaluer la consistance des niveaux de rétrodiffusion entre les différents modes d'insonification. La deuxième partie s'est intéressée à la recherche des caractéristiques discriminantes du signal rétrodiffusé en tenant compte de la géométrie d'acquisition de chaque mode d'insonification. La dernière étape du travail a porté sur des méthodes de fusion des données acquises. Cette étude s'est réalisée en deux approches ; la première considère des données venant du même mode d'insonification (intra-mode) et la seconde venant de modes différents (inter-mode), pour la cartographie des fonds marins. Les résultats expérimentaux obtenus mettent en évidence l'intérêt de la chaîne de traitement proposée et d'une architecture multi-mode sur les jeux de données réelles traitées.

Mots clés : *Système multifaisceaux, MBES multi-fauchée, rétrodiffusion, classification des fonds marins, descripteur, fusion d'information.*

Résumé étendu

Depuis 2010, iXBLUE, une de meilleures sociétés dans le développement des systèmes de navigation et d'imagerie sous-marins, a développé et commercialisé un système SONAR multifaisceaux innovant, SEAPIX, dédié au marché de la pêche. La réduction des rejets est l'un des défis les plus importants de l'activité de pêche moderne. Ceci pourrait être réalisé en utilisant une sélectivité acoustique pour discriminer les espèces de poissons et leur taille avant la capture. Le système SEAPIX a été développé dans ce contexte. Il a été conçu pour fournir un bon compromis entre le coût du matériel et les performances de détection dans la colonne d'eau [1]. Une cinquantaine de systèmes sont désormais en activité, principalement sur le marché pélagique. Le système SEAPIX fournit simultanément une carte bathymétrique précise qui donne, au pêcheur, une meilleure compréhension de l'environnement sous-marin. En outre, le système est capable de fournir une carte de rétrodiffusion acoustique calibrée à haute résolution du fond marin. Cette thèse vise à explorer et développer une méthode robuste de classification des fonds marins en utilisant les capacités multi-fauchées du système SEAPIX. Elle a été réalisée en collaboration entre iXBLUE et le laboratoire LAB-STICC (Laboratoire en Sciences et Techniques de l'Information, de la Communication et de la Connaissance) de l'institut de l'IMT Atlantique et de l'ENSTA Bretagne (Ecole Nationale Supérieure de Techniques Avancées).

Suite au but de la thèse, deux principales fauchées d'insonification du système ont été exploitées : fauchée transversale (mode bathymétrie) et fauchée longitudinale (mode longitudinal). Le mode bathymétrie correspond au mode de fonctionnement des systèmes multifaisceaux classiques (MBES). Dans la classification des fonds marins, les données MBES sont généralement exploitées en deux tentatives : mesurer la dépendance de la rétrodiffusion (BS) par rapport à l'angle d'incidence ou extraire des caractéristiques texturales à partir des images (mosaïque /waterfall). La discrimination des fonds marins à l'aide de la dépendance angulaire de rétrodiffusion est une méthode bien connue qui a été prouvée dans de nombreuses études classiques [2–4]. Elle peut être faite à l'échelle locale ou globale. Dans celle locale, la classification a été réalisée via la comparaison de niveau de rétrodiffusion sur les pixels ayant le même angle d'incidence [3, 4]. Dans celle globale, la dépendance BS en fonction de l'angle d'incidence (profil de rétrodiffusion) est utilisée. Dans ce cas, une hypothèse d'homogénéité est faite pour tous les pixels d'une même fauchée. La classification est obtenue par comparaison de la forme de ces profils [5–7]. Dans l'approche texturale, le type de sédiment est caractérisé par une structure locale (appelée texture) dans l'image. L'analyse de texture est une méthode bien connue pour la classification des images du fond marin [8–10]. Dans le mode longitudinal, un profil de rétrodiffusion complète est enregistré pour chaque pixel au nadir. Cette mesure est nettement plus robuste que celle acquise dans le mode bathymétrie car le profil longitudinal est obtenu sur un grand intervalle d'angle d'incidence et aucune hypothèse d'homogénéité n'est nécessaire. Par contre, ce profil est limité sur les pixels au nadir comme pour un système mono-faisceau (SBES).

La chaîne d’acquisition et de traitement SEAPIX a été étudiée en détail pour la détection de la colonne d’eau et de la bathymétrie [1]. Lors d’une première étape de notre travail, nous devons vérifier que la mesure BS est cohérente entre les différents modes d’insonification. Cela a été vérifié par la mesure de similarité entre les données BS acquises sur chaque mode. Nous décidons également d’utiliser des méthodes supervisées étant donné que, dans le contexte de l’activité de pêche, le vrai type de sédiments du fond marin est nécessaire, et non pas les classes abstraites. Dans la problématique de la classification, nous allons considérer les deux aspects : extraction des caractéristiques discriminantes et fusion des données. La procédure d’extraction de caractéristiques va condenser le grand volume de données dans un ensemble de données raisonnable tout en conservant l’information discriminante [11–13]. En ce qui concerne le second aspect, nous considérerons deux niveaux distincts de fusion de données : intra-mode et inter-mode. La fusion de données intra-mode est réalisée sur des résultats de classification obtenus sur deux lignes de levés superposées acquises en mode bathymétrie. Le but de ce processus de fusion est d’attribuer une valeur de classe unique pour chaque pixel de la carte des sédiments de sortie. Dans la fusion inter-mode, le but est de fusionner les résultats de classification donnés par le mode bathymétrique sur une grande zone de couverture avec les résultats de classification robustes obtenus par le profil du mode longitudinal. La combinaison de ces modes devrait améliorer les résultats de la classification des fonds marins obtenus par des méthodes classiques avec les données du mode bathymétrique uniquement.

La thèse est organisée comme suit :

Au chapitre 2, nous passons d’abord en revue des connaissances de base sur la rétrodiffusion du fond marin. Nous décrivons également les principaux systèmes acoustiques utilisés. Ensuite, nous présentons en détail notre système MS-MBES SEAPIX et ses multiples modes d’insonification.

Ensuite, le document est divisé en deux parties. La partie I est dédiée à la description détaillée du système d’acquisition et à l’analyse des données de rétrodiffusion. Il est composé de deux chapitres. Au chapitre 3, la chaîne complète d’acquisition et de prétraitement du système est décrite. Nous expliquons les différentes capacités du mode imagerie et montrons les résultats sur un vrai jeu de données acquis sur une zone de référence. Au chapitre 4, nous appliquons une analyse statistique pour vérifier la cohérence des données acquises entre les différents modes d’insonification. Cette analyse est faite en utilisant la mesure de similarité de la divergence de Kullback-Leibler. Dans la partie II, nous présentons nos travaux sur l’exploitation des données de rétrodiffusion à la classification des fonds marins. Cette partie est divisée en trois chapitres. Tout d’abord, au chapitre 5, nous commençons par une revue des méthodes de classification standards. Ces méthodes standards correspondent à différentes tentatives dans la littérature comprenant la tentative de dépendance angulaire à l’échelle locale (méthode basée sur le niveau), la tentative de dépendance angulaire à l’échelle globale (méthode basée sur le profil) et la tentative texturale (méthode basée sur la texture). Les résultats de la classification sont ensuite affichés sur l’ensemble de données réel. Ensuite, au chapitre 6, nous proposons et étudions nos propres méthodes d’extraction des caractéristiques discriminantes. Deux catégories de caractéristiques sont considérées : les caractéristiques statistiques (moyenne, variance) et les caractéristiques texturales (histogramme des gradients orientés, covariance spatiale). Ils sont évalués via un test de validation croisée pour la performance discriminante. Dans le dernier chapitre 7, nous présentons nos tentatives de classification du fond marin en combinant des informations (les caractéristiques sélectionnées exposées dans le chapitre précédent) dans deux contextes : la fusion intra-mode et la fusion inter-mode. La fusion intra-mode consiste en la fusion de la carte de classification obtenue en utilisant le mode bathymétrique conventionnel. Il est réalisé sur la base des stratégies consensuelles, où nous pondérons chaque source par leur contribution à la fusion. Dans la fusion

inter-mode, nous explorons des méthodes pour combiner les informations entre les deux modes d'insonification différents. La méthode proposée est basée sur celle des ensembles de niveaux variationnels, où nous développons le contour segmenté pour obtenir la meilleure similarité entre les caractéristiques de la zone segmentée actuelle et celles de référence.

Enfin, le chapitre 8 résume nos études et présente quelques perspectives qui se produisent au cours de notre recherche.

Introduction

Since 2010, iXBLUE, a leading company in the development of underwater navigation and imagery systems, developed and commercialized an innovative multi-beam SONAR system, SEAPIX devoted to the fishery market. Discard reduction is one of the most important challenges in modern fishery activity. This could be achieved using acoustic selectivity to discriminate fish species and size before catch. The SEAPIX system was developed in this context. It has been designed to provide a good tradeoff between hardware cost and detection performances in the water column [1]. About fifty systems are now in operations mainly on the pelagic market. SEAPIX system provides simultaneously a precise bathymetry map which gives, to the fisherman, a better understanding of the underwater environment. Furthermore, the system is able to give high resolution calibrated acoustic backscatter map of the seabed. The aim of this work is to explore and develop robust seafloor classification method using the multi-swath capabilities of the SEAPIX system. This thesis was conducted in collaboration between iXBLUE and the laboratory LAB-STICC (Laboratoire en Sciences et Techniques de l'Information, de la Communication et de la Connaissance) of the institutes of IMT Atlantique and ENSTA Bretagne (l'Ecole Nationale Supérieure de Techniques Avancées).

In our works, we have to study how to use the multiple swath capabilities of the system to improve the classification performances. Two main insonification swaths of the system have been exploited: across-track swath (bathymetry mode) and along-track swath (longitudinal mode). The bathymetry mode corresponds to operation mode of classical Multi-Beam Echo Sounder (MBES) systems. In seafloor classification, MBES data are usually exploited using two attempts: measuring the backscattering strength (BS) dependence versus incidence angle or extracting textural features from backscatter mosaic/waterfall images. Seabed discrimination using backscatter angular dependence is a well-known method that has been proven in many classical studies [2–4]. The analysis can be made at local or global scale. In the local ones, the classification was carried out via the backscatter level comparison on the pixels with the same incident angle [3, 4]. In the global ones, the BS dependence as the function of incident angle (backscatter profile) is used. In that case, a homogeneity hypothesis is made for all pixels in a same swath. The classification is obtained by shape comparison of these profiles [5–7]. In the textural approach, the sediment type is assumed to be characterized by local structure (called texture) in the image. Textural analysis is a well-known method for seabed image classification [8–10]. Using the longitudinal mode, a full backscattering strength profile is recorded for each pixel at nadir (along track). This measure is clearly more robust than the one using the across-track swath because the longitudinal profile is obtained on a large incidence angle interval and no homogeneity hypothesis is needed. But the measurement is restricted on the pixels at nadir as for a Single-Beam Echo Sounder (SBES).

The SEAPIX acquisition and processing chain was studied in details for water column and bathymetry detection [1]. At a first step in our work, we need to check that the BS measurement is consistent among the different modes of insonification. This has been verified via similarity measure [14] between the data acquired on each mode. We also decide to use a supervised clas-

sification scheme since, in the context of fishing activity, the true type of seafloor sediment is needed, not abstract classes. In the classification problematic, we will consider the two aspects: discriminant features extraction and data fusion. The feature extraction procedure will condense the large volume of data into a reasonable dataset while conserving the discriminant information [11–13]. Concerning the second aspect, we will consider two distinct levels of data fusion: intra-mode and inter-mode data fusion. Intra-mode data fusion is the fusion of the classification results obtained on two overlapped survey lines acquired in the bathymetry mode. The goal of this fusion process is to assign a unique class value for each pixel in the output sediment map. In the inter-mode fusion, the goal is to fuse the classification results given by the bathymetry mode on a large coverage area with the robust classification results obtained on the along track with the longitudinal mode. The combination of these modes is expected to improve the traditional seafloor classification results obtained with the bathymetry mode’s data only.

In this document, we present the whole chain of exploiting this MS-MBES system for seafloor classification, which consists of the acquisition campaign, the extraction of backscatter data, the data analysis for consistency check, the extraction of discriminant features, and the classification with the fusion methods. It is organized as follow:

In *chapter 2*, we first make a review of the basic knowledge on seafloor backscatter. We also describe the main acoustic systems in use. Then, we present in detail our MS-MBES system and its multiple operating modes.

The document is then divided in two parts. **Part I**, is dedicated to the detail description of the acquisition system, and of the analysis of the backscatter data. It is composed of two chapters. In *Chapter 3*, the full acquisition and preprocessing chain of the system is described. We explain the different imaging mode capabilities and show the results on a true data set acquired on a reference area. In *Chapter 4*, we apply a statistical analysis to check the consistency of the data acquired among different insonification schemes. This analysis is done using the similarity measure of Kullback-Leibler divergence. In **Part II**, we present our works on exploiting the backscatter data for seafloor classification purpose. This part is divided into three chapters. First, in *Chapter 5* we begin by a review of standard classification methods. These standard methods correspond to different attempts in literature consisting of the angular-dependence attempt in local scale (level-based method), the angular-dependence attempt in global scale (profile-based method), and the textural attempt (texture-based method). Classification results are then shown on the real data set. Next, in *Chapter 6*, we propose and study our own methods of extracting discriminant features. Two categories of features are considered: statistical features (mean, variance) and textural features (histogram of oriented gradients, spatial covariance). They are evaluated via cross-validation test for the discriminant performance. In the last *Chapter 7*, we introduce our attempts in classifying the seafloor in combining information (the selected features exposed in the previous chapter) in two contexts: intra-mode fusion and inter-mode fusion. The intra -mode fusion consists of the fusion of obtained classification map using the conventional bathymetry mode. It is realized based on the consensus strategies, where we ponder the sources by their contribution in the classification during the combination. In the inter-mode fusion, we explore methods to combine classification information between the two different modes of insonification. The proposed method is developed in the variational level-set segmentation framework, where we evolve the segmented contour to obtain the best similarity between features in current segmented zone and the training ones.

Finally, *Chapter 8* summarizes our studies, and presents some perspectives that occur during our research.

Seafloor mapping sonar system

In the context of seafloor classification, we first introduce some basic information about our exploited data: the backscattering strength. This data is commonly exploited in different studies such as seafloor characterization [4,15], seafloor classification [8,9,16,17] or seafloor imaging [18]. Three main types of acoustics systems have been developed for backscattering strength acquisition and analysis: single-beam echo sounder (SBES), multi-beam echo sounder (MBES) and side-scan SONAR (SSS). In such a context, iXBLUE introduced a new MBES system in 2010, called SEAPIX dedicated to the fishery market. This system offers multi-swath capabilities that can be selected on-the-fly.

This chapter is organized as following: we first introduce the notion of backscattering strength. Next, we present several commercial acoustic systems with their in-use context. In the end, we describe the exploited system in the thesis, and its different functionalities.

2.1 Seafloor Scattering

In underwater applications, sound waves are the most efficient means thanks to their long travel distance (up to kilometers) without significant attenuation. The level of attenuation depends on their frequency and is more important in the high frequency. While traveling, these waves carries a certain amount of acoustic energy and can be measured via their amplitude or their intensity (proportion to the squared of amplitude).

Seafloor is defined as the rough surface at the interface between the water-column and the underground stratified sediment. This surface is a boundary between environments with different impedance. As a result, while a sound wave encounter this surface, it will be reflected, transmitted and scattered. Usually, in active sonar imaging system, the scattered signal is measured in the same direction as the emitted signal which is then called backscattered signal. The backscattered signal strength will depend on the seafloor characteristics, which consist of both seafloor nature (sediment hardness) and seafloor interface (surface roughness). At high frequency, upon a few tens of kilohertz, only the first layer of the stratified seabed will contribute to the backscatter signal.

The strength of the scattering of the seafloor is characterized by the scattering cross section σ defined using equation (2.1) as in [19]. The scattered energy, proportion to mean-square scattered pressure $\langle |p_s|^2 \rangle$, is proportional to the incident energy $|p_i|^2$ and the insonified surface As , and inversely proportional to the square of distance from the insonified seafloor to the measure point r_s^2 .

$$\langle |p_s|^2 \rangle = |p_i|^2 As \sigma \frac{1}{r_s^2} \quad (2.1)$$

In this equation, we notice the mean operator $\langle . \rangle$ in the scattered energy. This operator signifies an idealized average over the ensemble of individual scatters inside the insonified area.

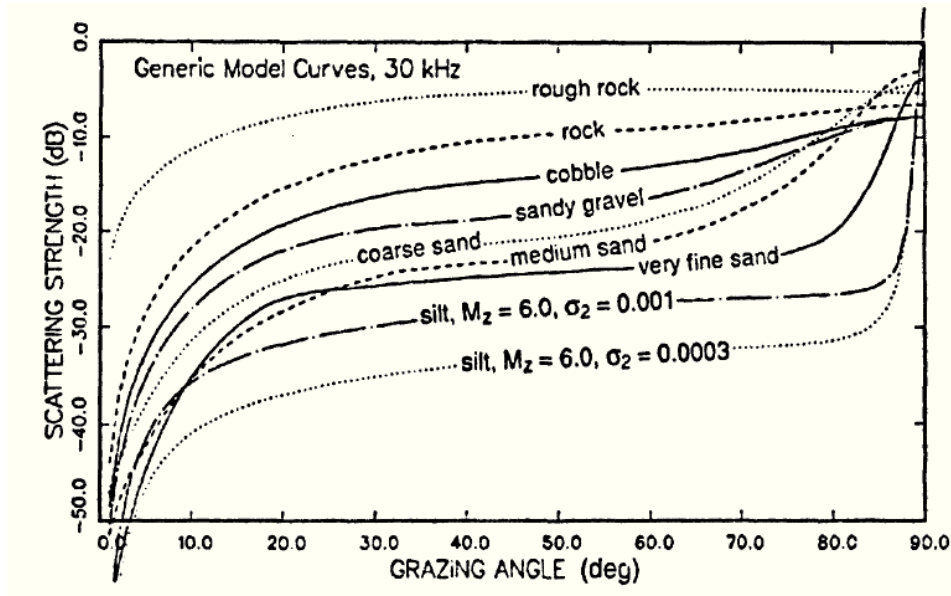


Figure 2.1 – Modeling of backscatter strength from different types of seafloor: rough rock, rock, cobble, sandy gravel, coarse sand, medium sand, very fine sand, and silts in APL 1994 [20]. This modeling was realized at the frequency of 30 [kHz]. The curves were expressed in the function of grazing angle, which was supplement to incident angle.

The backscatter strength value depends not only onto the nature of seafloor but also on the acoustic frequency and the incident angle. Different physical models were introduced to describe this information such as Kirchhoff model for large roughness seafloor ($\leq 20^\circ$ angles [20]), composite roughness model [2]. In Table 2.1, we present the different physical parameters utilized in these models, which were introduced in the APL 1994 [20]. In Figure 2.1, the modeling of different types of seafloor was presented at frequency of 30 [kHz], and we observe the strong discrimination of this information in the seafloor classification. From these models, we observe that not only the profile shape is a potential discriminant feature for the classification, but also, the backscatter level is discriminant in the range of incident angles (20° - 80°). In addition, by exploiting these physical models, it should be possible, in principle, to estimate geophysical parameters. This was not part of our study but could be envisaged as a perspective.

Table 2.1 – Parameters in physical model introduced in APL 1994 [20]

Param.	Physical meaning	Definition
ρ	Density ratio	Ratio of sediment mass density to water mass density
ν	Sound speed ratio	Ratio of sediment sound speed to water sound speed
δ	Loss parameter	Ratio of imaginary wavenumber to real wavenumber for sediment
γ	Spectral exponent	Exponent of the bottom relief spectrum
W_2	Spectral strength	Strength of bottom relief spectrum (in $[\text{cm}^4]$) at a wavenumber of 1 $[\text{cm}^{-1}]$
σ^2	Volume parameter	Ratio of sediment volume scattering coefficient to sediment attenuation coefficient

Since the modeling of the backscatter profile using physical parameters is not easy, more simple modeling have been used. For instance several heuristic models were introduced such as simple Lambert [21], IFREMER [22]. Even though these models were not able to provide the seafloor physical parameters, they have been commonly used and give sufficiently good discrimination for seafloor classification purpose [3, 22].

Seafloor classification can also be done using the images formed with the backscatter signals recorded at each ping, either in the waterfall image or in the fully georeferenced mosaic [8, 10]. There are mainly three attempts. The first attempt consists in extracting the textural information obtained from the seafloor mosaic or waterfall image. In the second attempt, the classification is obtained using the backscatter profiles (or their model parameters) that are reconstructed from the images knowing the incidence angles at each pixel [5, 6], [7]. In the last attempt, the classification is realized based on the backscatter distribution according to the acquired incident angle [16, 23, 24].

The distribution of the backscatter was also concerned in a lot of studies. As amplitude (resp. intensity) information, it was supposed to follow the Rayleigh (resp. exponential) distribution. In the study of Middleton [25], it was proposed to follow the gamma distribution because the acquired backscatter value was often obtained from an average of several backscatter intensity. These propositions were generalized to the Rayleigh mixture distribution [26] (amplitude), K-distribution [3, 27], log-normal distribution [28].

2.2 Classical systems

In the interest of the backscatter information, a lot of acoustic systems were introduced to acquire this information, in military as well as in civil commercial applications. These systems could generally be sorted into three main categories: Single-Beam Echo Sounder (SBES), Side-Scan SONAR (SSS) and Multi-Beam Echo Sounder (MBES). In this section, we describe the principle of each of these systems as well as their domains of applications.

2.2.1 Single-Beam Echo Sounder

SBES systems mounted on moving vessels were first used to analyze the underwater environment : measuring the bathymetry profile by detecting the first echo reflected from the seabed, analyzing the habitats using the acoustic signals reflected by the biomass present in the water column, estimating underground sediments structures by detecting the reflected echoes from deep internal interfaces. Moreover, the shape of echoes reflected by the seabed is related to the hardness and roughness of the first layer. So, these systems are commonly used as seafloor classification tools. Main commercial software using SBES data for seafloor classification are RoxAnn (Sonavision), IMPULSE (MaritimeWay) and SIVA (SEMANTIC TS).

2.2.2 Side-Scan Sonar

Since the emission aperture angle of SBES is only of a few degrees, the analysis is just limited to region at the nadir of the vessel track. SSS systems broaden the coverage of the insonified area to both port and starboard sides. In these systems, acoustics time-series signals capture backscatter information from a much larger range of incidence angles. It is then expected that this system could better distinguish different types of seafloor by exploiting the backscatter profile response as described in Figure 2.1. But, in practice, this technique is difficult to use with side-scan data for three main reasons. First, it is difficult to know the acoustic and electronic parameters (Source Level, acoustic Sensitivity, amplified gain) of commercial side-scan sonar in

order to get a full calibrated data values. Second, since the bathymetry profile is not known, a flat seabed hypothesis is assumed. Using this assumption the estimated incident angle value is biased as well as the BS level. Last, in estimating the seabed backscatter profile response from the swath signal, it is assumed that the seabed is homogeneous all along the swath. A better approach is to use textural features as discriminant features: With SSS, the seabed is insonified at high incident angle value. Textural information is then clearly visible on side-scan images. This is better reinforced when using higher emission frequency typically a few hundredth of kHz. The most popular commercial softwares available are SIDEVIEW (Maritimeway), GeoTexture (Kongsberg), Eca/Triton (SeaClass).

2.2.3 Multi-Beam Echo Sounder

SSS systems provide a good segmentation of the seafloor when textural features are present. But textural shape depends a lot upon insonified angle and range, and there are not absolute measurement criteria. Also, in conventional SSS, absolute BS level could not be well estimated as previously noted. With a MBES systems, sonar characteristics are better known and a full bathymetry profile can be obtained at each ping across track of the vessel. This capacity comes from the fact that the system forms multiple beams across track (typical value is 256) at reception using digital beamforming techniques. For each direction, a temporal signal is obtained, and a detection algorithm is used to extract the time of the first echo reflected by the seabed. Samples inside a time window before and after the seabed time echo are also stored. These signals, called snippet, correspond to the amplitude signals reflected from the beam footprint. These amplitude values combined with the known bathymetry profile can be precisely compensated to compute absolute BS values versus incidence angle. By combining all of the snippet series from each beam, a full backscatter profile can be reconstructed for each swath. Depending on the combination algorithm resp. average, max, nearest distance, different type of images can be constructed, resp. sidescan, Truepix or Snippet images. Due to the beamforming process, MBES backscatter images are more robust to multipath which is particularly useful in shallow water environment. But, in general, MBES systems provide lower resolution in the along-track direction and a lower range/depth ratio. However, to increase this ratio, a double emission head can be used. MBES systems gather more complete and precise measurements than SBES and SSS together. The ability to obtain backscatter value vs incidence angle make it a powerful tool for seabed classification purpose. The exploitation of the BS angular dependence for seafloor classification purposes was presented in many studies [5, 23, 24]. Main software commercial products are Multiview (MaritimeWay), SonarScope (Ifremer). High resolution multi-beam systems can also deliver high resolution side-scan like images. Textural based approach may be then applied simultaneously.

2.3 Multi-Swath Multi-Beam Echo Sounder

2.3.1 Historical

iXBLUE has begun to develop an innovative acoustic system, SEAPIX, since 2010 in the project Op-tipêche [29]. This system was defined in order to combine the following objectives:

- Optimized price/performances ratio adapted to the fishery market
- Medium performance in resolution (2° beam, at least 300m range)
- Bathymetry map IHO 1st order

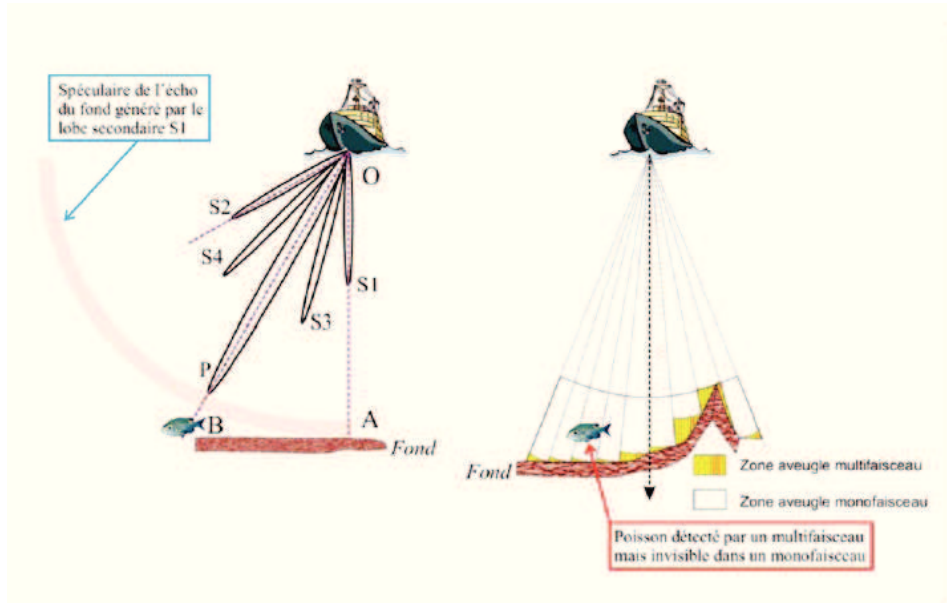


Figure 2.2 – Potential of MBES system in fishery market [29]. The left image shows the advantage of beam-forming in a direction (focusing on the signal in this direction and reducing signals from the other directions). The right image indicates the ability of MBES systems to detect fishes on a larger coverage than SBES.

- Detection and analysis of schools of fish
- Frontal insonification for security navigation and fish detection
- Backscatter sidescan image visualization and Seafloor type identification

SEAPIX architecture was based on a conventional MBES system architecture. This allow to deal with, first, the problematic of fishery detection/identification in the water-column level with a larger view than the SBES systems. This is illustrated in Figure 2.2. Besides, the MBES system is also capable of providing robust information about seafloor bathymetry and seafloor discrimination.

SEAPIX geometry is based on a traditional Mills-Crossed structure used for MBES. This system is composed of two linear antennas, one oriented along track the vessel and the other one across track. In a traditional system, the along track antenna is the emission antenna and the across track antenna is the reception antenna, on which signal beamforming is done. In SEAPIX, the two antennas are identical and can be used either in emission or reception mode. Beamforming can be done at emission and reception.

System specifications were defined in [29], as a trade-off between price and performance. They are displayed in Table 2.2. The frequency f of $150kHz$ with a band of $10kHz$ allow to obtain high-resolution information ($\approx 10cm$ in the seafloor) while the propagation range is still about several hundred meters. The working range of reception angles was quite open, from -60° to 60° , to cover a large aperture under the sounder. Beam aperture varies from 1.6° at nadir to 3.2° at 60° emission/reception angle.

One of the main SEAPIX objectives was to image in front and in the side of the vessel simultaneously for navigation security purpose and fish detection. Figure 2.3 illustrated the first prototype geometry: The two antennas were rotated 45° from the vessel's axis. Therefore, by forming the emission beam at 45° , one part of the insonified swath is oriented in front of the

Table 2.2 – SEAPIX configurations

Param.	Definition	Value
f	Working frequency	150 [kHz]
τ	Pulse width	0.1 [ms]
N	Number of sensors per antenna	64
θ_r	Reception angles	64 equi-angles from -60° to 60°
$\theta^{(-3dB)}$	Apertures of antenna (elevation \times azimuth)	$1.6^\circ \times 120^\circ$
L	Antenna's length	38 [cm]
Sv	Sensibility in emission	133 dB@1uPa
Sh	Sensibility in reception	-196 dB@1uPa

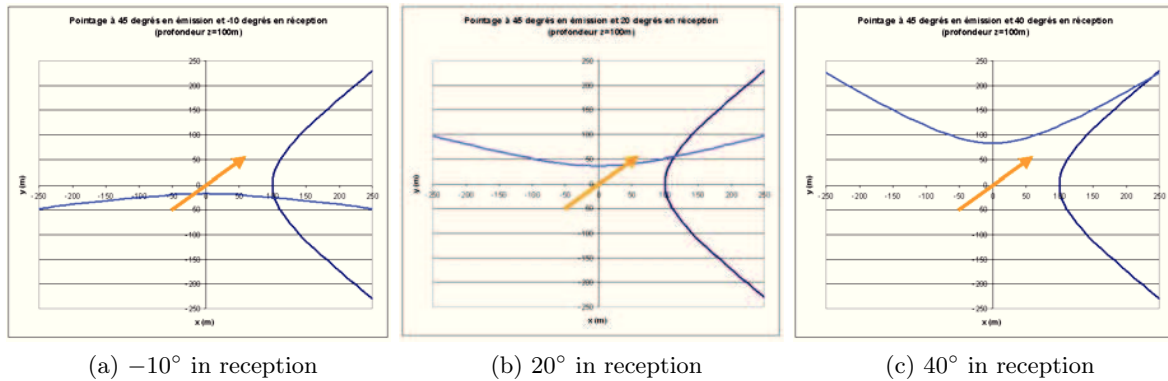


Figure 2.3 – First insonification strategy in [29]: emission at 45° (dark blue swath). The vessel heading angle is illustrated by yellow arrow. The reception scanned the insonified swath to acquired the information in vessel frontal (-10° in Figure 2.3a, 20° in Figure 2.3b, 40° in Figure 2.3c).

vessel and the other part on the side of the vessel. The beam-forming on reception antenna scanned this swath and provided bathymetry and backscatter information in front and on the side of the vessel. But, in practice, echograms and images, recorded using this geometry, are difficult for user to visualize and interpret. It was then decided to come back to a more natural geometry by placing the two antennas as in a conventional system: one antenna oriented in the vessel axis and the other perpendicular. Imaging in front and in the side is done by alternating the two antennas mode: First along track antenna is in emission mode which enable to image in a fore/aft direction. Then using the across track oriented antenna, the system is able to image on the port/starboard side.

By exploiting the scanning capabilities of the system, it is possible to image the full water volume under the vessel in a $120^\circ \times 120^\circ$ wide aperture. Application of SEAPIX in fisheries and ecosystem research is detailed in [1]. In this study, fish detection capabilities and bathymetry performances have been validated.

2.3.2 Current system

The three main insonification strategies that have been studied in this thesis are illustrated in Figure 6.2. These operating modes insonify the seafloor under different swaths illustrated in Figure 6.2: across-track swath in nadir (bathymetry mode - blue line), along-track swath in

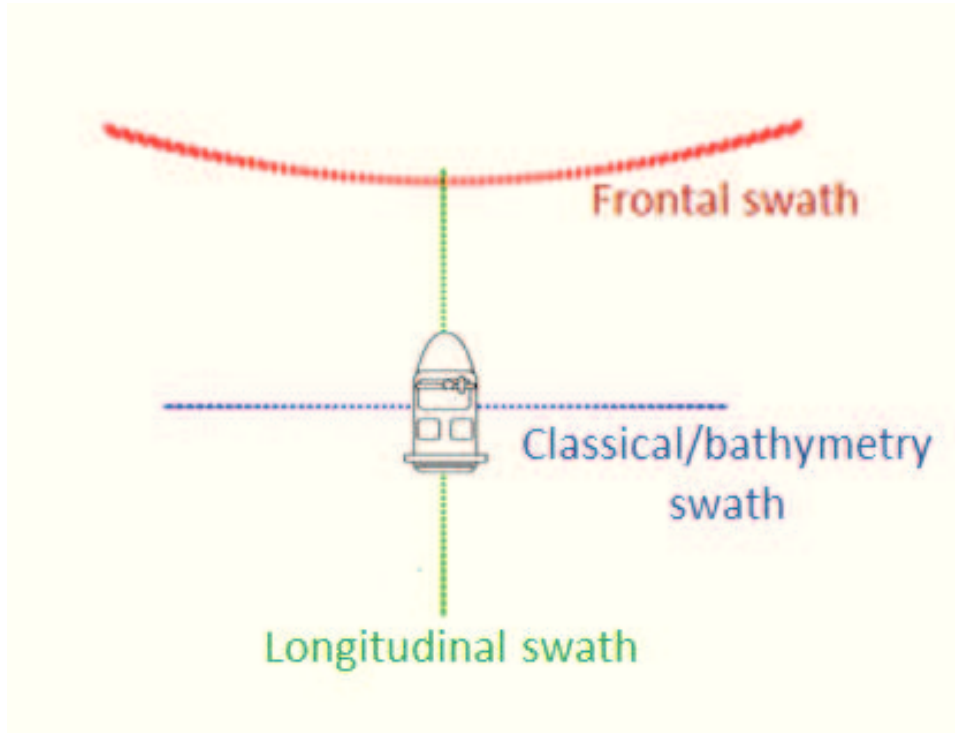


Figure 2.4 – Visualization of the SEAPIX insonified strategies: bathymetry mode (blue line), longitudinal mode (green line) and frontal mode (red line).

nadir (longitudinal mode - green line) and frontal across-track swath (frontal mode - red line). These modes can be used alternatively during the acquisition. We have proposed, then, to call this system a multi-swath MBES as opposed to a multi-spectral MBES. The description of these modes is presented more in details in the following.

2.3.2.1 Bathymetry mode

Principle of bathymetry mode is equivalent to the standard MBES systems. As a result, the emission antenna (antenna B) is positioned in the direction of vessel heading, and it insonifies the across-track swath in nadir ($\theta_i = 0^\circ$). In reception, the other antenna (antenna A) forms Nb beams, each of which acquires information from a predefined direction in the interval $[-60^\circ, 60^\circ]$ at 2-degree steps.

This mode is preferably used to acquire bathymetry thanks to its robustness and large coverage. So we call it the bathymetry mode. In that mode, a full backscatter image from port/starboard can also be obtained. This will be used to create full georeferenced mosaic backscatter image. But, in this mode, each pixel is insonified only at one incident angle. In the context of classification, it will be more interesting if pixels can be insonified to get a full backscatter profile from $[-60^\circ, 60^\circ]$. This is precisely what can be obtained from the second operating mode, the longitudinal mode.

2.3.2.2 Longitudinal mode

In the longitudinal mode, the backscatter profile is acquired by switching the antennas' role. The along-track swath is obtained by emitting with the antenna A (across-track antenna) while

receiving with antenna B (along-track antenna). When the vessel is moving along track, these pixels are scanned multiple times under different incident angles. The accumulation of these information, therefore, forms a backscatter profile. This profile is scanned in the full angle interval from -60° to 60° . We see that this mode exploits the antennas' capacity in both emitting and receiving signals, as well as their similarity in structure. The full backscatter profile is obtained only for the pixels on the vessel trajectory. The coverage is similar to a conventional SBES but with theoretically superior capability for seabed classification by recording full backscatter profile for each pixel.

2.3.2.3 Frontal mode

Since the backscatter information is more discriminant in the high incident angles (Figure 2.1), another operating mode is proposed, namely frontal mode. In this mode, the system exploits the beamforming in antenna B (along-track antenna) to insonify the across-track swath in front of the vessel by a predefined angle. As a result, the pixels, in this swath, are insonified under a larger interval of incident angles. Also, the seafloor's information is acquired in advance on the vessel track. The backscatter signal recorded using this mode is more efficient than by using the bathymetry mode because specular reflection is avoided at nadir. Hence, we obtain a better image continuity, and seafloor information from larger incident angles. On contrary, the bathymetry information is more difficult to obtain using this mode. A good scenario will be to combine the bathymetry and longitudinal mode by alternating these two modes during the acquisition. The system will thus provide a full robust and consistent bathymetry and backscatter measurements.

2.4 Conclusion

In the context of seafloor classification, acoustic systems are commonly exploited. The systems can be grouped into three main categories: SBES, MBES and SSS.

In this thesis, we used SEAPIX, a MBES system with some innovative capabilities developed for the fishery market. This system provides multiple operating modes (resp. bathymetry mode, longitudinal mode and frontal mode) to acquire seafloor information from different insonified swaths (resp. across-track swath in nadir, along-track swath in nadir and frontal across-track swath). The first mode proposes a good bathymetry profile as well as the classical backscatter information. The second mode provides a full backscatter profile for each pixel insonified along the vessel trajectory. The last mode offers a reasonable wide coverage of seafloor backscatter information, with larger incident/discriminating angles.

In this thesis, we have focused our study to the first two operating modes: bathymetry mode and longitudinal mode. While the first mode provides a comparable performance to the classical MBES system, the second one has a potential to improve the classification performance at nadir. In the last chapter, we study fusion methods to combine efficiently these two operating modes to produce a robust classification map.

Part I

Raw Data Processing

Backscatter data acquisition and processing

In the Chapter 2, the backscatter strength (BS), which measure the capacity of seafloor in reflecting signal in the direction of arrival [7, 18], was presented as a robust information for seafloor classification. The multi-swath multi-beam echo sounder (MS – MBES) system SEAPIX, which is exploited in this thesis, was also introduced as an equipment to acquire the backscatter information from multiple insonification scenarios.

In this chapter, we present first the standard acquisition and processing chain of a conventional MBES to compute the BS information. Then we describe specification of the acquisition and processing chain of the MS – MBES. The new capacities of this system will be illustrated by showing the processing results obtained under multiple imagery modes. From these results, we will explain the main interests of these additional modes of acquisition. All of these results have been obtained by processing a dataset that were acquired during a dedicated acquisition campaign organized in December 2015, on a reference area in la Ciotat Bay, in France.

This chapter is organized as follow. In Section 3.1, we first introduce the basic principle of an MBES system, as well as its standard acquisition chain. Next, in Section 3.2, we present the specificities of the SEAPIX acquisition chain. Latter, in Section 3.3, we explain the different methods that are commonly used to build backscatter image. This will be illustrated on the dataset acquired with SEAPIX system. In Section 3.4, we describe, in detail, the dataset and the acquired campaign. Afterward, in final Section 3.5, we explain the methods that have been used to gather all the information (computed BS data, navigation position and bathymetry data) for feature extraction and seafloor classification process.

3.1 Sonar principle

In this first section, we introduce the basic principles that a multi-beam echo sounder (MBES) system uses to obtain the seafloor information. The main phenomena that occur during a cycle of acquisition are presented in Figure 3.1. As an active SONAR system, MBES is composed of two antennas units, one for emission and one for reception, that are put in a Mills-crossed structure.

The acquisition cycle starts with an emission from the sounder system. This action takes place in the emission unit, where electric signal is transformed into acoustic signal. In this process, a projector, such as a piezo-electric ceramic, is used. It is capable to produce a pressure wave with specific frequency characteristics when a voltage V is applied.

The emitting signal travels equally in all directions in water environment. Therefore, its energy, measured as SL , is attenuated due to this dispersion and is expressed as a propagation loss PL . Besides, there is also an environment absorption of this signal while traveling, known as an absorption loss AL . All these losses are called as transmission loss TL .

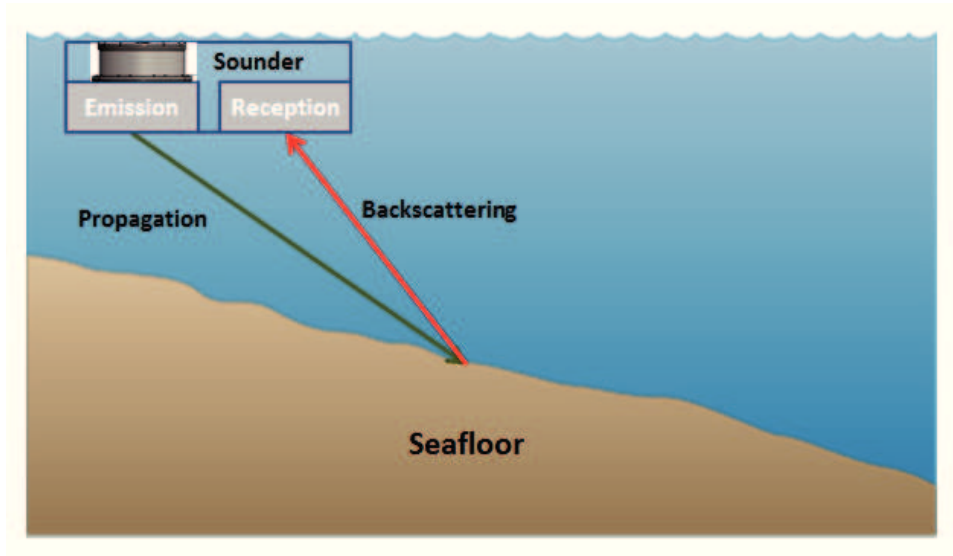


Figure 3.1 – Common active SONAR acquisition chain.

When the signal reaches to seafloor, it insonifies an area of seafloor A_s . In this area, the signal is mostly absorbed, reflected, and only a small part of energy returns to the sounder in the arrival direction (backscattering). The amount of backscattered energy depends on nature of the seafloor and its roughness and on the incident angle of the acoustic waves. The proportion normalized per unit area between the backscattered energy and the incident energy is called the backscattering strength BS of the seafloor.

While the backscatter signal goes back to the sounder, it suffers again another transmission loss. The acoustic signal level, EL , received at the transducer can be expressed via the SONAR equation (3.1).

$$EL = SL - 2TL + BS + 10 \log(A_s) \quad (3.1)$$

In the following, we present the details of the SONAR principle consisting of main phases: emission, transmission, backscattering and reception. The antennas are linear array composed of multiple sensors equally spaced. In SEAPIX, each antenna is composed of 64 sensors equally spaced at half a wavelength.

3.1.1 Beam-Forming

In this section, we present the beamforming principle commonly used in MBES system to form beam in a specific direction either in emission or in reception.

The antenna is supposed to be composed of a number N of sensors which are equally spaced by a distance δ . The center frequency of the pulse acoustic wave is f . To emit or receive from a specific direction θ_0 , the signal from each sensors k are simply delayed and summed. The temporal delay, applied to the signal of each sensor, is related to the emission/reception angle by the following relationship $t_k = k\delta \sin(\theta_0)/c$. For narrow band emitted signal, applying a temporal delay is equivalent to multiply the signal by a term of phase delay. The beamforming operation is then obtained as a complex weighting of antenna signals with weight $w_k = \exp(-j2\pi f k \delta \sin(\theta)/c)$. The emitted/received antenna response in any direction θ_0 , called the directivity function, is then given by the following expression: $D_{\theta_e}(\theta) = \left| \frac{\sin(N\pi f \delta / c (\sin(\theta) - \sin(\theta_e)))}{N \sin(\pi f \delta / c (\sin(\theta) - \sin(\theta_e)))} \right|^2$

An example of directivity function is displayed in Figure 3.2

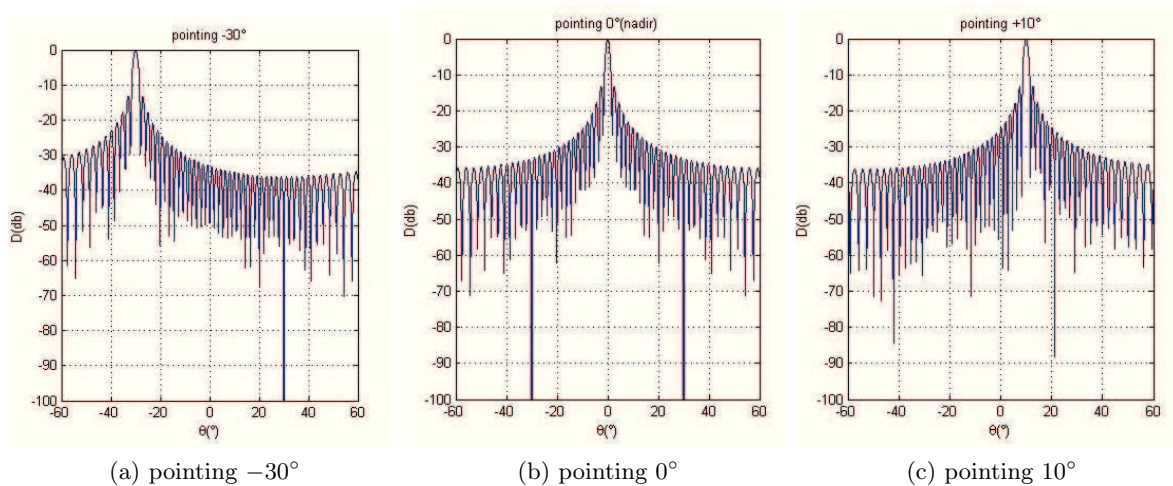


Figure 3.2 – Illustration of directivity function for the pointing direction of -30° , 0° and 10° . In this example, we use the parameters of SEAPIX system ($N = 64$, $\delta = 0.005\text{m}$, and $f = 150\text{kHz}$).

3.1.2 Emission

As an active SONAR system, MBES emits a signal into the underwater environment and wait for its return. Two types of modulation are currently used: continuous wave (CW) or frequency modulated wave (FM). The acoustic intensity emits by the N transducers of the antenna, in the focused direction θ_e at time t is as follow:

$$I(t, \theta_e) = \frac{|Np_e(t, \theta_e)|^2}{\rho_0 \cdot c} \quad (3.2)$$

For any other direction θ the emitted intensity is

$$I(t, \theta) = I(t, \theta_e)D_{\theta_e}(\theta) \quad (3.3)$$

The source level SL is defined as proportion of the pressure measured at $r = 1\text{m}$ from the emitting source $p(r = 1\text{m})$ and a reference pressure p_{ref} . It is proportional to the transducer sensibility Sv , which quantifies the electro-acoustic conversion. The Sv is defined as the output pressure p_{1V} measured from a distance of 1m while inputting 1V of electric signal at the transducer.

$$Sv = 20 \log_{10} \left(\frac{p_{1V}}{p_{ref}} \right) \quad (\text{dB}@1\mu\text{Pa}/\text{V}/\text{sr}) \quad (3.4)$$

Therefore, the source level becomes

$$SL(\theta_e) = 20 \log_{10} \left(\frac{p_e(r = 1\text{m}, \theta_e)}{p_{ref}} \right) \quad (3.5)$$

$$= 20 \log_{10} \left(\frac{p_{1V}}{p_{ref}} \cdot N \cdot V_e^{(rms)} \right) \quad (3.6)$$

$$= Sv + 20 \log_{10}(N) + 20 \log_{10}(V_e^{(rms)}) \quad (\text{dB sr}^{-1}) \quad (3.7)$$

where $V_e^{(rms)}$ describes the root mean square voltage applied into emitting antenna.

3.1.3 Transmission

The signal transmission takes place in the water environment, which disperses and absorbs the emitting energy. The overall transmission loss is the sum of two terms: propagation loss PL and absorption loss AL .

$$PL = 20 \log_{10}(r) \quad (3.8)$$

$$AL = \alpha r / 1000 \quad (3.9)$$

The absorption coefficient α is expressed in dB km^{-1} . It depends on the frequency, the temperature, the salinity and the pressure. This dependency is usually modeled using the François-Garrison formula [30, 31].

3.1.4 Reception

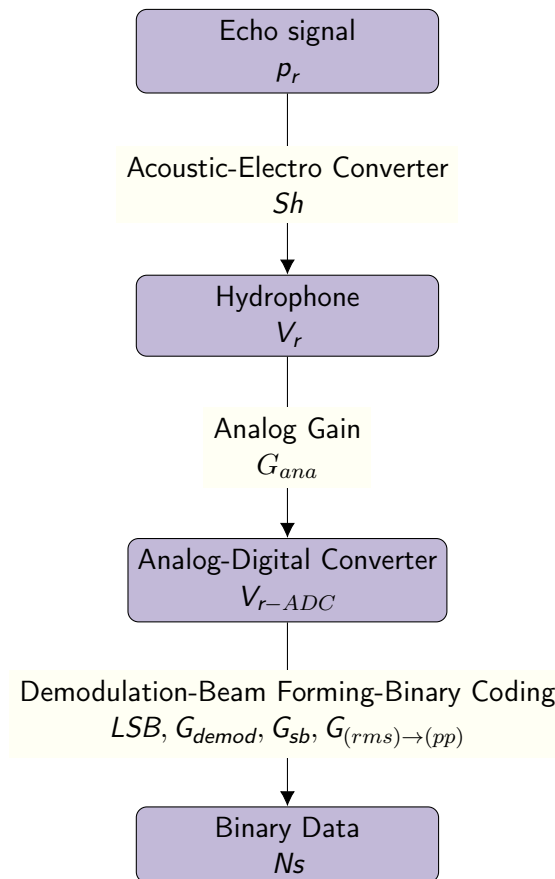


Figure 3.3 – Chain of processes in reception of an acoustic system.

Reception antenna is also a linear array that is usually longer than the emission antenna to get a better azimuth angular resolution. The beamforming is applied on the received signals to compute multiple beams in direction θ_r by applying a weighting factor $w_k = \exp(-j2\pi fk\delta/c \cdot \sin(\theta_r))$ for each sensor signal k . Signals coming from other directions are attenuated according to the directivity response of the antenna $D_{\theta_r}(\theta)$.

$$I_{\theta_r}(\theta) = I_{\theta_r}(\theta_r) D_{\theta_r}(\theta) \quad (3.10)$$

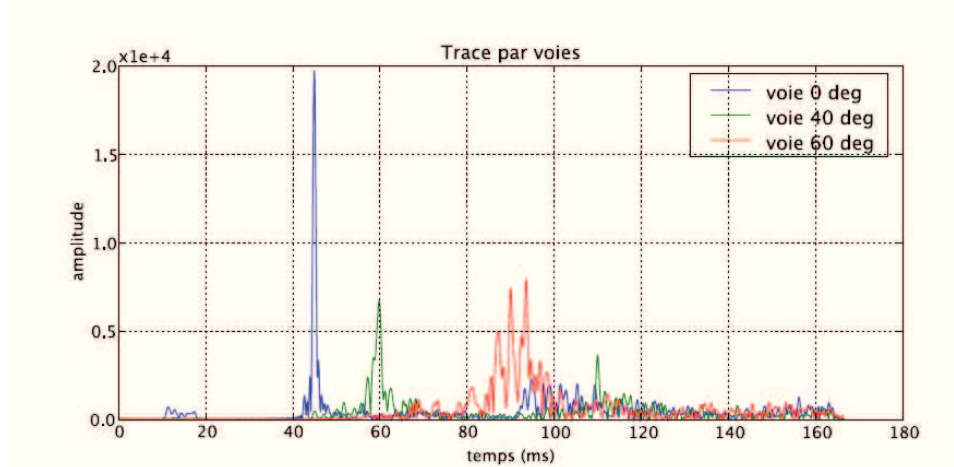


Figure 3.4 – Bathymetry detection: time-series signal of three beams from different directions (0° (nadir) - blue, 40° - green, 60° - red).

where $I_{\theta_r}(\theta)$ is the reception intensity, coming from the direction θ , measured in the beam forming at θ_r .

The received pressure signal is converted into an electronic signal V_r . The efficiency of the hydrophone conversion is characterized by the hydrophone sensitivity Sh which is defined as the output electric level measured while putting a pressure of $1\mu\text{Pa}$ into the hydrophone.

$$Sh = 20 \log_{10} \left(\frac{V_{1\mu\text{Pa}}}{V_{ref}} \right) \quad (\text{dB@1V}/\mu\text{Pa}) \quad (3.11)$$

The measured electrical signal is then expressed as

$$20 \log_{10}(V_r^{(rms)}) = EL_{\theta_r}(\theta_r) + Sh + 20 \log_{10}(N) \quad (\text{dB@V}) \quad (3.12)$$

After conversion into an electrical signal, the time amplitude values are baseband filtered, amplified and demodulated. The demodulated signals are digitized through an analog-digital converter (ADC). The acquisition and pre-processing chain in reception process is displayed in Figure 3.3.

3.1.5 Bathymetry detection

From each received time-series beam, an algorithm detects sample corresponding to the echo reflected by the seabed. Amplitude or phase interferometry null methods are used. For a ping, it gives a bathymetry profile, with number of values corresponding to the number of beam, for example Nb values in the case of SEAPIX.

3.1.5.1 Amplitude

The time-series signal p_i in beam direction θ_i can be divided in three parts. The upper part of the seabed echo contains information about the water column biomass contents. The second part around the seabed echo gives the piece of signals backscattered by the seabed from the insonified footprint. After the seabed echo, signal information is dominated by multiple-path signals and, if the frequency is low, refracted acoustic waves from the underground sediments. The signal echo

around the seabed is usually stronger than the other signals. As explained above, the seafloor echo can be detected as the position t_i maximizing the times-series amplitude.

$$t_i = \underset{t}{\operatorname{argmax}} (|p_i(t)|) \quad (\text{s}) \quad (3.13)$$

In case of low Signal to Noise Ratio (SNR), the barycenter *momenti* is preferably used instead of the maximum t_i . This value is calculated inside a window centered by t_i .

$$\hat{t}_i = \frac{\sum_{j=i-i_0}^{i+i_1} t_i(j) |p_i(t_j)|}{\sum_{j=i-i_0}^{i+i_1} |p_i(t_j)|} \quad (\text{s}) \quad (3.14)$$

where the window characteristics i_0, i_1 are determined via energy threshold from constant false alarm rate (CFAR) detection.

However, this detection method is less effective at large incident angles where the energy is spread (red line in Figure 3.4). In that case, a more efficient method, the interferometry method is used.

3.1.5.2 Interferometry

In the interferometry method, the reception antenna is divided into two sub-antennas. The beamforming is realized on each sub antenna (p_1, p_2) , and the interferometry $p_2 \bar{p}_1$ will give a phase shift

$$d\varphi = 2\pi \frac{d}{\lambda} (\sin(\theta) - \sin(\theta_0)) \quad (\text{rad}) \quad (3.15)$$

where θ_0 is the beam center direction. The interferometry phase is theoretically null in the direction of the beamforming process. So the bathymetry echo is obtained by searching the samples for which the phase interference is null. This method is not well suited to beam at nadir since the size of the footprint is small in that case. Hence, the interferometric phase will vary rapidly and the determination of the time of null phase will not be precise.

3.1.6 Target strength

In the sonar signal processing cycle in Figure 3.1, target strength TS describes the proportion of acoustic intensity reflected back to the system. More precisely, after acquiring the energy emitted from sonar system I_{inc} , the seafloor is considered as an imaginary source. The total energy power that the seafloor received on the surface is

$$W_e = \int_{A_s} I_e(p) dp \quad (\text{W}) \quad (3.16)$$

where I_e is the intensity emitting by the system. A part of this energy is absorbed into the sediment; another part is diffused in all directions. Only a small part is scattered back to system. It is measured via I_{r-1m} , which is the backscatter intensity measured at 1m from this imaginary source. The target strength is expressed as

$$TS = 10 \log_{10} \left(\frac{I_{r-1m}}{I_e} \right) \quad (\text{dB@m}^2/\text{sr}) \quad (3.17)$$

We remark that this term depends on the surface area A_s insonified by the sonar system. It is preferable to have an independent measurement of the insonified area by normalizing the target strength value to the insonified area. This normalized value is defined as the backscatter strength BS value and will be discussed in the next section 3.1.7.

Table 3.1 – Electro-acoustic systems parameters for Seapix

<i>Characteristics</i>	Notations	<i>Values</i>	<i>Units</i>
Number of sensors	N	64	(.)
Pulse width	τ	0.1	(ms)
Antenna A Projector Sensitivity	Sv_A	133.4	(dB@1 μ Pa/V/sr)
Antenna B Projector Sensitivity	Sv_B	131.9	(dB@1 μ Pa/V/sr)
Hydrophone Sensitivity	Sh	-196	(dB@1V/ μ Pa)
ADC resolution	LSB	69.3	(dB)
Beam-Forming Gain	G_{bf}	27	(dB)
Split-beam Gain	G_{sb}	6	(dB)
Demodulation Gain	G_{demod}	-6	(dB)
Resampling	G_{res}	0	(dB)

3.1.7 Backscatter strength

To avoid the influence of insonified surface in the target strength, the backscattering strength ($S_b[\text{sr}^{-1}]$, or $BS[\text{dB sr}^{-1}]$) is introduced as the backscatter intensity reflected by an insonified surface area of 1m^2 . Therefore, we can express the relation between the target strength and the backscattering strength as

$$TS = 10 \log 10 \left(\int_{p \in A_s} S_b(p) \cdot D_{\theta_e}(\theta_e(p)) D_{\theta_r}(\theta_r(p)) dp \right) \quad (\text{dB@m}^2/\text{sr}) \quad (3.18)$$

where the insonified surface is determined via the directivity in emission and in reception ($D_{\theta_e}(\cdot), D_{\theta_r}(\cdot)$).

In most of the cases, we make the assumption that the backscattering strength is constant all over the insonified surface, and the equation (3.18) can be simplified to

$$BS = TS - 10 \log 10(A_s) \quad (\text{dB@/sr}) \quad (3.19)$$

This term is preferred in describing the seafloor's nature, because it relies only on the incident angle θ_i under which the surface is insonified. The calculation of this term is realized via the sonar equation

$$BS = EL + 2TL - SL - 10 \log 10(A_s) \quad (\text{dB@/sr}) \quad (3.20)$$

3.2 SEAPIX Backscatter Processing

In this paragraph, the parameters of processing steps described above will be specified to the SEAPIX system. Some specific characteristics are displayed in Table 3.1.

3.2.1 Emission

SEAPIX system is composed of two similar antennas to emit in the along track or in the across track direction. Each of the antenna is characterized by a directivity at emission which has not yet been taken into account in the equation (3.7). The emission directivity depends on the pointing angle at emission θ_e and on the angle in the transverse direction θ_r . This two components have been measured and modeled as in Figure 3.5.

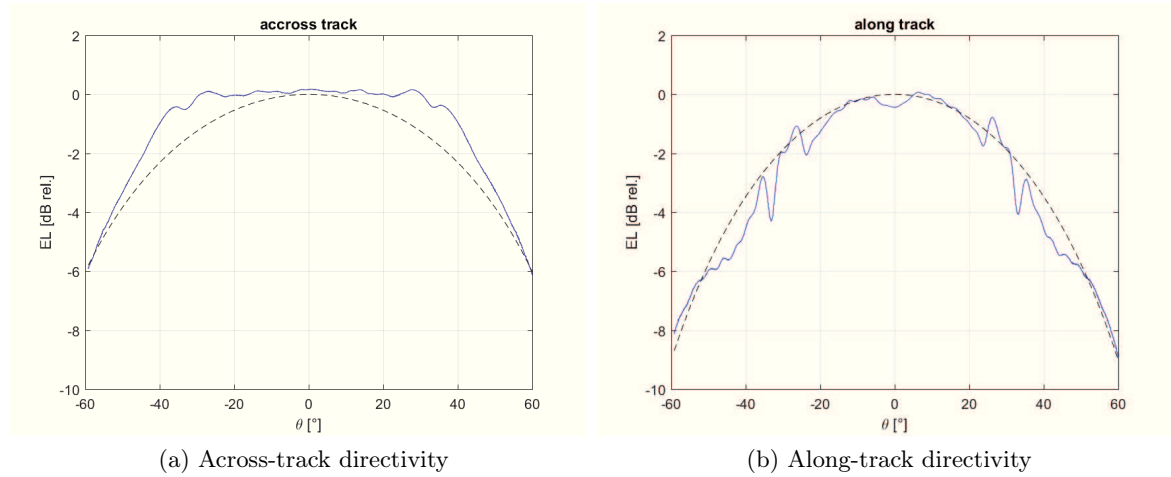


Figure 3.5 – Modeling the antenna directivity of system SEAPIX in two directions: across-track (Figure 3.5a) and along-track (Figure 3.5b). These models describe the evolution of the pressure/intensity at reception (EL in dB) as a function of incident angle θ (in degree).

$$D(\theta_e, \theta_r) = 10 \log_{10}(\cos(\theta_e)^2) + 10 \log_{10}(\cos(\theta_r)^6) \quad (\text{dB sr}^{-1}) \quad (3.21)$$

By introducing these terms in the equation (3.7), we have

$$\begin{aligned} SL(\theta_e, \theta_r) = Sv &+ 20 \log_{10}(N) + 20 \log_{10} \left(\frac{V_e^{(pp)}}{2\sqrt{2}} \right) \\ &+ 60 \log_{10}(\cos \theta_e) + 20 \log_{10}(\cos \theta_r) \quad (\text{dB sr}^{-1}) \quad (3.22) \end{aligned}$$

Also, there is a small dispersion in the sensitivity Sv value that has to be taken into account. These values are indicated in Table 3.1.

3.2.2 Reception

The acoustic signal received by the hydrophone is converted into an electric signal voltage V_r as:

$$20 \log_{10}(V_r) = EL + Sh + 20 \log_{10}(N) \quad (\text{dB@V}) \quad (3.23)$$

Then, this signal is digitized with an analog-digital converter (ADC) with 12-bit dynamic. This choice of ADC was a trade-off between the system cost and reverberation dynamic level [29]. The input level dynamic of the ADC is -0.7 to 0.7 [V]. To adapt the signal level to the ADC input dynamic, an analog gain G_{ana} is applied. The gain is not adaptive. It is composed of a static component of 8.5dB and a dynamic one from 0dB to 57dB. The dynamic part is adjusted depending on the conditions (range, type of seabed) before acquisition via a coefficient C .

$$G_{ana} = 8.5 + 57C \quad (\text{dB}) \quad (3.24)$$

$$20 \log_{10}(V_{r-ADC}) = 20 \log_{10}(V_r) + G_{ana}(C) + G_{(rms) \rightarrow (pp)} \quad (\text{dB@V}) \quad (3.25)$$

After ADC, the digital value of the signal is expressed in (3.26) with parameters value displayed in Table 3.1.

$$20 \log_{10}(N_s) = 20 \log_{10}(V_{r-ADC}) + LSB + G_{bf} + G_{demod} + G_{sb} \quad (3.26)$$

3.2.3 Information extraction

In this section, we will explain how the BS is computed. The starting point is the SONAR equation (3.20). The only parameter that has to be estimated is the surface area. For each received sample at time t_r , this area corresponds to the area that has been insonified by the acoustic pulse travelling inside the beam footprint between time interval $[t_r/2, t_r/2 + \tau]$ where τ is the temporal resolution of the emitted pulse. For CW pulse it is the pulse length, for FM pulse it is the inverse of the bandwidth. The beam footprint area corresponds to the region where the directivity level is more than -3dB . An example is displayed in Figure 3.6 where the insonified area is represented as a thin line crossing the beam footprint area.

To simplify the calculation of the S_b , we make several hypothesis. We first assume that the S_b is uniform inside the beam footprint. We then obtain the first approximation

$$TS = 10 \log 10 \left(S_b \int_{p \in A_s} D_{\theta_e}(\theta_e(p)) D_{\theta_r}(\theta_r(p)) dp \right) \quad (3.27)$$

$$= BS + 10 \log 10(A_s^{(theory)}) \quad (3.28)$$

where $A_s^{(theory)}$ takes into account the non-uniformity of the directivity function inside the insonified surface limited in a pulse width. This term is commonly too complicated to obtain an analytic formula. Therefore, two others simplification have been made

- The footprint region is limited to the -3dB directivity level (orange region in Figure 3.6).
- Inside -3 dB region, the directivity level is set to 1.

Using these two approximations we get:

$$A_s^{(theory)} \approx A_s^{(-3\text{dB})} \quad (3.29)$$

In conventional MBES geometry, where the emission is oriented across track, the $A_s^{(-3\text{dB})}$ area is computed as the product of the along-track length and the across-track length. The along-track length is always measured as $r\theta_e^{(-3\text{dB})}$ where r is the range and $\theta_e^{(-3\text{dB})}$ is the azimuth aperture angle. On across-track, two cases area considered: high incident angles and nadir angles. In high incident angles, the beam-insonified surface is large enough to cover the one corresponding to the system's pulse width τ . Therefore, the component is calculated via the pulse width and expressed as $c\tau/2/\sin(\theta_r)$. However, by approaching to the nadir, the pulse-width surface becomes too large for the beam to cover, and the insonified surface is limited by the beam's aperture $\theta_r^{(-3\text{dB})}$ at this time. The calculation of the component becomes $r \left| \tan \left(\theta_r - \frac{\theta_r^{(-3\text{dB})}}{2} \right) - \tan \left(\theta_r + \frac{\theta_r^{(-3\text{dB})}}{2} \right) \right|$. This estimation is summarized as:

$$A_s^{(-3\text{dB})} = \begin{cases} r\theta_e^{(-3\text{dB})} \frac{c\tau}{2\sin(\theta_r)}, & \text{if } \theta_r > \theta_0 \\ r\theta_e^{(-3\text{dB})} r \left| \tan \left(\theta_r - \frac{\theta_r^{(-3\text{dB})}}{2} \right) - \tan \left(\theta_r + \frac{\theta_r^{(-3\text{dB})}}{2} \right) \right|, & \text{if } \theta_r < \theta_0 \end{cases} \quad (3.30)$$

where θ_0 is the transition angle in between the two cases.

Simulation has been done to compare the value of surface area obtained by the approximation formula and the theoretical value. By dividing the surface into small pixels, directivity is calculated for each pixel and the theoretical surface value is calculated by summing the directivity of all pixels belonging to the insonified surface.

$$A_s^{(-3\text{dB})} = \sum_{p \in A_s} D_{\theta_e}(\theta_e(p)) D_{\theta_r}(\theta_r(p)) dr_e dr_r \quad (3.31)$$

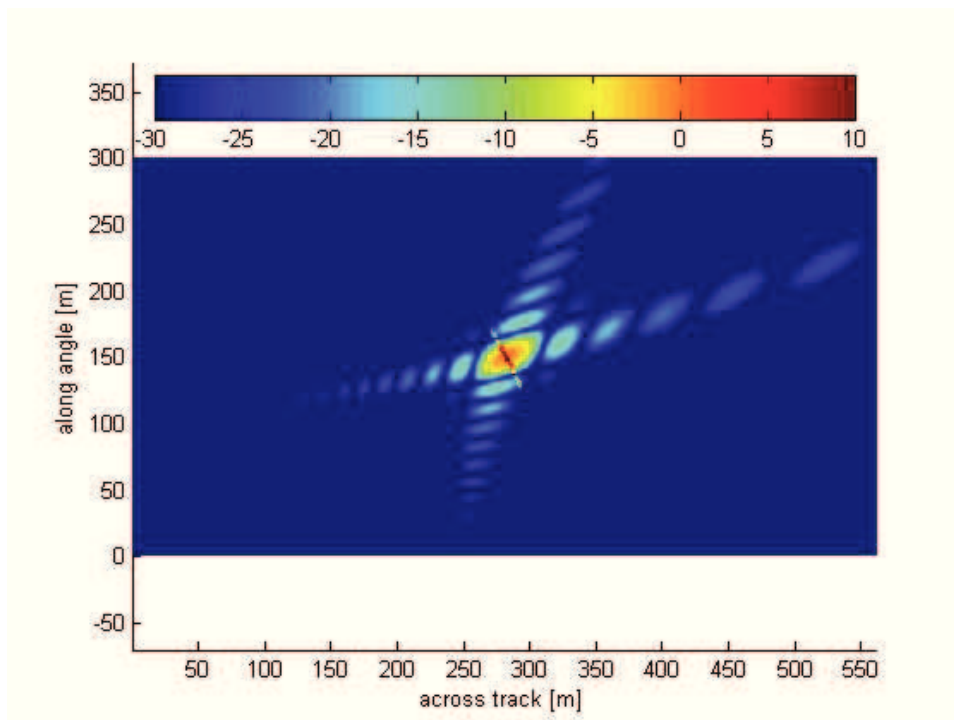


Figure 3.6 – Illustration of insonified surface: the simulation is realized for emission angle of 20° , reception angle of 40° at seafloor of 30m. The pulse width is chosen at 0.3ms for the visibility. The insonified surface corresponding to the sample at beam center is emphasized by increasing 10dB.

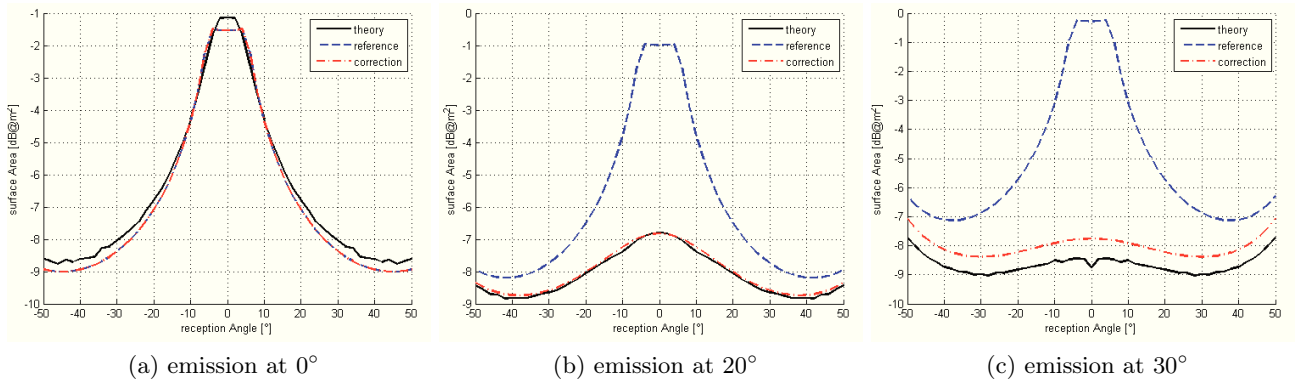


Figure 3.7 – Estimation of surface area insonified from different reception/incident angles with various emission angles (0°, 20°, 30° corresponding to Figure 3.7a, 3.7b, 3.7c). The theoretical area is displayed in black. The literature calculation and its correction are respectively displayed in blue and red lines.

where $dr_{(\cdot)}$ is the resolution on across track (r) and along track (e). In the simulation, the water depth is 30m. Figure 3.7a shows that the formula is well adapted for the across swath in nadir (black line for theoretical value with a pixel resolution of 1cm and blue line for the formula). Figure 3.7b, 3.7c show the results when the emission is tilted forward. A correction is proposed by replacing the reception angle with the incident angle for a better estimation of insonified surface's thickness

$$As_{(c)}^{(3dB)} = \begin{cases} r\theta_e^{(-3dB)} \frac{c\tau}{2 \sin(\theta_i)}, & \text{if } \theta_i > \theta_0 \\ r\theta_e^{(-3dB)} r \left| \tan\left(\theta_i - \frac{\theta_i^{(-3dB)}}{2}\right) - \tan\left(\theta_i + \frac{\theta_i^{(-3dB)}}{2}\right) \right|, & \text{if } \theta_i < \theta_0 \end{cases} \quad (3.32)$$

This correction changes nothing in the case of across-track in nadir, and it fits better in case of frontal across-track (red line in Figure 3.7b, 3.7c). However, this formula is not working with too large emission angle. It could be explained by the fact that the estimation of the length of insonified surface is no more adapted.

We have computed previously the BS value for each sample. This is the high resolution BS value useful for high details imagery analysis. Another important value to compute is the low resolution BS value $BS^{(LR)}$. This is the mean BS value computed for the whole footprint of each beam. This value is computed as

$$BS^{(LR)} = \frac{\sum_{p \in As_b} (TS_p)}{As_b} \quad (3.33)$$

where TS_p is the TS for the resolution cell and As_b is the beam footprint surface.

If the sampling frequency is higher than the resolution cell (which is the case of SEAPIX), the formula above should be corrected by the oversampling factor. This can be done either by downsampling the signal before computing the BS or, as an approximation, by dividing it by the oversampling factor. The $BS^{(LR)}$ is then obtain approximately by

$$BS^{(LR)} = \frac{\sum_{p \in As_b} (TS_p)}{As_b^{(3dB)} f_e \tau} \quad (3.34)$$

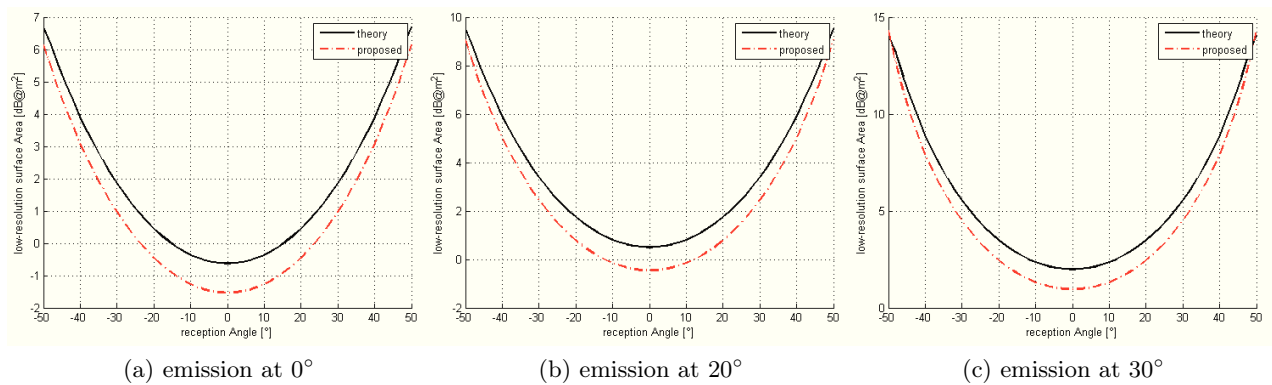


Figure 3.8 – Illustration of low-resolution surface area insonified from different reception/incident angles. The simulation is realized for emission angles at 0° , 20° , 30° at seafloor of 30 m. The theory and proposed estimation are respectively displayed in black and red lines.

where f_e is the sampling frequency

To compute the footprint area, the -3dB boundary of the directivity function is approximate by a polygon. A simulation was done to check the precision of this approximation. The simulation was realized for a water depth of 30m and the results are displayed in Figure 3.8. It shows an error of 1dB in between the theoretical value computed with the exact surface area and the approximate surface area, which is acceptable.

3.3 Backscatter Imagery Processing

In the previous section , we describe how to compute the TS or BS (high or low resolution) signals from the raw signals. In this section , we will explain the methods that are commonly used to build and visualize the backscatter images from the backscatter signals. First, we will apply these methods onto the classical imaging mode, the bathymetry mode. Then we will show results on other insonifications mode available with seapix , the longitudinal mode and the forward looking mode.

3.3.1 Backscatter imaging methods on the classical bathymetry mode

Table 3.2 – Time variable Gain 's parameters applied in different imagery types

Applied Gain	<i>TVG</i>		
Imagery type	side-scan	true-pix	snippet
Initial(%)	1	1	100
Medium(%)	1	1	25
Medium(m)	0	0	5
Final(%)	100	100	60
Gain Factor	3	1	50

Visualizing an image in a waterfall display is a common way in real-time on the operator screen. The waterfall image is build line by line. Each line represents the *TS* or *BS* value in the

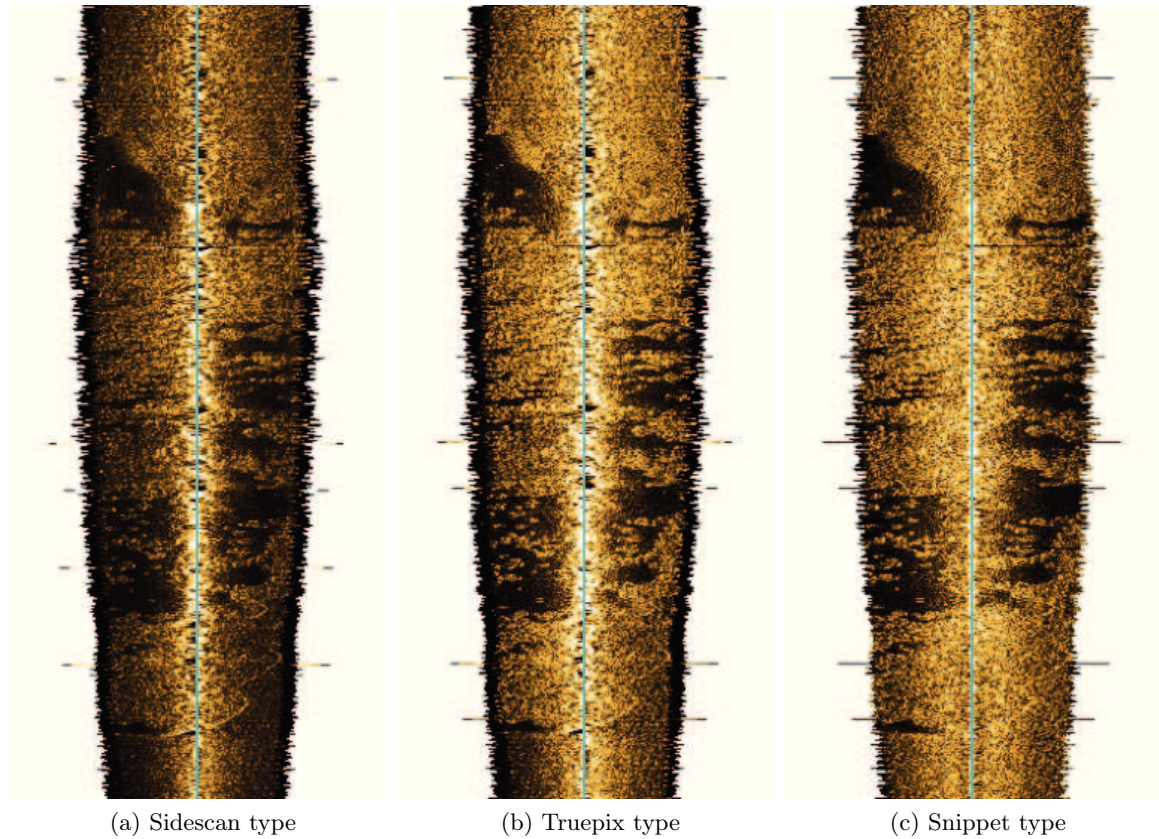


Figure 3.9 – Visualization of different imagery types of an MBES system: sidescan type (Figure 3.9a), truepix type (Figure 3.9b), snippet type (Figure 3.9c).

across-track direction. This swath is computed at a predefined spatial sampling frequency. In a SSS system, for each ping, there are only two time-series signals, one on port side and one on starboard side of the vessel. Each line of the waterfall image is simply the concatenation of these two signals. These signals can be represented as a temporal series: the slant range image, or spatially: the ground range image, which is obtained using a simple geometric projection of the time sample on the ground. In the case of a MBES system, there are multiple-beam signals on each side. In that case, a concatenation of the entire beams signal shall be done to reconstruct a sidescan like swath. There are three main methods that are currently used. Each of these methods will produce a different waterfall image: Sidescan, Truepix and Snippet images [32]. These methods are described in more details in the following paragraphs. This will be illustrated with waterfall images constructed with the SEAPIX data acquired during the acquisition campaign in la Ciotat (France) in December 2015.

Side-scan type In this method, the principle is to mimic the imaging process of a sidescan system. In the reconstructed sidescan (port or starboard), at each instant of time-series signal, the assigned value is the average value of all the samples across the beams (on port or on starboard) taken at this time. Advantages of the method are: simplicity, independence to the detection process, water column image. Disadvantages of the methods are: degradation with multipath and side lobes effects, incidence angle value is lost, no bathymetry correction, no BS value. The visualization of this imagery type is shown in Figure 3.9a.

True-pix type This imagery type was introduced by R2SONIC [33]. The difference with the sidescan reconstruction is that, at each time instant, the maximum of the signal across the beams is taken instead of the average. This maximum value should, in principle, correspond to the seabed echoes (or near the seabed echo). Advantages of the method are: simplicity, independence from the detection process, multipath and side lobe rejections are preserved, directions of arrival and bathymetry value are known. Disadvantages are: sensitivity to noise, objects shadows not preserved. The visualization of this imagery type is shown in Figure 3.9b.

Snippet type In this method, the swath image is reconstructed by the concatenation of each smaller time-series piece extracted from each beam around the seabed detection sample (soundings). Using all the soundings, a bathymetry profile is first constructed on across track. This profile is sampled at a predefined spatial across-track resolution. For each across-track sample, the beam angle is known. The assigned BS value for this sample is extracted from the corresponding beam and time. Advantages of this method are: multipath and side lobe effect rejections preserved, true BS value, incidence angle and bathymetry value are preserved. Disadvantages: sensitive to the detection process. If, for instance, no detection occurs on several beams, the images will be degraded. The visualization of this imagery type is shown in Figure 3.9c.

Waterfall Image Visualization Software has been developed to process and convert SEAPIX raw data into standard XTF file format. The processing module includes all the signal compensation stage described previously to produce calibrated TS/BS samples. Swath processing includes all the three methods (Sidescan, Truepix and Snippet). The sonar data are then imported in the DELPH software as standard sidescan data. The DELPH software is a complete suite of modules [34] developed and commercialized by iXblue to process sonar, seismic and magnetic data. The waterfall images, shown in Figure 3.9, are created using the DelphSonar module. A time variable gain (TVG) is applied to the swath data before being displayed on the screen. The parameters of TVG , defined in DELPH, are summarized in Table 3.2. These configurations aim at rescaling the gray-level of waterfall image for the visualization. At first glance, the waterfall images appear to be very similar except at the nadir where the bathymetry compensation is more visible for the snippet image. Besides, we find that on the first two imagery types (Sidescan and Truepix), the structures appear a bit more clearly on the display. This is somewhat surprising. But in fact, even so the images are better corrected with the snippet processing (which takes into account the bathymetry), small distortions are more visible. In the following study, we will use the snippet image as our reference image for further processing.

3.3.2 Multiswath Backscatter Imaging with Seapix

In Figure 3.10, three waterfall images of SEAPIX data acquired through different insonification modes are compared. These three images have been built with data acquired exactly on the same path (in this insonification scenario, the three modes are successively activated). On the right, the snippet images obtained with the bathymetry mode is represented. In the middle, the emission was tilted 20° forward the vessel. At left, the emission/reception antennas have been switched. When comparing the bathymetry mode and the frontal mode, we found that the frontal mode offers a better view of the seafloor (Figure 3.10b) in the nadir region than the bathymetry mode (Figure 3.10a). In the frontal image, the specular reflection is no more present and a better continuity of the seabed image is obtained. Also, since the incident angles are higher, seafloor structures appear more clearly. In the snippet frontal image, the surface normalization is not yet applied. This functionality will be included in future release of the processing software. On the

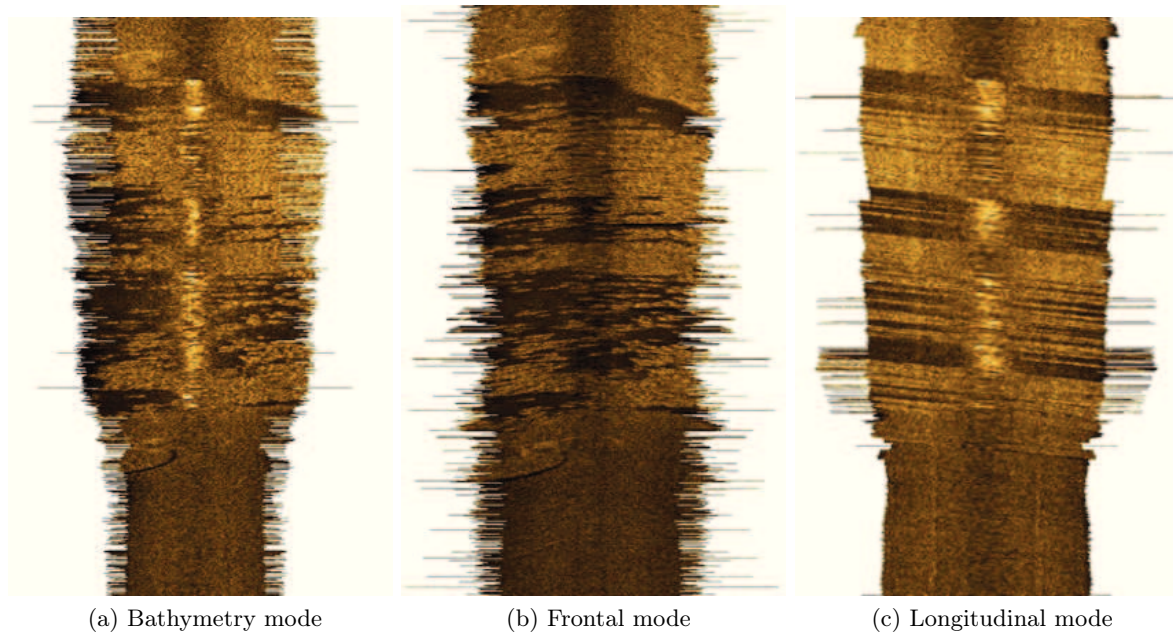


Figure 3.10 – Waterfall images of SEAPIX data acquired using different insonification modes: bathymetry mode (Figure 3.10a), frontal mode (Figure 3.10b), longitudinal mode (Figure 3.10c).

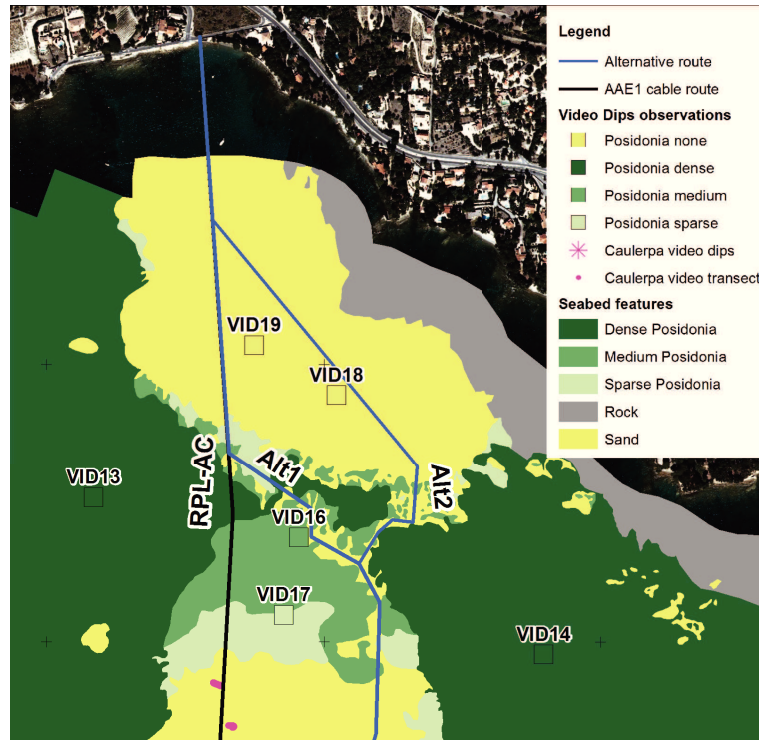
right, the waterfall image is built from the longitudinal mode. In this configuration, the insonified swath is aligned on the vessel trajectory. As the vessel is moving forward, the system will record the full *BS* profile response for each pixel under the vessel trajectory. The *BS* profile appears as oblique line in the display image. The angle is directly proportional to the vessel speed. As it will be discussed in more details later, the different types of seabed are clearly distinguishable.

3.4 Acquisition campaign

An acquisition campaign was organized in December 2015, in La Ciotat Bay in France. This dataset will serve as the reference dataset for the evaluation of the system performances and classification algorithms.

3.4.1 Selection of the reference area

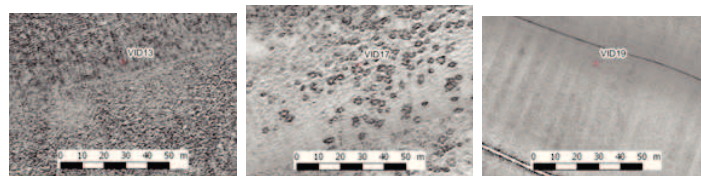
The bay of la Ciotat is located in the suburb of Toulon at the South of France, and is known for the maritime industry since 15th century. This zone is not only studied for scientific tests for acoustic systems, but is also familiar with fishermen. From some previous works, a precise classification map of this zone (Figure 3.11) is available. The area was surveyed with standard sidescan and multibeam sonar systems. Video and ground truth data were also collected by diver at some observations points which were precisely georeferenced. By correlating the ground truth data and the sonar images textures, geophysicists have manually constructed the sediment map of all the area. In this zone, we found mostly three main type of sediments: posidonia, rock and sand. The posidonia was further divided into three different classes depending on the posidonia density per m^2 . The sand is also different between the near-port region (normal sand) and the farther region (caulerpa sand). Besides, we found also a zone of sand ripples in the near-port zone (at video 18).



(a) Ground Truth



(b) Dense Posidonia (c) Sparse Posidonia (d) Sand



(e) Dense Posidonia (f) Sparse Posidonia (g) Sand

Figure 3.11 – Ground truth in the bay of la Ciotat, France: this zone briefly consists of the posidonias (dense: green, medium: dark green, sparse: light cyan) and the sands.

3.4.2 Survey parameters and dataset

Survey planning: An acquisition was planned in September 2015 knowing the classification map. 17 parallel lines path were defined to cover homogeneous regions of sediments for classification training and analysis, heterogeneous regions for the classification tests and also some ground truth observations points. To minimize the influence of depth variation onto the calibration, the survey lines were oriented from north-west to south-east following the seabed slope. Before starting the acquisition, the gain level was adjusted. Theinsonification scenario was defined to acquire alternatively three different types of swath: across-track swath (bathymetry mode), tilted forward across-track swath (frontal mode) and along-track swath (longitudinal mode). These swaths covered then exactly the same seafloor region. Besides, we also recorded data in a static mode. In this mode, the vessel was stationary and the system scanned the seafloor by pointing the frontal swath in different emission angles. This mode was applied on a homogeneous region. The idea was to study the influence of the emission and reception angles onto the BS values from the same type of sediment.

Table 3.3 – System specification during the campaign in la Ciotat in December 2015

Characteristics	Values	Units
Vessel speed	1.5	(m s^{-1})
recording length	200	(ms)
Dynamic Coef. (11 first lines)	0.5	(.)
Dynamic Coef. (6 last lines)	0.3	(.)

Besides the above predefined details, some other specifications of the acquisition can be found in Table 3.3. These choices were decided for the following reasons:

- A recording length of 200ms corresponds to a slant of about 150 m. This would guaranty to acquire the entire seafloor signal up to depth of 75m. In fact, the maximum depth in the survey area is 30m.
- The vessel speed was fixed to 1.5 m s^{-1} . It is a compromise between vessel stability and the slowest possible speed to ensure the best along-track sampling. With 200ms ping rate and with three different modes, the ping rate for each mode is 600 ms. This gives a ping every 0.9m in along track which corresponds to the along-track resolution given by the beam azimuth width (1.6°) at 30m depth.
- The across track distance between two parallel lines was chosen in order to have a swath overlap of 50%. The mean distance was set to 50m.
- The dynamic gain of the system during the acquisition (via C) was adjusted to avoid the saturation of the signals. More precisely, this coefficient was set to $C = 0.5$ for 11 first lines far from the coast, and to $C = 0.3$ for 6 last lines which were near to the coast.

Bathymetry and backscatter maps of the full dataset: The bathymetry map and the backscatter map of all the survey area are respectively shown in Figure 3.12 and 3.13. The detection soundings have been computed in realtime by an onboard system. The BS snippet signals have been computed according to the algorithms described previously. The georeferencing and interpolation of the bathymetry and the BS data have been done using the DELPH software. In the bathymetry map, we observe a variation in water depth from the coast (about 10 m) to

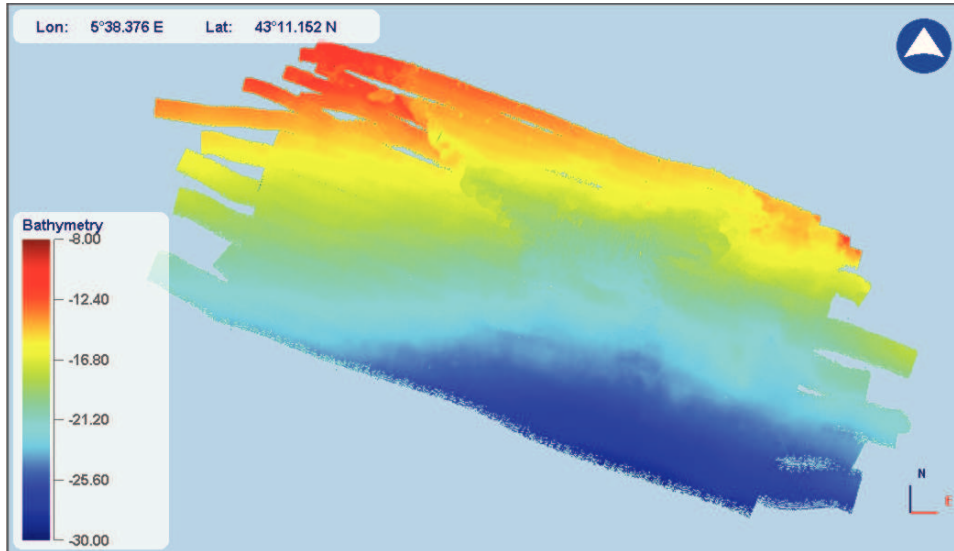


Figure 3.12 – Bathymetry map measured in the bay of la Ciotat, France.

the Mediterranean sea (30 m). A bias is observed in the slope of about 1° in across track and 0.5° in along track. Unfortunately, these bias are not compensated in our post-processing. The backscatter mosaic is built at 0.1m resolution .

Table 3.4 – Specifications of gain compensation for backscatter mapping in Figure 3.13

Imagery type	Snippet	
Applied Gain	<i>TVG</i>	
Acquisition Lines	1 – 11	12 – 17
SEAPIXtoXTF(dB)	28.5	17.1
Initial(%)	100	15
Medium(%)	20	10
Medium(m)	5	10
Final(%)	100	100
Gain Factor	40	150

Selection of reference region for analysis: Among the ground truth regions where video images were acquired, we have selected three regions, one for each type of sediment: dense posidonia, sparse posidonia and sand. The region’s size is decided following the homogeneity and the boundary on the survey area.

- Dense posidonia: 200×200 [m] at (43.181851309972529° North, 5.648129187018885° East).
- Sparse posidonia: 100×100 [m] (43.180111129972296° North, 5.651970018019026° East).
- Dense posidonia: 150×200 [m] (43.184112519972324° North, 5.651365781018998° East).

The data recorded on the reference region will first be used for evaluating the system consistency (Chapter 4). They will be used to study the statistical properties of *BS* distribution for each class and the similarity measure in between class. Then, the different feature extraction algorithms

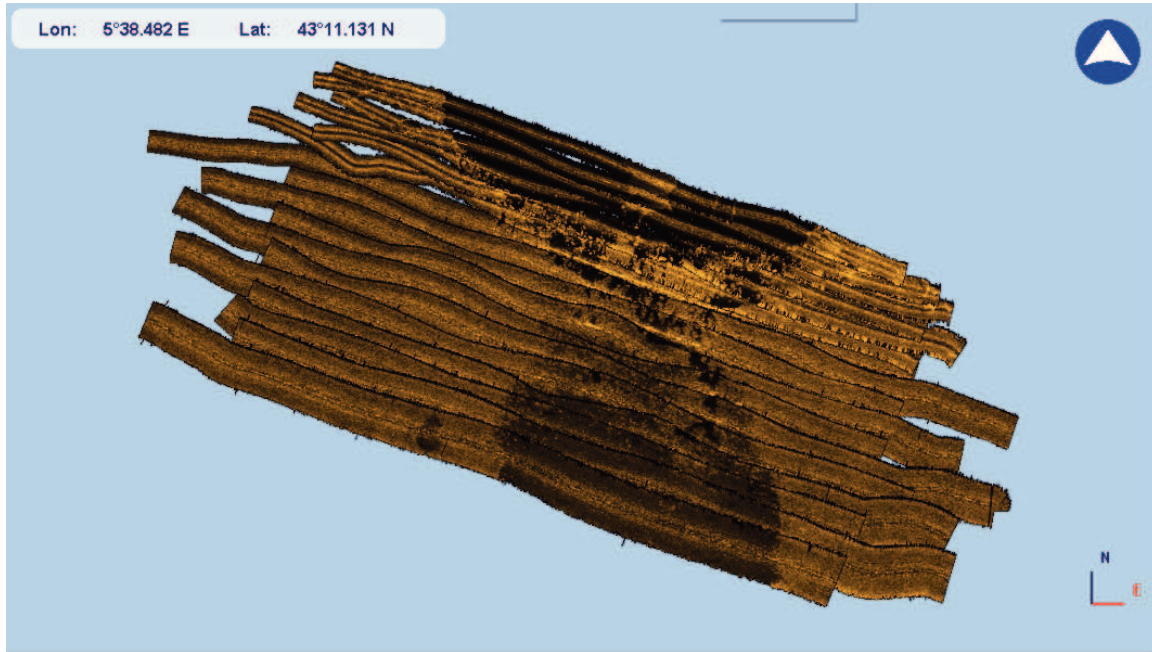


Figure 3.13 – Snippet-type visualization of the bay of la Ciotat (France): This visualization is based on the backscattering strength information extracted from the acquisition in December 2015.

will also be tested on this dataset in order to obtain the most discriminant ones (Chapter 7). Finally, these data will be used as the training base to classify the whole survey area.

3.5 Data collection for seafloor classification

The backscatter data are visualized in Figure 3.13. In the classification methods that we propose, the features for classification will not be extracted on the georeferenced backscatter mosaic image. Instead, the features are computed with all the data samples that belong to a region around each georeferenced pixel. The region size is defined by a radius that shall be computed according to the acquisition geometry. So for each pixel in the output map, at a preprocessing step, these following data are associated:

- Pixel position in 3D (center of the region) and radius
- Number of samples data collected in the regions
- Incidence angle and backscattering strength value for all of the samples data inside the region.

3.5.1 Data collection for the bathymetry mode

For the bathymetry mode, the radius of the region is roughly defined by the accuracy of the navigation and attitude data. The attitude accuracy is of the order of 0.5° or better in roll/pitch/heading. This has to be compared to the beam aperture width which is at best $1.6^\circ \times 1.6^\circ$. The navigation position accuracy is of the order of 1m. So we have considered that the uncertainty of the samples position is governed by the beam footprint size. We have fixed it to 2m. At 10kHz bandwidth with

a pinging rate of 600ms and at speed of 3 knots, the minimum number of independent samples data inside a 2m region is of the order of 100. In the dataset, the survey lines are almost parallel and the overlap ratio in between two lines is about 0.5. This means that a pixel is insonified with maximum two survey lines. For each pixel region, the angular distribution (via incident angle) will then be concentrating around two main values.

3.5.2 Data collection for the longitudinal mode

Longitudinal data refers to the data acquired from the longitudinal mode, which insonifies the along-track swath. As a result, each seafloor pixel, on the vessel trajectory, is insonified multiple times but from different incident angles. The distribution of incidence angle will spread all over the $[-60^\circ, +60^\circ]$ aperture in that case. For 30m water depth, the insonified swath is about 100m for $\pm 60^\circ$ reception aperture. At 3 knots, with 600ms pinging rate, each pixel will be insonified 100 times and the total duration of insonification is 60s. The variability of the position of the insonified pixel is directly related to heading variation during the insonification time. Assuming a 5-degree maximum heading variation during the time of insonification, the region size should be at least 5m. This value has been used to collect the data around each seafloor pixel for longitudinal mode.

3.6 Conclusion

In this section, we have presented the full processing chain to compute the backscattering strength value from the raw data and have shown first results on waterfall image of backscatter data for the three different swaths. We have, then, presented the survey campaign and the full dataset acquired with the MS-MBES using the three modes. Finally, we have explained how the samples data are collected around each pixel for later analysis and processing steps.

SEAPIX backscatter data analysis

In the previous chapters, we have presented the multi-swath multi-beam echo sounder (MS-MBES) system SEAPIX (Chapter 2), as well as its backscatter data processing (Chapter 3). In this chapter, a statistical analysis is dealt on the data acquired in December 2015 in la Ciotat (France), which was presented in Section 3.4.2. This zone composed of homogeneous regions of different types of seafloor: dense posidonia (DP), sparse posidonia (SP) and sand (S). The first analysis aims at characterizing data statistical distributions according to the incidence angles for each mode taken separately. The goodness-of-fit (GOF) of the data to classical BS statistical models is evaluated via the Kolmogorov- Smirnov test [35, 36]. The angular dependence of fitted distribution parameters is also considered to assess their discrimination capacity as a prelude for seafloor classification. The second analysis concerns the intermode (bathymetry and longitudinal) statistical comparison to evaluate the inter-mode consistency.

4.1 Statistical analysis for SEAPIX operating modes

Statistical distributions of MBES data have been widely studied and used in a classification context [3, 4, 27]. In this section, we look for a distribution to model our data. We will evaluate the classical models proposed in literature. Due to the angular dependence of backscattering strength (BS) [2, 4, 24], we study the angular distribution of data, which describes the distribution variation according to its incident angle. Therefore, the data are sorted into 51 angular sectors which are equally distributed from -50° to 50° (corresponding to the longitudinal mode's angle range in Section 3.5.2). Each angular sector range is 2° corresponding to the system beam's aperture.

In literature, different probability density functions have been proposed to model the BS distribution in linear scale (amplitude) such as: Rayleigh, Gamma [25], log-normal [28], Weibull [26], K [3, 27]. In logarithmic scale (dB), several studies proposed to model the BS distribution with

Table 4.1 – Proposed distribution of backscattering strength in literature.

Name	Density function	Parameters	Support
Rayleigh	$\frac{x \exp\left(-\frac{x^2}{2\sigma^2}\right)}{\sigma^2}$	σ	$[0, +\text{inf}[$
Gamma	$\frac{\beta^\alpha}{\Gamma(\alpha)} x^{\alpha-1} e^{-\beta x}$	α, β	$[0, +\text{inf}[$
Log-normal	$\frac{1}{x\sigma\sqrt{2\pi}} e^{-\frac{(\ln x - \mu)^2}{2\sigma^2}}$	μ, σ	$[0, +\text{inf}[$
Weibull	$\frac{k}{\lambda} \left(\frac{x}{\lambda}\right)^{k-1} e^{-(x/\lambda)^k}$	k, λ	$[0, +\text{inf}[$
K	$\frac{2}{\Gamma(L)x} \left(\frac{L\nu x}{\mu}\right)^{\left(\frac{L+\nu}{2}\right)} \frac{1}{\Gamma(\nu)} \mathbf{K}_{\nu-L} \left(2\sqrt{\left(\frac{L\nu x}{\mu}\right)}\right)$	L, μ, ν	$[0, +\text{inf}[$
Gaussian mixture	$\sum_{i=1}^K w_i \mathcal{N}(\mu_i, \sigma_i)$	$\{w_i, \mu_i, \sigma_i\}, i = 1..K$	$] - \text{inf}, +\text{inf}[$

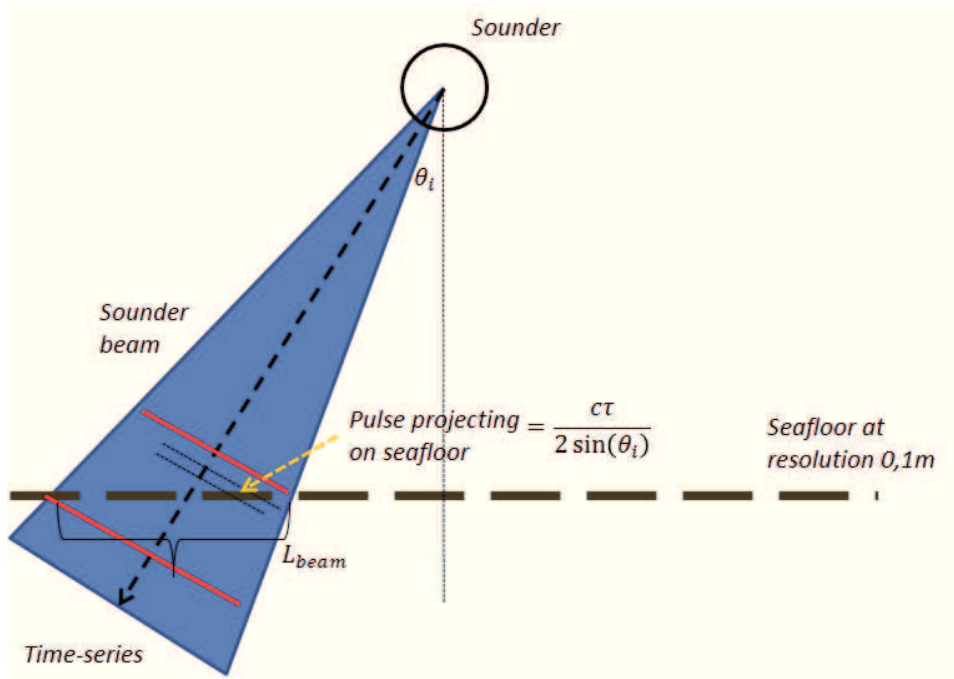


Figure 4.1 – Illustration of the estimation L parameter (K-distribution) on across-track.

a distribution of Gaussian mixture (GM) [6, 37]. The description of these distributions is expressed in Table 4.1. In this section, we carry out the data distribution analysis on both scales. In the linear scale, the distribution parameters can be related to physical characteristics of the seafloor [22]. In the logarithmic scale, we are looking for a robust distribution model for the classification stage.

All the proposed distributions have been fitted using the statistics and machine learning toolbox in MATLAB. The K-distribution estimator, however, is not available in the toolbox, so we use the ones recommended by Redding in [38]. Recalling that the K-distribution also demands an input parameter L signifying the number of times that a pixel is insonified. We present, in the following, our estimation for this parameter L , which is related to two axes: along-track and across-track.

Along-track: In the acquisition campaign 3.4.2, the distance between 2 successive pings was around 1m while the swath average width was around 2m. It means that there is a spatial superposition in between 3 successive swaths:

$$L_{along} = 3 \quad (4.1)$$

Across-track: The estimation on this track is illustrated in Figure 4.1. The acquired dataset was defined with the resolution 0.1m on this track. However, the number of information in the beams varies according to incident angles θ_i .

Denoting $L_{beam}(\theta_i)$ the length of footprint at the incident angle θ_i on this track, the number of independent information at this incident angle is an integer value

$$N_i(\theta_i) = \frac{L_{beam}(\theta_i)}{L_{resolution}(\theta_i)} = \frac{L_{beam}(\theta_i) \sin(\theta_i)}{c\tau/2} \quad (4.2)$$

where

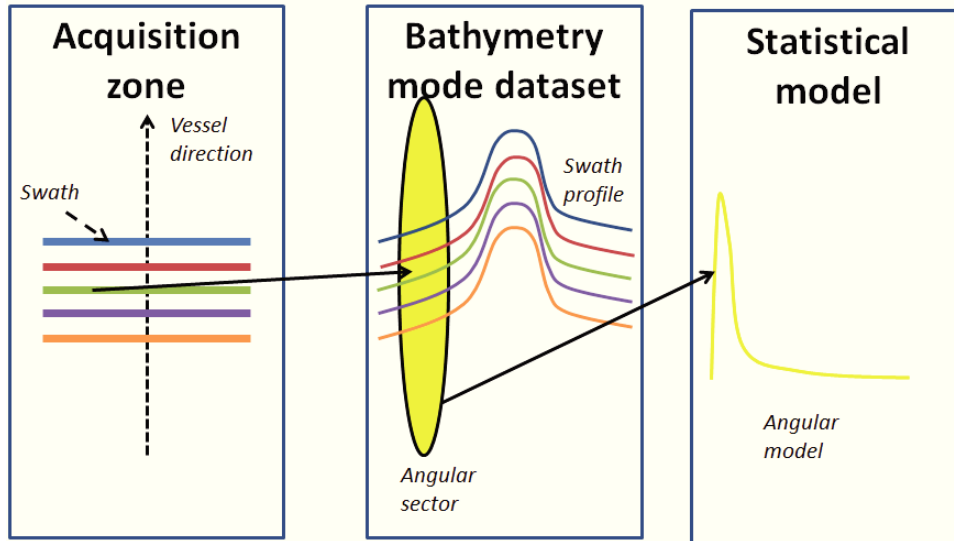


Figure 4.2 – Visualization of the distribution analysis process on the bathymetry mode.

- c : sound celerity in water environment (1500m s^{-1}).
- τ : pulse width of SEAPIX system (0.1ms).

On the other hand, the number of data samples in this beam is $Ns(\theta_i) = L_{beam}(\theta_i)/0.1$. As a result, we have

$$L_{across}(\theta_i) = \frac{Ns(\theta_i)}{Ni(\theta_i)} \quad (4.3)$$

We determine the value of parameter L as the combination between the along-track and across-track:

$$L(\theta_i) = L_{along} \cdot L_{across}(\theta_i) = 3 \cdot \frac{Ns(\theta_i)}{Np(\theta_i)} \quad (4.4)$$

The GM distribution also requires a parameter N corresponding to the number of Gaussians. In this study, we limit this number N in the interval $[1, 10]$, and select the value which provides the best Bayesian Information Criterion (BIC) [39].

We assess the goodness-of-fit via the Kolmogorov-Smirnov test [35, 36] applied to each previously mentioned model. This test gives a value (p -value) in the interval $[0, 1]$ expressing the probability of rejecting the proposed distribution hypothesis. The interpretation of this p -value is:

- p -value < 1 : proposed model validates the GOF test.
- p -value $= 1$: proposed model is not suitable for our data.

The two following sections report GOF results and analysis for both bathymetry and longitudinal modes.

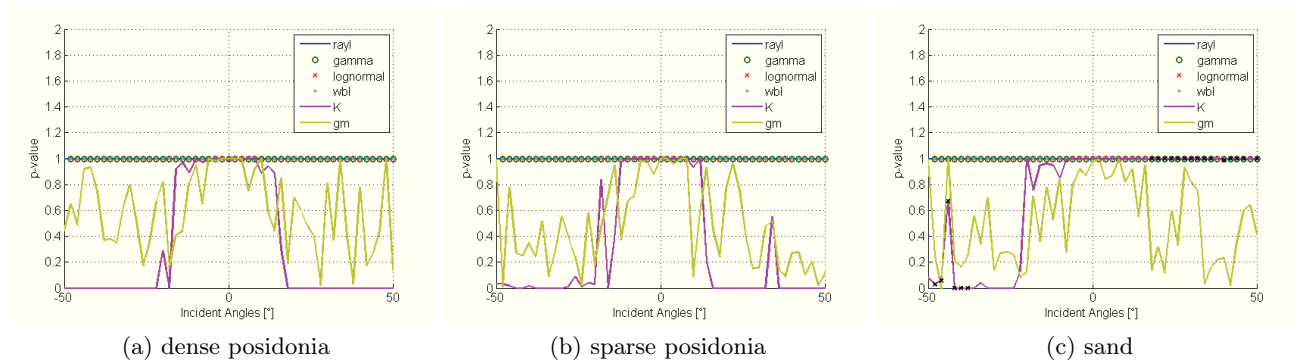


Figure 4.3 – Visualization of the goodness-of-fit for data in the bathymetry mode. The distribution evaluation is displayed via p -value estimated from different angular sectors in $[-50^\circ, 50^\circ]$. The considered distributions compose of Rayleigh (blue -), Gamma (green o), Log-normal (red \times), Weibull (cyan .), K (violet -) and Gaussian Mixture (yellow -). Results are reported for three seafloors: posidonias (dense - Figure 4.3a and sparse - Figure 4.3b), sand (Figure 4.3c).

4.1.1 Bathymetry mode distribution analysis

We first introduce the data collection strategy for the distribution analysis of this mode in Figure 4.2. Beginning at the acquisition zone, acquired data are the BS profile measured on the whole across-track swath. For an angular sector (yellow region), the data is accumulated on different swaths. This angular dataset contains the samples, in the acquired data, that were insonified in the incident angle range of the angular sector.

This section consists of two main tasks on the angular dataset:

1. Determination of the data distribution for this mode via a GOF test.
2. Extracting and comparing the fitted distribution parameters to the references in literature.

We report in Figure 4.3 the GOF (whose degree is expressed by the p -value) of the proposed distributions to the bathymetry mode's data in the different angular sectors. The visualization of the proposed models is displayed in Figure 4.4 on two angular sectors (high incident angle 50° and nadir angle 6°) on our considered seafloors (DP, SP, S). The result shows that:

- In linear scale, K-distribution is the best model for our data (violet line). However, this model doesn't fit well in the nadir zone ($\approx 20^\circ$ – radius in nadir).
- In logarithmic scale, GM offers a good GOF (yellow line).

But we observed some artifacts in linear scale that we will try to explain by the following arguments:

- In the nadir angles, we have mostly one unique independent information $N_i = 1$. The parameter L (K-distribution) becomes $L = 3 \cdot \frac{L_{beam}}{0.1} \approx 24$ for 30m depth, which is too large. This makes K-distribution model unsuitable in the nadir.
- In some angular sectors, the K-distribution estimator doesn't work with the estimated parameter L . We, therefore, tunes this parameter in $[1, 10]$ to obtain K-form distribution model. We display these results, on the GOF curve for the K distribution, with the black cross " \times ". This phenomenon principally happens in the sand region, and on the vessel's

4.1. Statistical analysis for SEAPIX operating modes

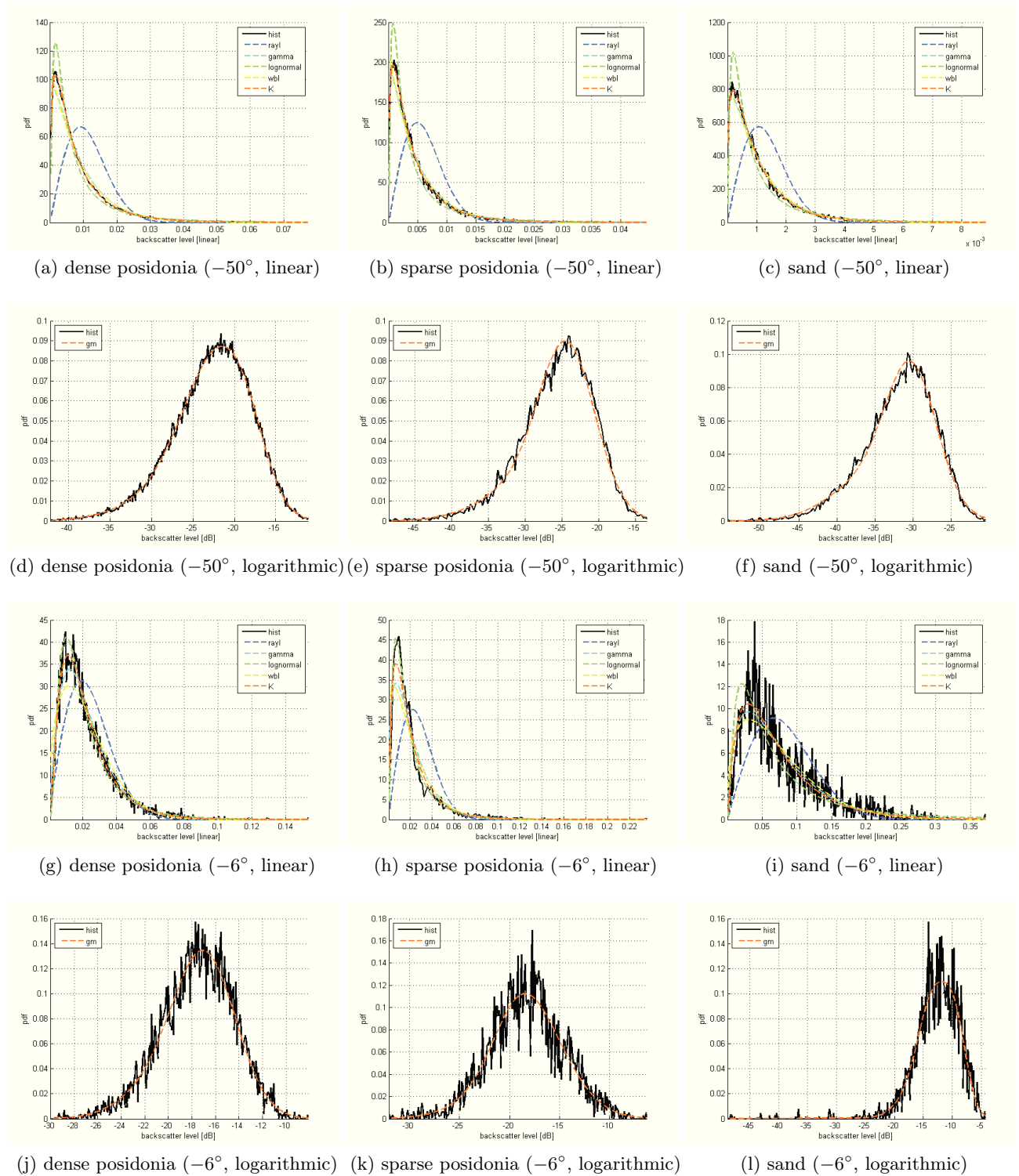


Figure 4.4 – Visualization of distribution fitting process on the data of 2 angular sectors: incident angle 50° and 6° . The proposed distributions are Rayleigh (blue), Gamma (cyan), Log-normal (green), Weibull (yellow), K (orange) in linear scale, and Gaussian Mixture (orange) in logarithmic scale. They are compared to the empirical distribution, which is the normalized histogram (black). The fitting process is done for different types of seafloors (dense posidonia, sparse posidonia and sand).

port side. We recall that the 12-bit ADC supports the *BS* about -53dB in our case. It, therefore, influences the most on the sand region where the *BS* was pretty weak (less than -30dB in average - Figure 4.5b).

We, next, investigate the angular dependence of the parameters extracted from these two distributions in linear and logarithmic scale. Since the GM is composed of a set of Gaussian components defined with two components (Table 4.1), the displayed parameters $\mu_{\text{dB}}, \sigma_{\text{dB}}$ are a linear combination of those components.

$$\mu_{\text{dB}} = \sum_{i=1}^K w_i \mu_{G(i)} \quad (4.5)$$

$$\sigma_{\text{dB}} = \sum_{i=1}^K w_i \sigma_{G(i)} \quad (4.6)$$

They correspond to the *BS* average and variance in the logarithmic scale. Moreover, we also display, in the logarithmic scale (Figure 4.5b), the reference *BS* profile of some typical sediments at frequency of 100kHz [20].

- Figure 4.5a (resp. 4.5b) display the evolution of the parameter μ (K-distribution) (resp. μ_{dB} (GM)) according to the incident angles in linear scale (resp. logarithmic scale). This angular evolution is realized on different types of seafloor (blue - DP, green - SP, red - S), and it characterizes well the *BS* profile of these seafloors.
 - In logarithmic scale (Figure 4.5b), we find the similar *BS* level of the sand in acquisition zone to those referenced in literature. Even though SEAPIX system operates at a different frequency of 150kHz , it still gives a good system consistency in acquiring the *BS* data.
 - The form of these *BS* profiles expresses some reasonable characteristics of the considered seafloors:
 - * *BS* sand curve is characterized by a strong backscatter level in low incident angles (nadir). The backscatter level decreases slowly when the incidence angles increases. This curve may be interpreted as moderately hard and rough sediment.
 - * The posidonia curves shows a small angular dependence, where *BS* level is mostly not affected by the angular angle. This angular behavior is generally associated with a rough interface. The fact that the *BS* level is lower than for the sand in nadir, and stronger in high incident angles maybe due to the attenuation of this sea-grass living in the sand.
- Figure 4.5c (resp. 4.5d), display the parameters L (resp. N) in linear (resp. logarithmic) scale. Due to the calculation complexity, these parameters are studied only in the interval $[1 \ 10]$. We found a small coherence between these parameters where both L, N are approximate to 3 in high incident angles. This is interesting because L represents the number of times a pixel was insonified while N could be understood as the number independent information sources in the data. We remind that K-distribution was not really adapted in the sand region and L was regulated to have a K-form distribution.

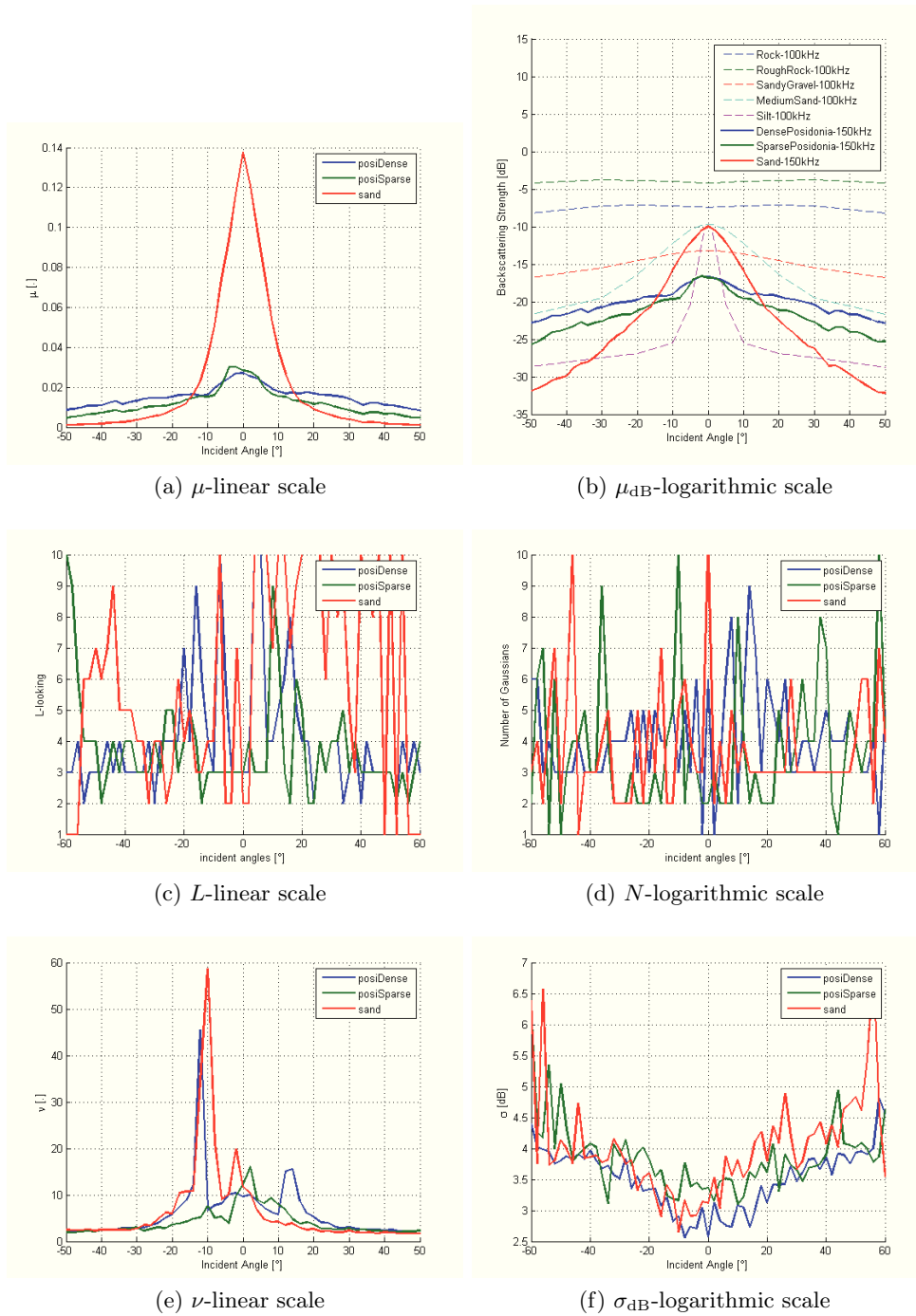


Figure 4.5 – Evolution of distribution parameters estimated in bathymetry mode as a function of incident angles in three-class case-study (dense posidonia - blue, sparse posidonia - green, sand - red). The distribution is the K-distribution for linear scale data and GM for logarithmic scales. Figure 4.5a, 4.5c, 4.5e shows the development of μ , L , ν (K-distribution) while the Figure 4.5b, 4.5d, 4.5f displays the evolution of μ_{dB} , N , σ_{dB} (GM-distribution).

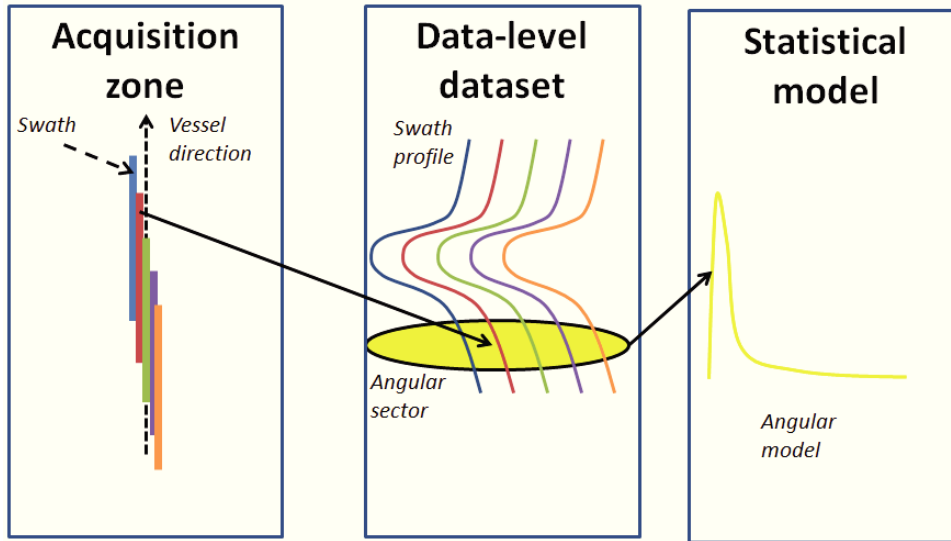


Figure 4.6 – Visualization of the distribution analysis process of the data-level dataset on longitudinal mode.

- Figure 4.5e and 4.5f) present the second-order parameters ν (K-distribution) and σ_{dB} (GM). We observe a small shifting of these curves, which can be explained by the fact that we do not take into account the seafloor slope in our BS computation. (Section 3.4.2). These figures also show an equivalent level of these parameters between the considered types of seafloor. These parameters, therefore, shouldn't be good characteristics for the discrimination of these types of seafloor.

4.1.2 Longitudinal mode distribution analysis

In this section, we will analyze the data in two different manners: data-level and pixel-level. On the one hand, we use the data-level dataset to investigate the consistency of the acquisition system SEAPIX. On the other hand, we demonstrate the advantage of this operating mode via pixel-level dataset. Consequently, the distribution analysis applied on these datasets is also composed of the following steps:

- Determination of the data distribution for these dataset via GOF test.
- Extracting and comparing the fitted distribution parameters to the references.

4.1.2.1 Data-level distribution analysis

As previous section, we first present the data collection process for the data-level dataset in Figure 4.6. We organize the acquired data in this mode in the same manner as in the bathymetry mode. It means that each acquisition swath is used to produce a BS profile, and the data-level dataset is an ensemble of these profiles. For each angular sector, the data is accumulated on different swaths. This angular data-level dataset contains the samples which were insonified in the incident angle range of the angular sector. As a result, the coherence of the data-level dataset and the bathymetry mode dataset will indicate the system consistency in acquiring the BS data.

Next, we report the GOF test of the proposed distribution models on the data-level dataset. Figure 4.7 shows similar results than for the bathymetry mode's: the K-distribution best fits in linear

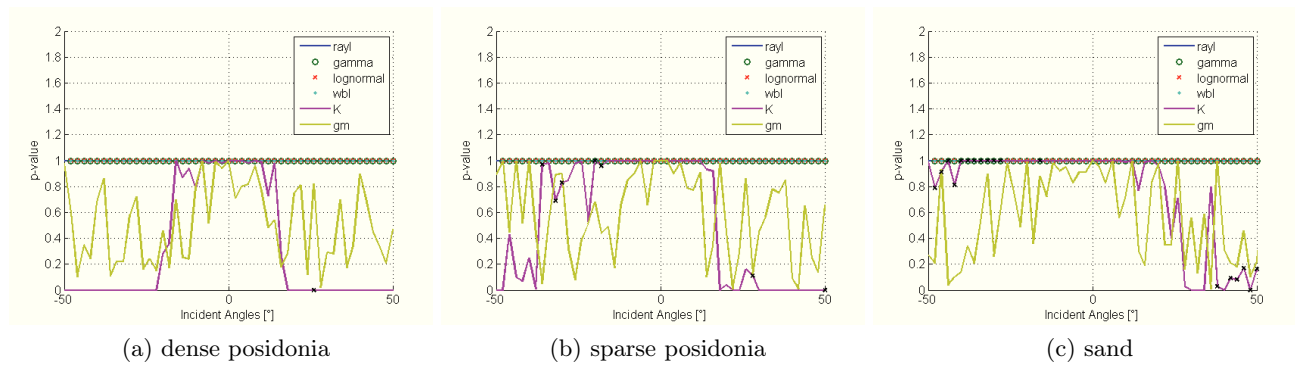


Figure 4.7 – Visualization of distribution fitting for data-level dataset of the longitudinal mode. The distribution evaluation is displayed via p-value estimated from different angular sectors in $[-50^\circ, 50^\circ]$. The considered distributions are Rayleigh (blue -), Gamma (green o), Log-normal (red \times), Weibull (cyan \cdot), K (violet -) and Gaussian Mixture (yellow -). The fitting process is done for the three different seafloor types: posidonias (dense - Figure 4.3a and sparse - Figure 4.3b), sand (Figure 4.3c).

scale and GM in logarithmic scale. We have also the same difficulties in fitting the nadir’s angular sectors (less than 20°) in linear scale, and the fitting doesn’t work well on the sand seafloor. We exploit the same strategies of tuning the parameter L (K-distribution) to represent the data via a K-form distribution in linear scale.

Figure 4.8 shows the evolution of the fitted distributions’ parameters. We observe the same angular behavior according to the seafloor type as in the bathymetry mode.

- The angular dependence of the first order parameter (resp. μ , μ_{dB}) and second order ones (resp. ν , σ_{dB}) of the fitting distributions (resp. K-distribution, GM) in linear and logarithmic scale. This dependence varies according to the insonified seafloors for the first order parameter while the second order ones doesn’t. The BS profile (expressed via first order parameter) is spikier in the hard sediments as sand while mostly absorbed in the posidonias.
- The BS in logarithmic scale (expressed via μ_{dB}) shows a good consistency to the backscattering profile recorded in the state-of-the-art [20].

4.1.2.2 Pixel-level dataset distribution analysis

Figure 4.9 presents the data collection process for this pixel-level dataset. In this process, we exploit the fact that a seafloor pixel, in vessel trajectory, is insonified multiple times under a large range of incident angles. This process is realized through the following steps:

1. Pixel-level dataset collection: Representing a seafloor pixel with a BS profile.
 - (a) Accumulating pixel’s data from different swaths.
 - (b) Sorting these data into the angular sector according to their incident angle.
 - (c) Representing each angular sector by the BS average from the angular data.
2. Assuming an homogeneous seafloor type, accumulating average values on successive seafloor pixels for each angular sector.

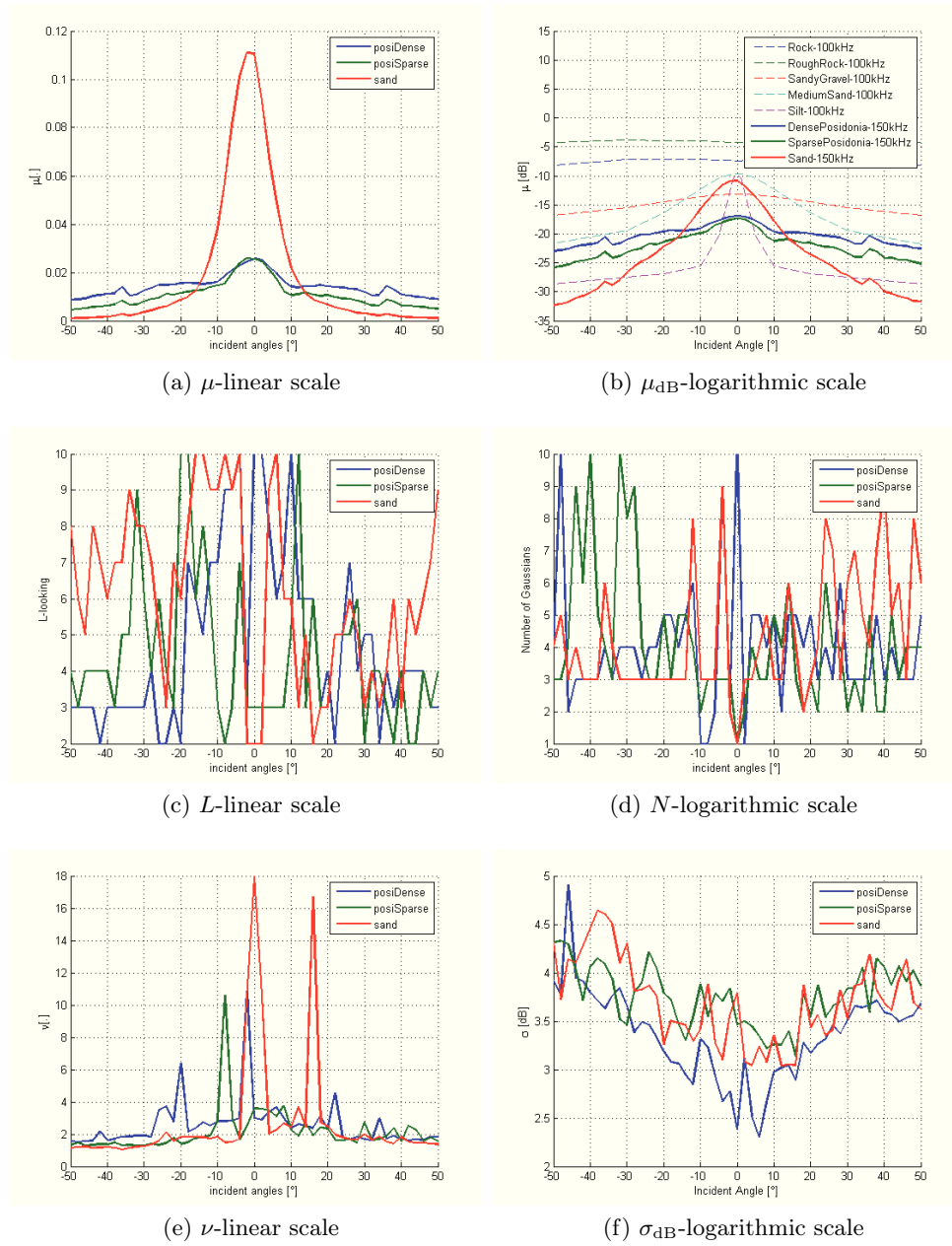


Figure 4.8 – Evolution of distribution parameters estimated in data-level dataset of the longitudinal mode as a function of incident angles in the three-class case-study (Figure 4.5). The distributions compose of K-distribution and GM to describe the acquisition data in linear and respectively logarithmic scales. Figure 4.8a, 4.8c, 4.8e shows the development of μ , L , ν (K-distribution) while the Figure 4.8b, 4.8d, 4.8f displays the evolution of μ_{dB} , N , σ_{dB} (GM-distribution).

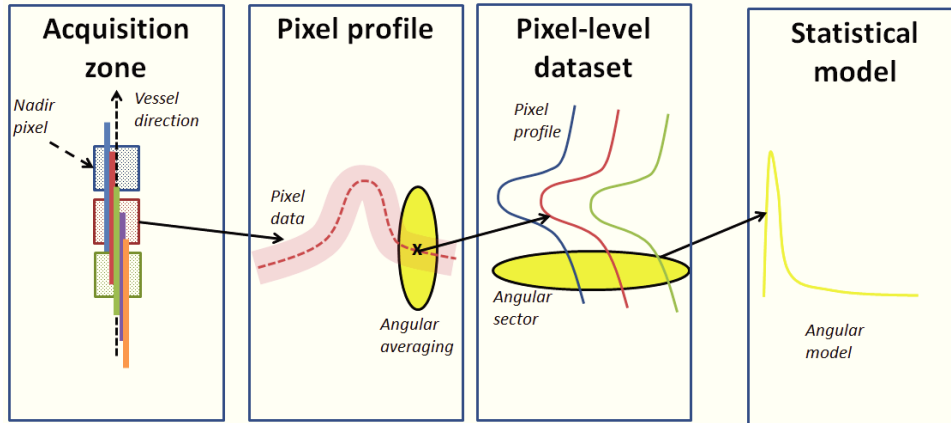


Figure 4.9 – Visualization of the distribution analysis process of the pixel-level dataset on longitudinal mode.

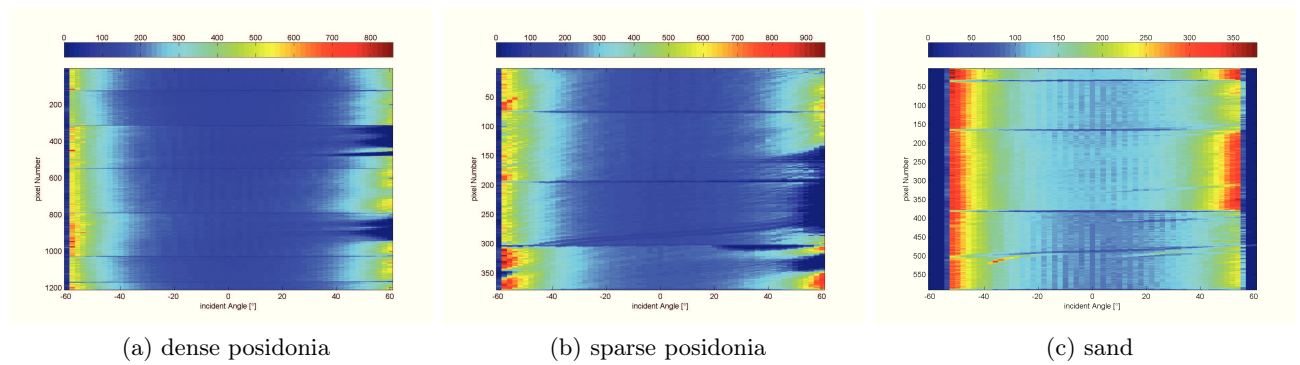


Figure 4.10 – Visualization of pixel’s sample number in angular sectors , which is used to generate the backscatter profile. This information is extracted for the three considered classes (dense posidonia - Figure 4.10a, sparse posidonia - Figure 4.10b, sand - Figure 4.10c).

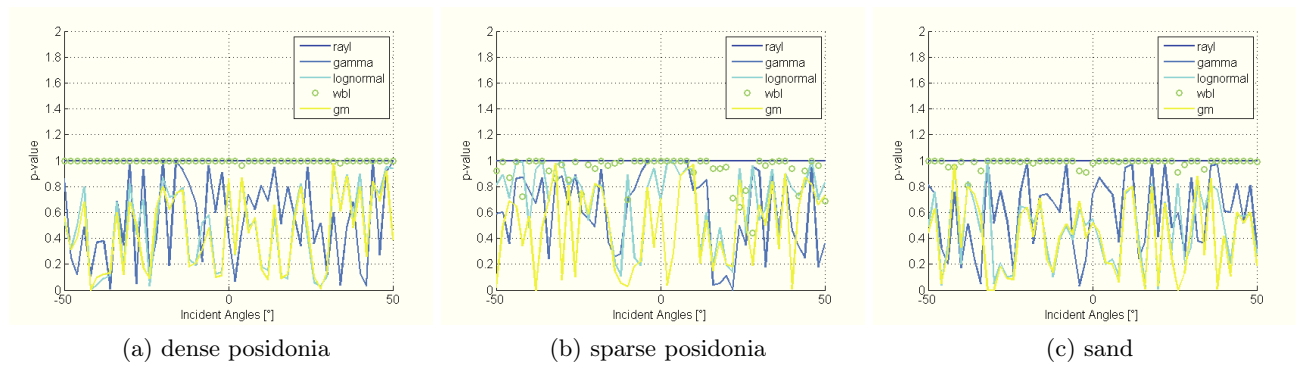


Figure 4.11 – Visualization of distribution fitting for pixel-based data in the longitudinal mode. The distribution evaluation is displayed via p-value estimated from different angular sectors in $[-50^\circ, 50^\circ]$. The considered distributions compose of Rayleigh (blue -), Gamma (light blue -), Log-normal (cyan -), Weibull (green o), and Gaussian Mixture (yellow -). The fitting process is separately realized for the seafloors: posidonias (dense - Figure 4.11a and sparse - Figure 4.11b), sand (Figure 4.11c).

We report, in Figure 4.10, pixel’s number of samples in each angular sector. This number is mostly constant in the same angular sector, and it varies to the incident angle (the number of samples was greater in high incident angles). It is reasonable because the bathymetry didn’t vary a lot inside the analysis region. It means the pixel’s representing value is equivalent in the same angular sector in the term of statistical analysis. Next, we observe a lack of samples in some high incident angles, especially outside the incident angle range of -50° to 50° . It is caused by the yaw variation during acquisition, which made some samples drop outside the vessel trajectory. This confirms again the choice of considered angular range in Section 3.5.2.

We next report the GOF results in Figure 4.11. We display in Figure 4.12 the distribution modeling of the pixel-level dataset from two different angular sectors (high incident angle 50° and nadir angle 6°). We remark that we don’t exploit K-distribution in this test because we fail in estimating its parameters. The result shows that the log-normal distribution offers a better fit in linear scale while the GM always shows a good performance in logarithmic scale. We find this result quite reasonable. Because of the large number of samples in the angular sectors in Figure 4.10, the sector’s representing value obtained via mean operator displays the effect of the central limit theorem. This phenomenon is displayed the most clearly in logarithmic scale where the GM becomes a Gaussian distribution in Figure 4.13a.

We investigate, in Figure 4.13, the evolution of fitted model parameters. These models are the log-normal model in linear scale and GM model in logarithmic scale since these two models have been found to give the best fit to our data set.

- The GM first order parameter μ_{dB} , representing the backscatter level in logarithmic scale, shows a good coherence to those ones in the bathymetry mode and the data-level longitudinal mode except for a difference of 2dB in level. This difference could be explained from the fact that, in the pixel-level data analysis, the data are first averaged in linear scale before entering to the model in logarithmic scale.
- The *BS* profile in logarithmic scale (μ_{dB}) shows a good consistency to the reference ones in [20].

4.1. Statistical analysis for SEAPIX operating modes

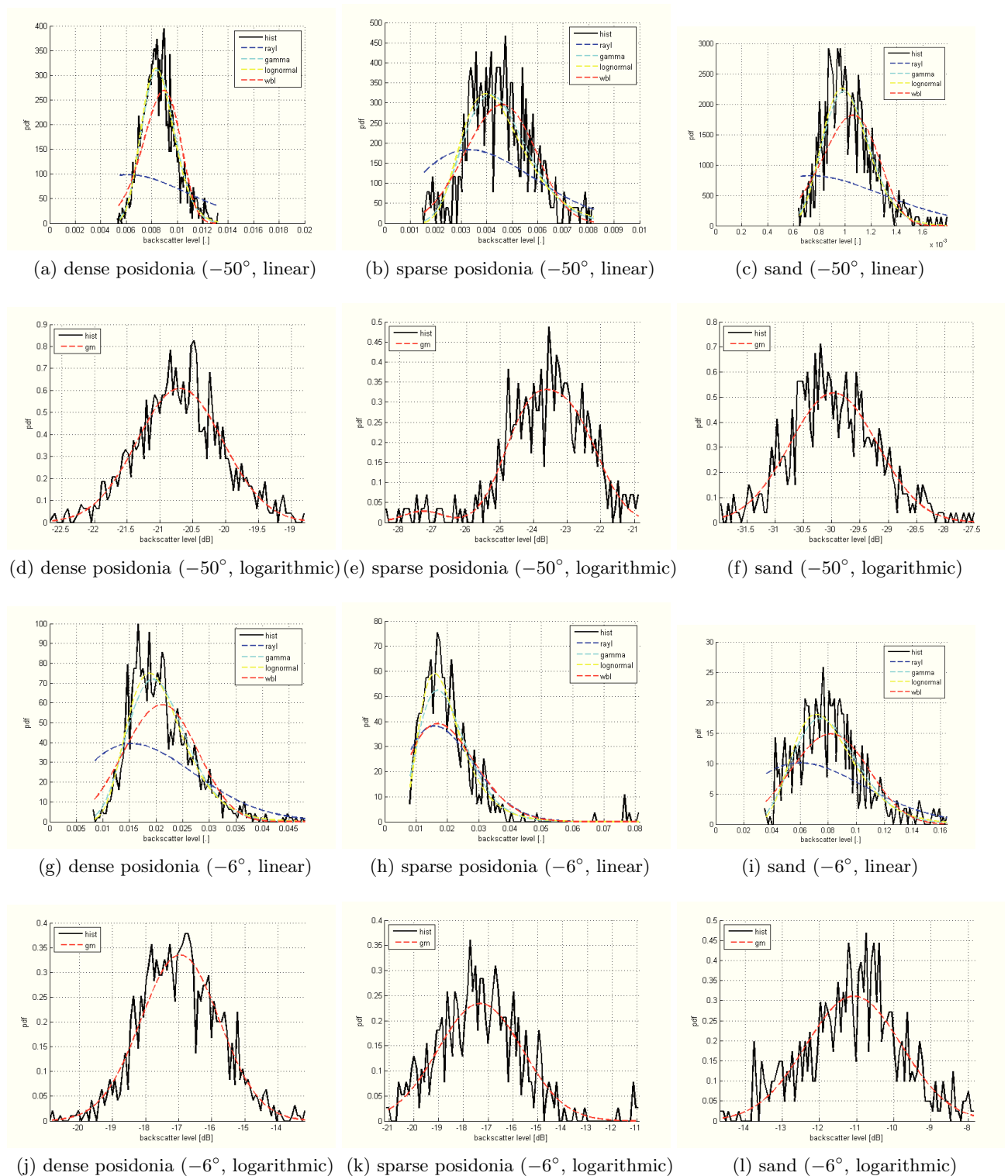


Figure 4.12 – Visualization of distribution fitting process on the pixel-level dataset from two angular sectors: incident angle 50° and nadir angle 6° . The proposed distributions compose of Rayleigh (blue), Gamma (cyan), Log-normal (yellow), Weibull (red) in linear scale, and Gaussian Mixture (red) in logarithmic scale. They are compared to the empirical distribution, which is the normalized histogram (black). The fitting process is realized for different types of seafloors (dense posidonia, sparse posidonia and sand).

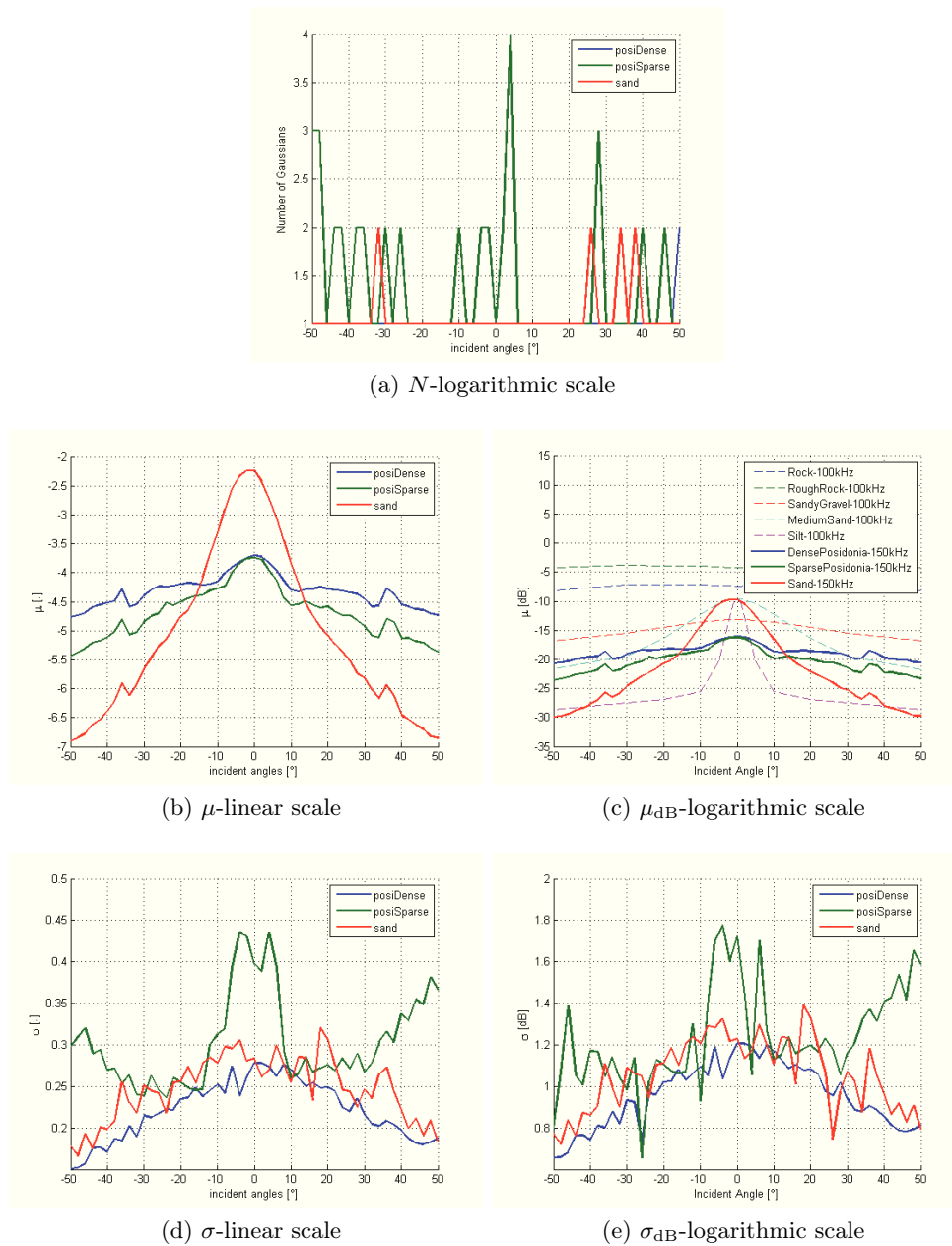


Figure 4.13 – Evolution of distribution parameters estimated in pixel-level dataset (longitudinal mode) as a function of incident angles. The distributions are the Log-normal for the linear scale and GM for the logarithmic scale. These distributions’ characteristics are extracted for the three types of seafloor (dense posidonia - blue, sparse posidonia - green, sand - red). Figure 4.13b, 4.13d displays the evolution of μ, σ (log-normal distribution) while Figure 4.13c, 4.13a, 4.13e displays the evolution of μ_{dB}, N, σ_{dB} (GM-distribution).

- In logarithmic scale, the second order parameter (σ_{dB}) is reduced from those ones in the bathymetry mode and data-level datasets, especially in the higher incident angles where the angular sector's sample number is more important.
- In the linear scale, the distribution parameters have the same form to the ones in the logarithmic scale, but is more normalized. This similarity could be explained from the log-normal model whose parameters are measured in logarithmic scale.

4.2 Inter-mode statistical analysis

In this section, we compare the data from the bathymetry and longitudinal modes in two manners:

- Visualizing the distribution features (median and quantiles) extracted from the datasets.
- Using the similarity measure of distribution models to evaluate the coherence between models and between seafloor types. We use the GM model (in logarithmic scale) because it works well on all three datasets.

In order to evaluate the system consistency, we will use the two following datasets: the bathymetry mode dataset and the longitudinal data-level dataset since these dataset should represent the same distribution (Figure 4.2, 4.6).

4.2.1 Visualization of BS distribution features

In this section, we will compare two distribution characteristics of three datasets (bathymetry mode, data-level, pixel-level) on each angular sector

- Average BS value: the consistent BS acquired with the dataset.
- BS dispersion: the variation of BS acquired with the dataset.

Even though the GM model proves its performance in fitting all three datasets in logarithmic scale, it is complicated to display these characteristics via its parameters. On the one hand, the previous representation (via $\mu_{\text{dB}}, \sigma_{\text{dB}}$) is also not the best manner for displaying our data because the distributions are not pure Gaussian. On the other hand, it is better to extract the distribution characteristics in linear scale because it conserves their physical meaning.

In this section, we will present our data with the data box-plot representation [40]. These characteristics will be extracted in linear scale and visualized in logarithmic scale.

- Average BS value: BS level.
- Two quantiles [0.25, 0.75]: BS dispersion.

In Figure 4.14, we first report the comparison between the two dataset: bathymetry mode (blue line), longitudinal data-level (red line). The BS levels are very consistent: max difference 1dB in the posidonias 4.14b). Also the dispersion expressed by the range between the two quartiles is consistent.

Next, we compare the longitudinal pixel-level dataset (green line) to the others. Figure 4.14 shows

- A consistent BS level between the pixel-level dataset and the others.

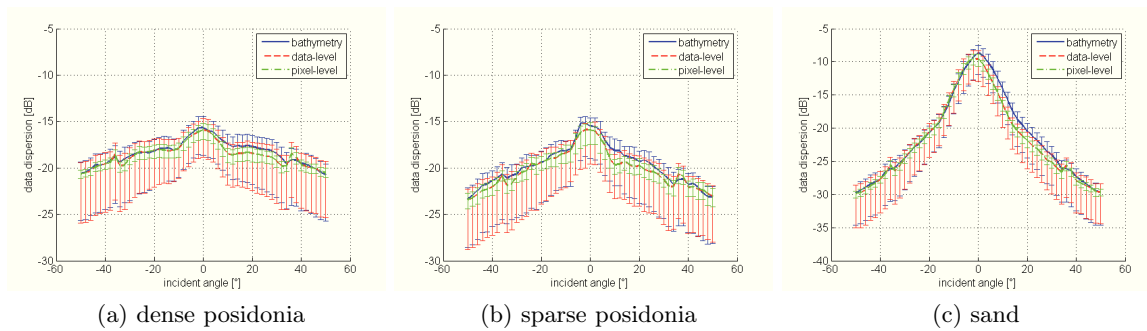


Figure 4.14 – Visualization of three features of in logarithmic scale: mean and quantiles (0.25,0.75). They are presented for each type of sediment (Figure 4.14a: dense posidonia, Figure 4.14b: sparse posidonia, Figure 4.14c: sand). The characteristics are extracted from the different operating modes’ data (-b: bathymetry mode dataset, -r: longitudinal data-level dataset, -g: longitudinal pixel-level dataset).

- A great reduction in data dispersion. On the one hand, this reduction is due to the data collection process of pixel-level dataset via the use of an averaging operator (Figure 4.9). On the other hand, the homogeneity hypothesis of seafloor is better respected in the longitudinal mode because the acquired data were mostly restricted in the vessel trajectory.

In conclusion, the good coherence between the distribution parameters extracted from the two bathymetry mode and longitudinal data-level datasets shows a good system consistency in acquiring the *BS* data. In the pixel-based approach a lower dispersion is observed which make this approach very promising for seafloor classification.

4.2.2 Distributions comparison

In the previous section 4.2.1, we find a good coherence, via statistical distribution parameters, between the data acquired from the bathymetry mode and the longitudinal mode. In this section, we exploit the Kullback-Leibler divergence [14] in order to interpret this coherence via the similarity measure between two distributions [41–43]. We use the GM models (logarithmic scale) in the similarity measure for its fitting performance (Section 4.1). We focus our study only on the two following datasets: bathymetry mode dataset, longitudinal data-level dataset.

The Kullback-Leibler divergence is presented as

$$\text{KL}(p, q) = \int_x p(x) \log \left(\frac{p(x)}{q(x)} \right) dx \quad (4.7)$$

where $p(\cdot)$, $q(\cdot)$ are the distributions of 2 compared datasets.

In order to obtain a more relevant interpretation, this similarity measure is applied on our distributions in logarithmic scale 4.1. We remark that this divergence, however, is not symmetric. Therefore, we exploit a symmetric form of this divergence, which is also known as Jeffreys divergence [14, 44].

$$\text{SM}(p, q) = 0.5 (\text{KL}(p, q) + \text{KL}(q, p)) \quad (4.8)$$

Even though this divergence is not a distance (because of not satisfying triangular inequality properties), it still offers a way to quantify the similarity or difference between two distributions [41, 43, 45]. In our case, this divergence is used to evaluate the similarity in two ways:

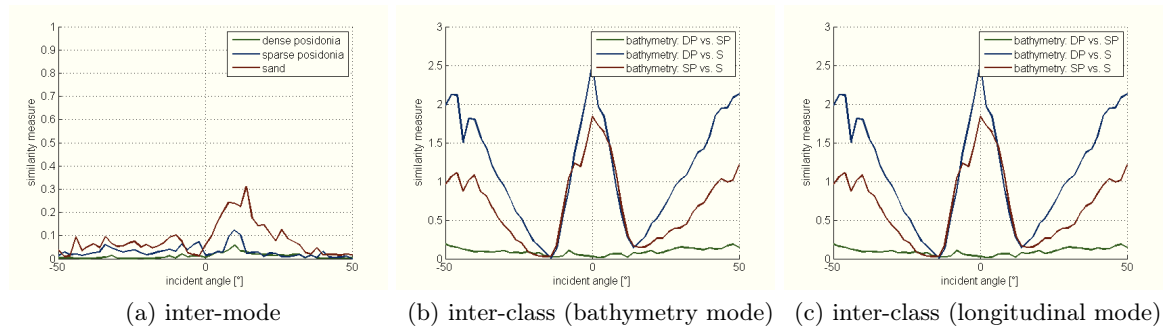


Figure 4.15 – System consistency interpretation via the similarity measures: inter-mode coherence and inter-class discrimination (between different types of sediments for the same mode). Figure 4.15a presents the inter-mode coherence by comparing the same seafloor data (dense posidonia - blue, sparse posidonia - green and sand - red) acquired from the bathymetry mode and the longitudinal mode. Figure 4.15b (resp. 4.15c) displays the inter-class discrimination between dense posidonia - sparse posidonia (green), dense posidonia - sand (blue), sparse posidonia - sand (red) via the data acquired from the bathymetry mode (resp. longitudinal mode).

- Inter-mode coherence: the similarity between distributions recorded from different operating modes on the same seafloor (Figure 4.15a).
- Inter-class discrimination: the differences between distributions from the same operating mode on different seafloors. This measure may, thus, evaluate the capacity of distributions to discriminate seafloor (Figure 4.15b and 4.15c).

Figure 4.15a reports the inter-mode coherence on the different types of seafloor: dense posidonia (blue), sparse posidonia (green) and sand (red). On the other hand, Figure 4.15b (resp. 4.15c) gives the inter-class discrimination via the data acquired from the bathymetry mode (resp. longitudinal mode). The results show

- A good system consistency: the inter-mode coherence is much more important than the inter-class discrimination for the both operating modes. It signifies that the data, acquired from these modes, could be exchanged during the classification of these data without clear influence onto the classification result.
- Angular dependence classification: the inter-class discrimination varies as a function of the incident angles (more discriminating in the high incident angles). The class confusion happens in the interval $[10^\circ, 20^\circ]$, which corresponds to the interaction region in the backscatter level in Figure 4.5b (bathymetry mode) and 4.8b (longitudinal mode).
- Posidonias confusion: the discrimination capacity based on distributions of both posidonias is weak, which is mostly equivalent to the inter-mode coherence. It signifies a difficulty in discriminating posidonias seafloors while exploiting independently the angular information. Otherwise, we observe a small angular dependence discrimination of these classes. Combining with the different angular forms in Figure 4.5b, a backscatter profile could be more useful for their classification.

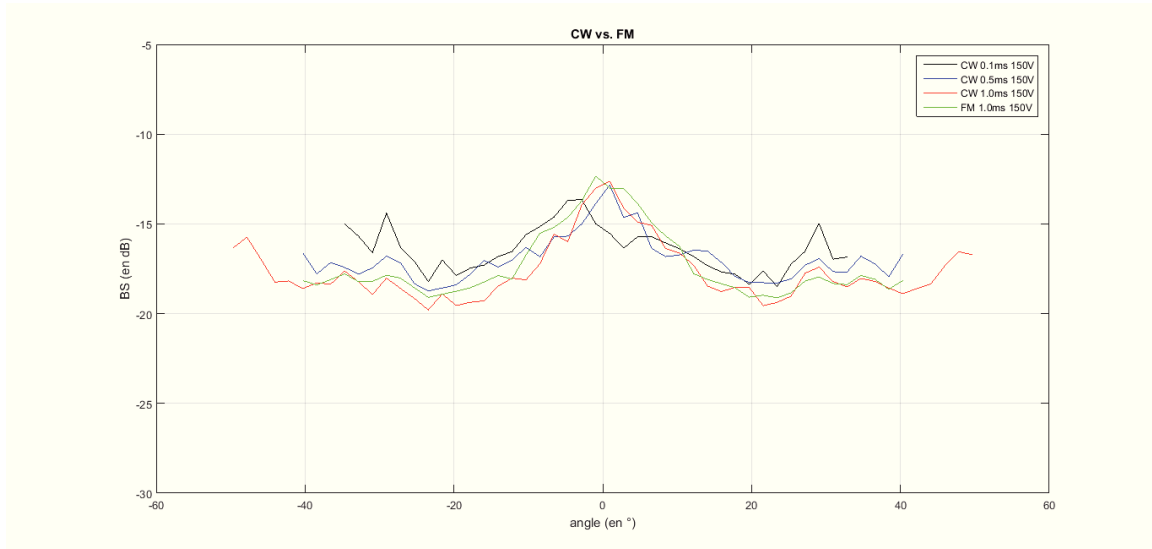


Figure 4.16 – Verification of system consistency SEAPIX in different pulse modulations: CW (0.1ms - black, 0.5ms - blue, 1ms - red), FM (1ms - green).

4.3 Pulse modulation consistency

In this thesis, we exploit the system SEAPIX with the constant wave (CW). Recently, it has been verified that we also have a consistency in the *BS* acquired from CW and FM (frequency modulated) modulation. This test is realized on a new dataset acquired in la Ciotat in 2017 using the bathymetry mode. In this study, the *BS* level is compared between:

- Different pulse width lengths CW: 0.1ms, 0.5ms, 1ms
- FM modulation: 1ms

The result is displayed in Figure 4.16. We have a good consistency of 2dB between the different CW pulse-widths, and there is no difference between different types of modulation.

4.4 Conclusion

In this chapter, we have first presented a statistical analysis of the data distribution acquired on the different operating modes (bathymetry and longitudinal). This distribution analysis is usually applied in classical methods of seafloor classification [37, 46]. We have fitted our data distribution to the physical-meaning distributions (Rayleigh, Gamma, Log-Normal, K in linear scale) and the mathematical ones (Gaussian Mixture in logarithmic scale). The goodness of fit test (Kolmogorov-Smirnov) points out that:

- In linear scale, the K-distribution is the best to model the data for the bathymetry mode and the data-level in longitudinal mode. The pixel-level data in the longitudinal mode should be modeled by the log-normal distribution.
- In logarithmic scale, the GM shows a good performance in fitting our data for all three datasets (bathymetry mode, longitudinal data-level, longitudinal pixel-level).

Then, we realized the system consistency in acquiring the *BS* data via two manners. On the one hand, we compared, between all three datasets, the dispersion of *BS* data in each angular sector. On the other hand, we compared the measures of:

- The coherence of the data acquired from the bathymetry and longitudinal modes.
- The discrimination of different seafloors via the data acquired from the same mode.

These results depict 2 important points:

- SEAPIX system is consistent in acquiring the *BS* data, especially in classification.
- In next studies, these are the exploited datasets:
 - Bathymetry mode’s dataset works for the classification between the sand and the posidonias via the difference of the *BS* distribution, especially in the high incident angles. However, the distribution similarity between the dense and sparse posidonia will cause difficulties in their discrimination.
 - Longitudinal mode’s pixel-level dataset demonstrated as the most robust dataset.

Part II

Seafloor classification

State of the art of seafloor classification and application to SEAPIX

Backscattering strength (BS), which is the intensity backscattered by the seafloor, is the basic information used for seafloor classification as the BS varies according to the seafloor nature. In this thesis, we present a new acoustic system, namely SEAPIX, to acquire such BS information and investigate its exploitation for seafloor classification. This system is capable of functioning as classical multi-beam echo sounder systems through the acquisition of across-track backscatter information. Moreover, it also embeds a new operating mode, namely longitudinal mode, which acquires the BS information from along-track swaths. Within this mode, we obtain for each pixel in the vessel trajectory a fully-characterized BS profile which describes the dependence of the BS with the incident angle. Overall, SEAPIX is regarded as a multi-swath multi-beam echo sounder (MS-MBES) system. In the last chapters, we presented, in detail, the functioning principles (Chapter 2) and the post-processing (Chapter 3) of this system. Besides, we also realized an analysis of the BS data acquired from this system (Chapter 4). In this chapter, we further investigate the application of state-of-the-art seafloor classification techniques on the BS data acquired by this system. This study will draw conclusions of interest for our main contributions on feature extraction and seafloor classification introduced in the next two chapters.

In the literature, the BS data are often acquired from three main categories of acoustic systems: single-beam/sediment echo sounder (SBES), side-scan sonar (SSS) and multi-beam echo sounder (MBES) [5, 47–51]. These systems rely on temporal acoustic signals which convey information on water column, seafloor and subsurface layers. Each category of systems may however involve specific features, which in turn lead to different classification methods. SBES system acquires only one temporal signal in the vertical direction, so that the classification is restricted to the nadir area. The proposed methods typically rely on a segmentation of the received BS signal with respect to the seafloor response as well as subsurface responses. The classification may rely solely on the extracted seafloor response [17, 47] or seafloor characteristics obtained from this signal (hardness, roughness, etc.) [48]. SSS system acquires BS seafloor information on two sides (port/starboard) at high incident angles. Under a hypothesis of flat seafloor, these BS data can be processed to create a mosaic image of the seafloor. Textural analysis techniques are applied on the mosaic image to achieve seafloor segmentation [50, 51]. MBES system can be regarded as an extension of the SBES. It collects temporal signals in many different directions using digital beamforming at reception.

The classification methods for MBES systems exploit two types of information: raw BS data from each beams [5, 23] or mosaic images (Section 3.3) [8, 10]. In the next sections, we will address

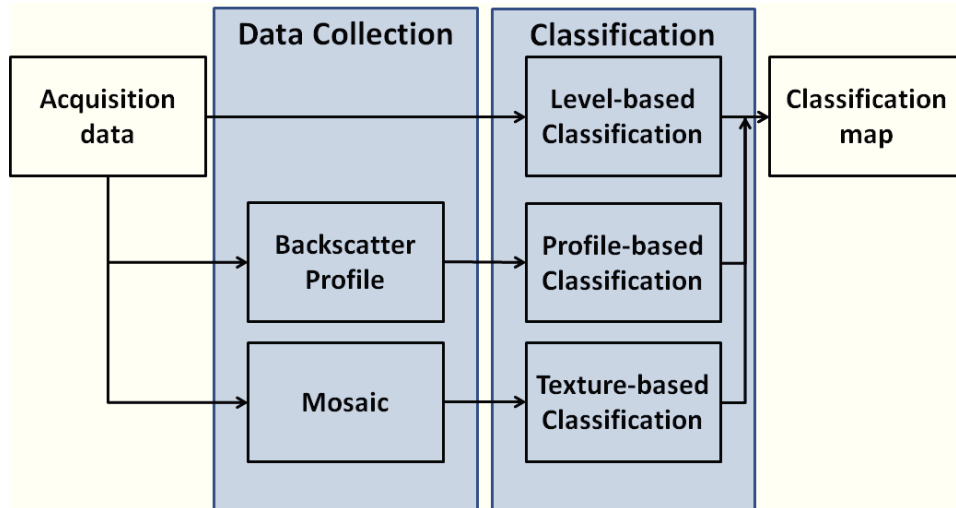


Figure 5.1 – Diagram of the conventional classification methods: namely level-based method, profile-based method and texture-based method.

Table 5.1 – Evaluation of the level-based approach for the considered three-class case-study (dense posidonia - DP, sparse posidonia - SP and sand - S) in the analysis zone. The result is displayed in percentage. The color stands for our evaluation on the good predictions (green - good rate (>80%), orange - medium rate (50%-80%), red - bad rate (<50%).

	DP (67250)*	SP (10000)	S (17250)
DP	91	5	4
SP	41	34	25
S	33	1	66

*:number of pixel in each class.

two state-of-the-art methods for the *BS* approach, Level based and profile based, and one method for the mosaic approach, texture based. Overview of studied classification methods are displayed on Figure 5.1. These methods will be applied on the dataset collected with theMS-MBES system SEAPIX in December 2015 in la Ciotat (France). The area is composed of 3 main classes: dense posidonia (DP), sparse posidonia (SP) and sand (S).

5.1 Level-based classification

This section presents the *BS* approach applied to seafloor pixels. For each pixel in the map, we collect all the BS values and incidence angles for each sample inside this pixel (pixel-level data). This data collection is made for each survey line separately. So for each pixel in the map, the incidence angle will be mostly constant.

In the literature, different studies showed that the *BS* level varies according to the incident angle [23,24,52]. We also verified that a Gaussian Mixture (GM) model works well in a logarithmic scale for the data acquired by the bathymetry mode in Section 4.1. As a result, we exploit an angular-dependent GM model over the considered angular range.

The classification is realized on the acquired data within a Maximum Likelihood (ML) framework:

- Training phase: We divide the training dataset according to 61 incident angle sectors uniformly distributed from -60° to 60° . In each angular sector, a probabilistic model is built from the data belonging to this angular sector. As a result, we derive 61 angular-related three-class models (namely for dense posidonia, sparse posidonia and sand seafloor types).
- Classification phase: For any acquired data, we first select an appropriate model from the training ones according to the associated incident angle. From this model, we evaluate the likelihood of the acquired BS for the different seafloor types and assign the seafloor type corresponding to the greatest likelihood.

We may also point out the difference in the spatial resolutions of the data in the two directions:

- 1m resolution for the along-track direction which corresponds to the product of the vessel speed and pinging rate.
- 0.1m for across-track direction which corresponds to the pulse bandwidth.

As described in Section 3.5.1, in the bathymetry mode, the classification grid resolution has been fixed to 2m. Consequently, any seafloor pixel will contain about 40 samples. Each sample is classified and the pixel-level classification is obtained through a simple majority voting rule over all the elementary sample classifications.

Table 5.1 reports the classification performance of this approach on the case-study zone (described in Section 3.4.2) composed of three classes (DP, SP and S). We first note an important confusion between the two posidonia classes (34% recognition rate of sparse posidonia). Even though the classification performs better for the sand class, but the correct classification rate is not higher than 66%. In fact, this result have been anticipated in Section 4.1 where we found a high similarity between the angular-dependent BS distributions on the posidonia classes (Figure 4.15).

Figure 5.2 displays the classification map on the whole acquisition zone via DELPH. The classification is realized separately on each acquisition line. In areas covered by different acquisition lines, we select one line corresponding to the last passage. From these results, we may draw the following conclusions:

- A good classification of the sand from the posidonias.
- A poor classification between the dense and sparse posidonia classes as in the analysis zone (Table 5.1).
- A larger confusion in the areas with incident angles within $[10^\circ, 20^\circ]$. This issue also appeared in the analysis of the angular-dependent distribution of the BS in Chapter 4 in Figure 4.5b.
- There is a complete confusion, in the Southern area of the map, between the sparse posidonia and the caulerpa sand. The latter has not been represented in the training database since we don't have collected the data around the ground truth observations. This sand class, however, is more similar to the sparse posidonia in terms of BS level distribution in Figure 3.13.

Overall, the level based BS approach performs well only for the sand class, but reaches poor discrimination performance for the two posidonia classes. This method performs very poorly in the near-nadir angular sector $[10^\circ, 20^\circ]$.

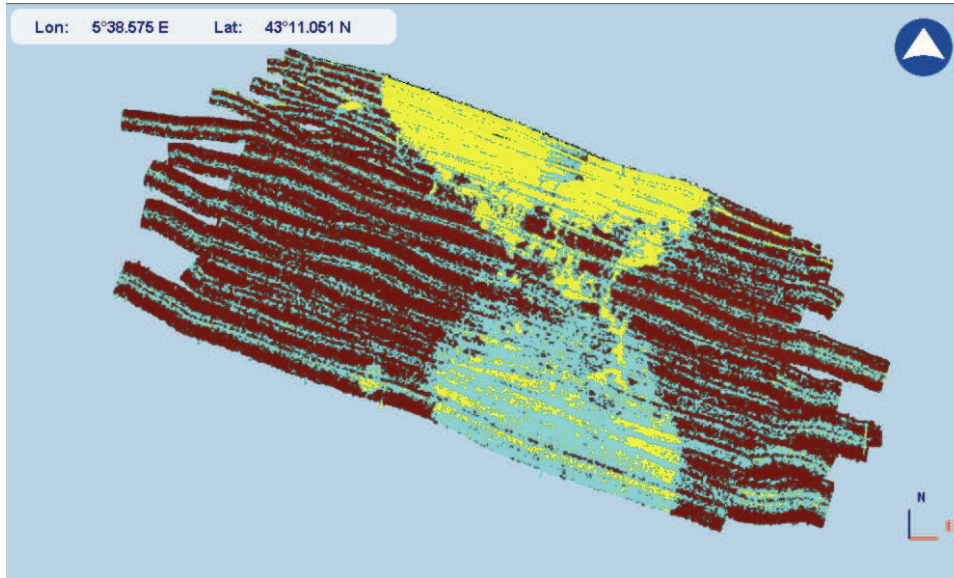


Figure 5.2 – Visualization of the level-based classification on the dataset in la Ciotat (France), in December 2015, acquired by MS-MBES SEAPIX. This region is composed of 3 main classes: dense posidonia (brown), sparse posidonia (blue) and sand (yellow). The classification result is displayed in the resolution 2m.

Table 5.2 – Evaluation of the profile-based approach in the considered three-class case-study (Table 5.1). The result is displayed in percentage. The color stands for our evaluation on the good predictions (green - good rate ($>80\%$), orange - medium rate ($50\%-80\%$), red - bad rate ($<50\%$)).

	DP	SP	S
(2487)*	(1349)	(487)	(660)
DP	84.35	9.64	6.01
SP	28.48	62.99	8.53
S	0	1.42	98.58

*:number of pixel in each class.

5.2 Profile-based classification

In this section, we present the second *BS*-based approach. In this approach, the seafloor type is assumed homogeneous for all pixels in the swath (homogeneity hypothesis on the whole swath). The backscatter profile over the entire angular range will be used for the classification. Because of the important number of samples in a swath, we generate a representing swath *BS* profile as follows:

1. Sorting the swath *BS* data into the 51 angular sectors of size 2° uniformly distributed from -50° to 50° . This choice of angular sector allows us to exploit the distribution studied in Section 4.1.1.
2. Representing each angular sector with the average of the linear *BS* value [6], which is also used in Section 4.1.2. The GM model has been chosen to represent these profile based data because we have previously demonstrate in Section 4.2, that:

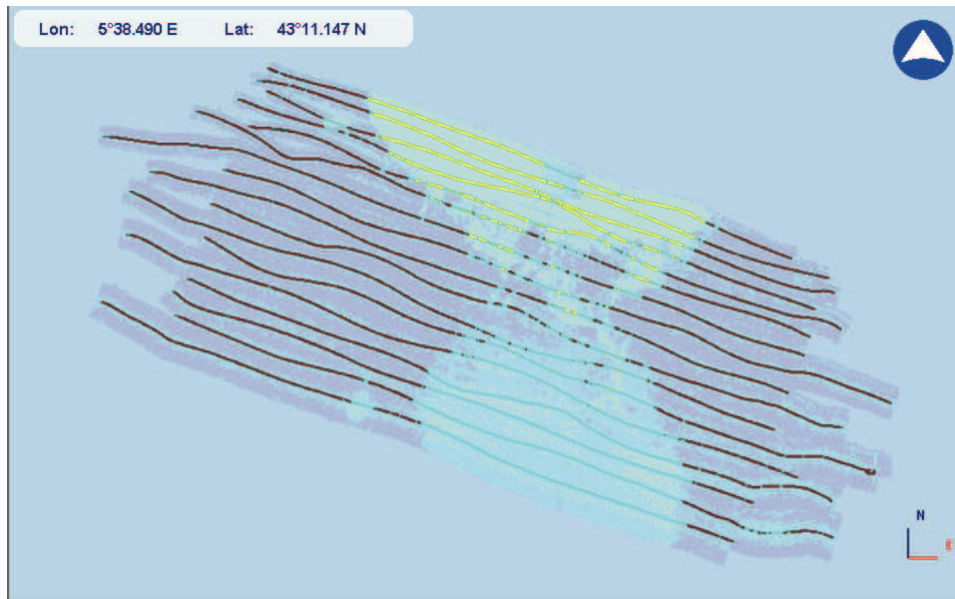


Figure 5.3 – Visualization of the classification with multi-dimension attempt of profile-based method in la Ciotat (France) in the considered three-class case-study (Figure 5.2). This classification is applied on the data acquired in December 2015 with the MS-MBES SEAPIX. The profile-based classification result is displayed on the vessel trajectory with the bold color. The level-based classification result, obtained previously, is displayed with the light color.

- The *BS* data distribution acquired from the bathymetry mode and the longitudinal mode are consistent.
- The GM model is the best model for this representation.

Based on profile data, we realize the classification with two approaches: statistical approach, and model-based inversion [7].

Statistical approach As in [6], this approach is regarded as a multivariate extension of the classification scheme described in the previous section. We also use a GM model with a diagonal covariance matrix (i.e., assuming a statistical independence across angular sectors) and the classification of a given profile is issued from a ML criterion. This classification is assigned to the position of the vessel where the signal was emitted, projected onto the seafloor.

We report the classification performance of this method for the analysis zone (Table 5.2). This method improves the classification rate of the sand (98%), and also distinguishes better the sparse posidonia (63%). We further compare this approach to the level-based classification reported in the previous section for the entire zone in Figure 5.3. We draw the following conclusions:

- The profile-based method depicts much more homogeneous result. We even have a better discrimination between the dense and sparse posidonias.
- This result also shows a good coherence in the transition region of these methods.
- We still observe a confusion between the caulerpa sand and the sparse posidonia in some regions, especially in the South of the area. This confusion is actually caused by the difference between the sand region on the North side (training zone) and the one in the South:

Table 5.3 – Description of IFREMER parameters in simplified version.

Parameter	Signification
α	main lobe's width in nadir zone.
A	amplitude of the first component. It shows the contribution of specular component in the profile. It is often equivalent to the maximum of the backscattered intensity.
β	backscatter attenuation in high incident angles.
B	contribution of this Lambert law in high incident angles.

at nadir, the sand on the training zone is more specular and this is clearly observed in the mosaics in Figure 3.13.

Model-based inversion approach We also explore a model-based inversion [7]. There are two approaches, either a physical parameter inversion or a heuristic model inversion. Even though, it would be better to use a physical model [2, 53], we don't have retain this method for many reasons. First, the popular physical model of Jackson is only valid for frequency under $100kHz$ while SEAPIX frequency is $150kHz$. Secondly, this model was not applied to posidonia seafloor type. Next, the physical model contains a complicated formula, which makes it difficult in the inversion process. Ultimately, because our thesis focuses on classification purposes, we only need a good heuristic model describing our data. In our study, we use the model introduced by IFREMER [22, 54, 55]:

$$BS(\theta_i) = Ae^{-\alpha\theta_i} + B \cos^\beta(\theta_i) + Ce^{-\gamma\theta_i} \quad \text{if } \theta_i < G \quad (5.1)$$

$$BS(\theta_i) = B \cos^H(\theta_i) \quad \text{if not} \quad (5.2)$$

where

- $Ae^{-\alpha\theta_i}$ describes the specular pike in nadir.
- $B \cos^\beta(\theta_i)$ describes the Lambert law in the high incident angles.
- $Ce^{-\gamma\theta_i}$ performs a transition between these 2 models above.
- $B \cos^H(\theta_i)$ describes the Lambert law in the very high incident angles defined by critical angle G .

In our study, we choose a simplified version of this model, which only combines the first and second components as proposed in [54]. This choice is motivated by the fact that:

- the two first components contain enough information for classification purposes (described in Table 5.3).
- for the considered angular range $[-50^\circ, 50^\circ]$, there is no need to exploit the fourth component.
- the third component is used for regularization issues, which are not as important for classification.

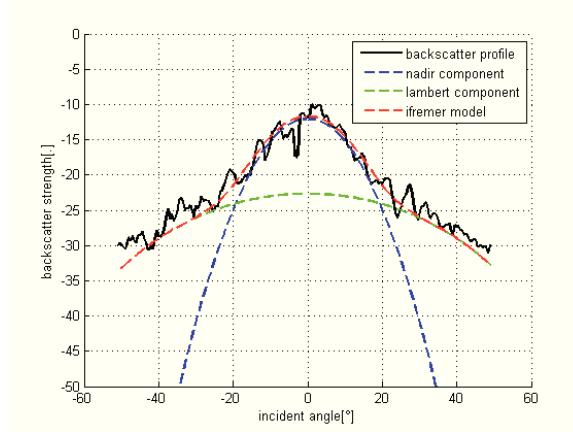


Figure 5.4 – Backscatter profile modeling with simplified IFREMER model. The first component describes the nadir response (blue line) while the second component describes the high-incidence response as a Lambert model (green line). The combination of these two components constructs the IFREMER model (red line).

Overall, our backscatter model is given by (Figure 5.4):

$$BS(\theta_i) = Ae^{-\alpha\theta_i} + B \cos^\beta(\theta_i) \quad (5.3)$$

This model-based approach requires a good compensation of the BS data. However, since we did not compensate the seafloor slope in our postprocessing 3.4.2, we apply the following simple correction to our BS profile for the modeling :

1. The profile is smoothed with a 20° large window. This value is large enough to denoise the large response of posidonia area and small enough to keep the shape of the specular response of the sand.
2. The true center beam is identified at the maximal backscatter level.
3. The correction is applied by shifting the profile so that the center beam is at the incident angle of 0° .

We extract model parameters (A, α, B, β in (5.3)) for all BS profiles and use these parameters as features which we rely on for classification. We consider the following classification models:

- To evaluate the contribution of each of the four parameters independently , we consider parameter-specific classification model using a GM model and a ML criterion.
- We also achieve a classification using the feature vector formed by the four parameters. As classifier, we use a Random Forest (RF) [56], which has been proven to be a good performance classifier in literature, and also give a measure of the importance of each parameter. This importance is measured as the increasing of the prediction error while permuting each variable across out-of-bag observations. We compute random forests composed of 50 trees using the squared-root of the number of feature dimension as number of variables for each decision split and a bootstrap rate of 0.5.

Figure 5.5 displays the distribution of the model parameters. It depicts some characteristics of the considered seafloor types:

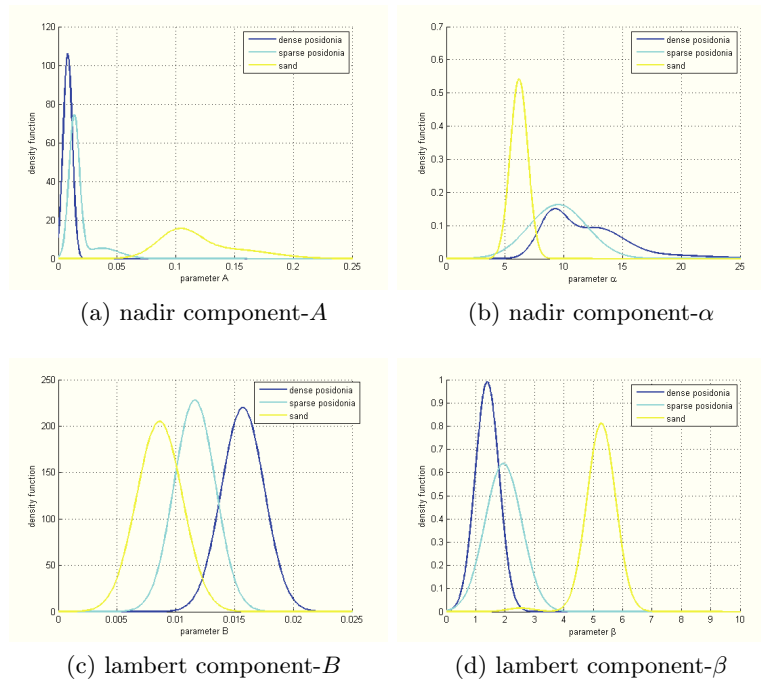


Figure 5.5 – Visualization of distribution fitting for IFREMER parameters: The distribution fit is realized for different incident angles and different types of seafloor

- The sand reflects more in nadir with a high peak (parameter A) and a narrow lobe (parameter α). Besides, it has a higher decreasing rate in high incident angles.
- The posidonia classes have a larger lobe and lower peak at nadir.

Figure 5.6 displays the classification of the whole acquisition zone using model parameters as feature vector. These results demonstrate that

- Specular peak parameter (A) and high-incidence attenuation (β) works well on discriminating the sand from the posidonia classes. This result is emphasized both by the distribution of model parameters (Figure 5.5a, 5.5d) as well as classification results (Figure 5.6a, 5.6d).
- It is difficult to distinguish the two posidonia classes. Their model parameters greatly overlap in Figure 5.5. The most discriminant parameter B between these three classes (in Figure 5.5c) result in poor classification results when used solely (Figure 5.6c).

Similar conclusions can be drawn from the random forest analysis. Figure 5.7a displays the resulting measure of feature importance for the discrimination of sand and posidonia areas. This figure stresses the important contribution of parameters A and β in classifying the sand class. Figure 5.7b depicts the measure of feature importance for the 3-class case. Parameter B seems to be the most important among the four parameters in this context.

Figure 5.7c displays the classification map of the acquisition zone using as feature vector all model parameters and a RF classifier. The result depicts classification performance similar to the multivariate statistical method, including the misclassification of the Caulerpa sand area. In conclusion, the profile-based method demonstrates a good classification, even between the dense and sparse posidonias. This classification is also coherent with the level-based method

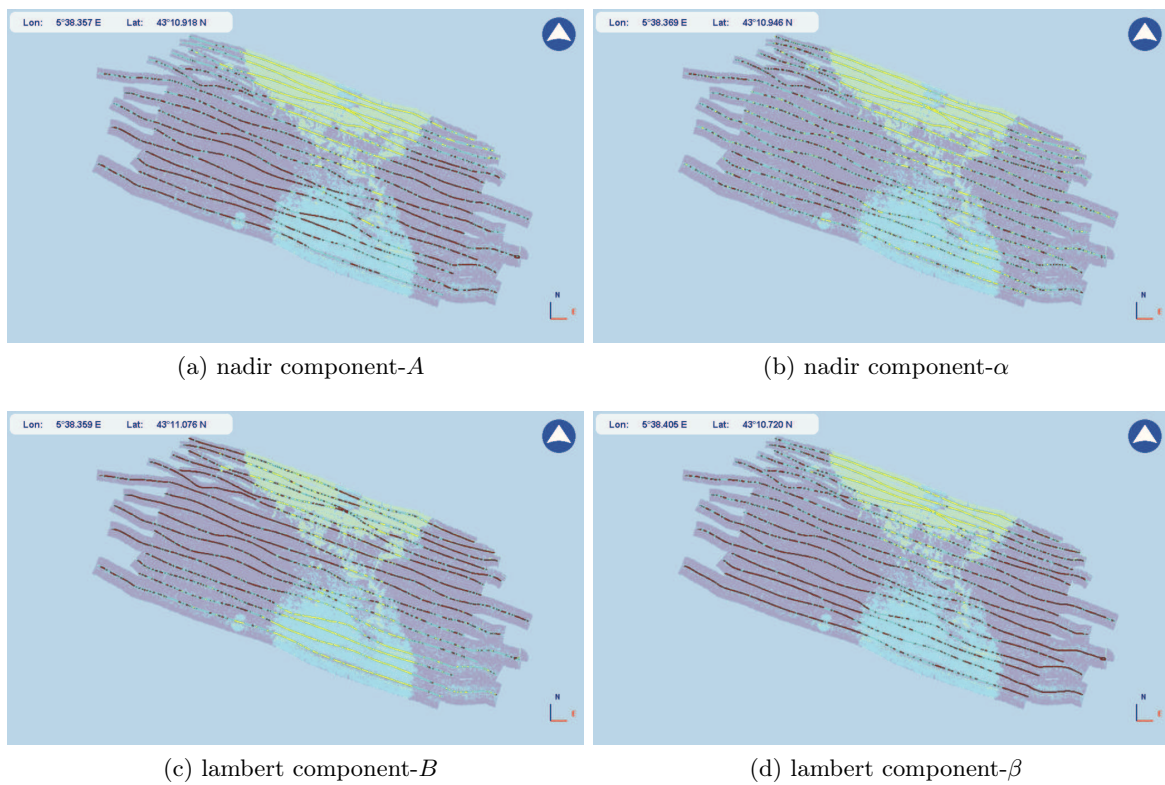


Figure 5.6 – Visualization of the seafloor classification in the bay of la Ciotat using IFREMER model parameters as feature vector in the considered three-class case-study (Figure 5.2). Figure 5.6a (resp. 5.6b, 5.6c, 5.6d) displays the classification based on the parameter A (resp. α , B, β). The parameter classifications are put in the vessel trajectory while the level-based classification is used as a background (blurred color).

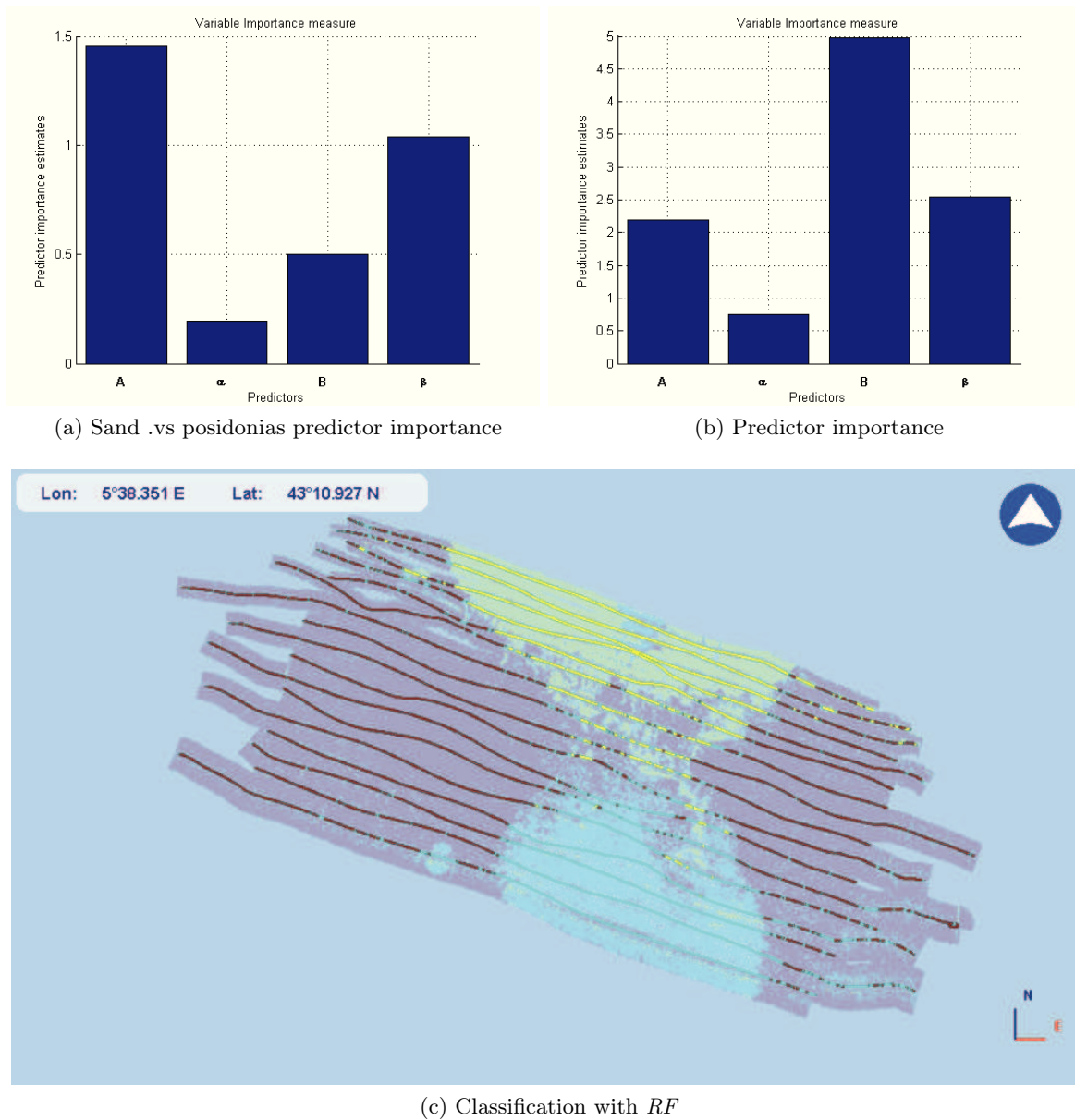
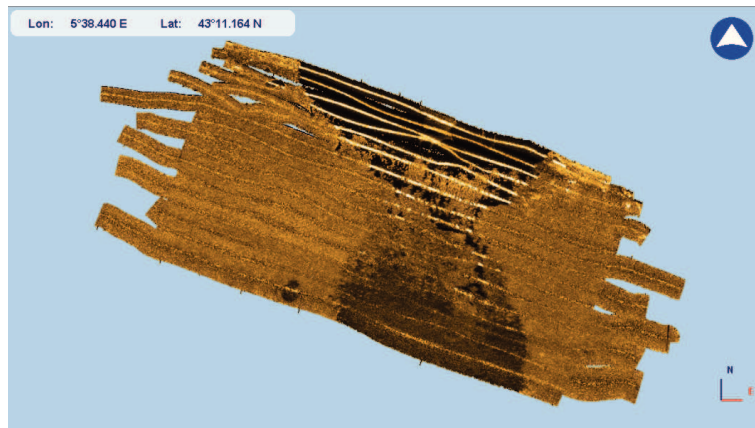
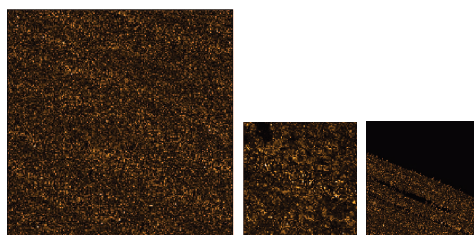


Figure 5.7 – Study of seafloor classification with classifier *RF* in the bay of la Ciotat (France) in the considered three-class case-study (Figure 5.2). The measure of predictor importance of 2 classes (resp. 3 classes) is displayed in Figure 5.7a (resp. 5.7b). The classification result with all four parameters is displayed in Figure 5.7c.



(a) Mosaic



(b) dense posidonia (c) sparse posidonia (d) sand

Figure 5.8 – Snippet mosaic constructed from the acquisition in la Ciotat (resolution of 0.5 [m]). The analyze/training zones are successively displayed in Figure 5.8b, 5.8c, 5.8d.

presented in the previous section. The model-inversion method does not lead to significantly better classification performance compared with the direct application of statistical classification model applied to *BS* profiles.

5.3 Texture-based classification

In this section, we present the mosaic approach for seafloor classification. Texture analysis techniques are exploited for the classification on mosaics from SSS systems [50, 51], or MBES systems [8, 10]. The computation of the mosaic image was described in Section 3.4.2. We select snippet-type mosaics for which image pixel is built with the true samples on the seabed (Section 3.3).

Texture-based techniques rely on the extraction and characterization of the textural information of each seafloor type. In this section, we work only on data collected on the analysis zones, which are composed of homogeneous regions. At a first step, to have a reliable texture analysis, it is necessary to remove the angular dependency on each analysis zone which shares the same backscatter profile. The mosaics of these regions are displayed respectively in Figure 5.8b (dense posidonia), 5.8c (sparse posidonia) and 5.8d (sand). However, visually no remarkable texture feature was observed.

The Histogram of Oriented Gradient (*HOG*) is a popular feature in texture classification [11, 13, 57, 58]. Therefore, we select this feature for our study. It is extracted on the mosaic of the analysis zone with the following parameter setting as in [11]:

Table 5.4 – Cross-Validation test on the textural feature *HOG* in the considered three-class case-study with RF (Table 5.1). The result is displayed in percentage. The color stands for our evaluation on the good predictions (green - good rate (>80%), orange - medium rate (50%-80%), red - bad rate (<50%).

Truth .vs Predict	DP	SP	S
DP	99.95	0.04	0.01
SP	45.79	54.20	0.01
S	53.54	0.16	46.30

- A feature is extracted for each pixel p_0 by defining a block of size 16×16 [m] in its neighborhood.
- Each block contains 4 cells of size 8×8 [m] corresponding to the top-left, top-right, bottom-left and bottom-right.
- In each cell $C(i)$, pixels are sorted into 9 groups via the direction of their gradient ∇p . Each group represents a direction, which is equally distributed in $[0^\circ - 180^\circ]$.
- These groups are used to construct the histogram of direction, whose bin $B(j)$ is represented with a value calculated as:

$$HOG(i * 9 + j) = \sum_{p \in C(i)} w_p \cdot |\nabla p| \quad (5.4)$$

where $w_p = \exp(-|p - p_0|^2 / 2/64)$ is the Gaussian weight on distance of pixel to the center.

- The feature is obtained by normalizing these histograms.

A *RF* classifier is selected for the classification based on the *HOG* feature vector. The *RF* is composed of 50 trees and we use all features at each node in the training phase for the construction of the trees. The evaluation relies on a k -fold cross-validation test. The analysis data are used to extract $k = 10$ partitions. In each partition, we use 90% of the samples for training and 10% as test set. The results are summarized in Table 5.4.

They show a large confusion between the classes where all data are classified as the dense posidonia. It means these mosaics are unfortunately not different in term of textural information (Figure 5.8), as noted visually. In Section 3.4.1, we presented the posidonias and the sand (Figure 3.11b, 3.11c, 3.11d), as well as their mosaics (Figure 3.11e, 3.11f, 3.11g). These mosaics, however, were acquired with a SSS, which provided a good resolution, and we did find some repeatable structures for these seafloors, which a texture-based analysis could rely on. However, SEAPIX system, given its targeted fishery market, was not primarily aimed to address high-resolution imagery and the resulting mosaics (Figure 5.8b, 5.8c, 5.8d) do not reveal fine-scale structures.

5.4 Conclusion

In this section, we reviewed state-of-the-art approaches for seafloor classification and their direct application to SEAPIX system. More precisely, given the characteristics of SEAPIX system, we explored the three classic frameworks, namely level-based methods using raw *BS* data, profile-based methods based on a swath homogeneity hypothesis and texture-based methods applied to

seafloor mosaics. In agreement with the analysis of SEAPIX BS data in Chapter 4, we draw the following conclusions:

- The level-based methods, which work on local pixel information, provide a classification result on the entire study region. We find a reasonably good classification rate at high incident angles, but a large confusion for incident angles in the interval of $[10^\circ - 20^\circ]$. Overall, the BS level may be considered as discriminative feature in high incident angles.
- Results obtained with both the model-based and statistical profile-based methods confirm that BS profiles are relevant descriptors for seabed classification, however at the expense of the intra-swath homogeneity hypothesis which may not be fulfilled.
- Texture-based features lead to poor discrimination performance, which suggests a low textural content of the mosaic derived from SEAPIX data for the considered study zone. These results also point out the information loss in the construction of the image mosaics, where for each seafloor pixel all the elementary BS data are averaged.

These conclusions motivate the framework described in the next two chapters according to the following guidelines:

- Extracting information directly from the raw *BS* data rather than the compressed mosaic. This strategy maximizes our exploitation of the richness of the acquired data. This strategy also adapts to both bathymetry and longitudinal modes. In particular, the latter mode only acquires information along the vessel trajectory, which offers an exceptional angular-dependent distribution of acquired data but on a restricted coverage;
- Combining the advantages of the two acquisition modes: the bathymetry mode only offering a reasonable classification performance, but on a large spatial region and the longitudinal mode leading to much greater seafloor recognition performance but limited to the vessel trajectory.

Feature extraction for seafloor classification from Multi-swath MBES system

In this chapter, we study how a multi-swath capability for multi-beam echo sounder systems (MBES) can be used to improve performances in seafloor classification. These new kinds of mapping sonar system are able to simultaneously insonify the seafloor on multiple swaths either along or across the vessel trajectory and thus to record backscattering strength (BS) versus incidence angle as information for seafloor classification. Across-track BS measurements correspond to data recorded by conventional MBES systems and represent the response from a large seafloor area. Using this information to classify seafloor type necessitates a homogeneity hypothesis. When the insonified swath is oriented along the vessel trajectory, a full BS profile is locally recorded for each resolution cell at nadir. No homogeneous hypothesis is required to exploit BS versus incidence angle but the spatial extent of classification results is drastically restricted to the nadir. In this chapter, we assess the reliability of data from each acquisition mode and introduce novel strategies on extracting useful features for a multiswath system. Two types of features are studied: statistical properties (mean, variance) and textural characteristics (Histogram of Oriented Gradients (HOG), spatial covariance). These features are evaluated as classification features on a real dataset. From this dataset, along-track mode gives more robust performances than those from across-track. Second, the traditional BS mean (versus incidence angle) feature is more informative in the task of seafloor classification whatever the acquisition mode. For data from the across-track swath, the results suggest the combination of mean and spatial covariance to slightly improve performances. For data from the along-track swath, the study reveals that the BS mean versus incidence angle is the better choice.

6.1 Introduction

To observe underwater environment, acoustic imagery systems are the most efficient because of the low absorption of sound waves in water. Existing underwater imagery systems can be grouped into three main types: single-beam echo sounder system (SBES) [47, 48], side-scan sonar system (SSS) [50, 51] and multi-beam echo sounder system (MBES) [1, 4, 59, 60]. MBES systems are mainly used to obtain 3D bathymetry map of the seafloor. But they also provide a precise measurement of the BS dependency upon incidence angle. Since BS profile is a well-known discriminating feature in seabed type, MBES systems are commonly used for seafloor characterization [59, 61], segmentation [4, 49, 60, 62], or geophysical parameter inversion [7, 63].

Since 2010, iXBlue has developed SEAPIX, an MBES based on a steerable symmetric Mills Cross geometry, which is a unique MBES system on the market with steering capabilities in transmit and receive on both antennas. This full multi-swath MBES (MS-MBES) is able to image the full water column and sea bottom by scanning in the fore/aft and port/starboard directions. Transmitted beams are stabilized in roll or pitch and receiving beams are motion compensated using an embedded motion reference unit. SEAPIX was designed to address the fishery market. Its design was therefore optimized to meet the best trade-off between hardware cost and level of performances [1]. The purpose of the study is to develop and evaluate the capabilities of MS-MBES for seafloor backscatter imagery and characterization. Three main swath configurations have been considered:

- Insonification along the across-track swath: This is the classical configuration used for bathymetry profile measurement.
- Insonification on a forward looking across-track swath: Any tilt angle in between 0° to 40° from vertical can be selected. Using this mode, the specular reflections that commonly occur at nadir are eliminated, ensuring a full continuity of backscatter image from port to starboard.
- Insonification in the along track direction (also called longitudinal): Using this mode, a bathymetry profile is obtained in the fore/aft direction. Also, for each pixel at nadir, the full angular backscatter response (from -60° to $+60^\circ$) can be obtained.

Each of these three swaths gives complementary information on the backscatter response of the seabed. By correctly processing all of these measurements, we expect that an MS-MBES will improve the classification rate compared to a conventional MBES system.

The MS-MBES performances are evaluated on a real dataset recorded on a reference area. This area was previously surveyed using SSS, conventional MBES systems and video. Ground truth samples were also extracted, so a complete and precise interpretation map was obtained by the geophysicists. The seabed is mainly composed of three types of sediments: dense posidonia (DP), sparse posidonia (SP) and sand (S). A supervised classification algorithm has been applied on this reference dataset: for each of the three types of sediments, a region of interest was selected on which a set of features are computed (mean, variance, textural information). A classifier is then trained on the selected regions and a classification rate is measured. Classification rate has been measured using a random forest based classifier. It has been verified that classifier type (bayesian, neural net) doesn't have any significant impact on the classification results. Using this procedure, we have then tested different type of features for each insonification scheme.

The chapter is organized as follow: first, problem statement is presented in Section 6.2. The MS-MBES system is described in more details in Section 6.3.1. The real dataset is depicted in Section 6.3.2. The different types of features computed on each configuration are explained in Section 6.4. Last, results on evaluating different sets of features are given in Section 6.5.

6.2 Problem statement and related work

In our study, we focus on two of the three swath configurations: conventional across-track swath and along-track swath visualized in Figure 6.1. As briefly stated in the previous section, each of these two configurations gives different seafloor backscatter information. Using conventional insonification along the across track swath, the system measures the backscattering strength at only one incidence angle for each pixel in the swath. But this information is given on the full

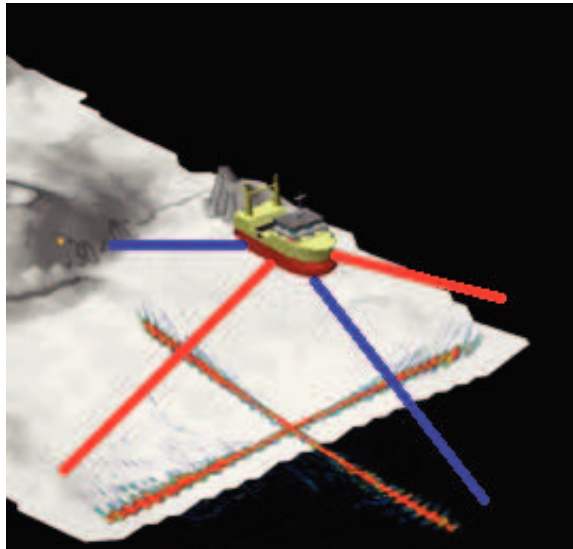


Figure 6.1 – Visualization of SEAPIX operating swaths: conventional across-track swath (red line), and along-track swath (blue line).

port/starboard coverage. Using insonification on the along-track swath, the system measures the full backscatter angular response for each pixel but this information is restricted to nadir pixels. Given the differences in the acquisition geometry, different features will be extracted to address seafloor characterization as detailed below.

We will first give a state of the art of main existing along-track and across-track systems in used for seafloor characterization. In the along-track system categories, ie. system that uses the along track direction to collect acoustic data, we will mention single-beam echo-sounder (SBES) systems and forward looking sidescan system. In SBES system, the seafloor is insonified by one beam at vertical with a small aperture (a few degrees in practice). The backscatter time-series is used directly as classification features [17], or indirectly to estimate geophysical classification-parameters [15]. In [47, 48], response of seafloor to different operating frequencies was studied to verify its frequency dependence. This characteristic was further exploited to extract the frequency-dependent parameters via principle component analysis (PCA) for seafloor classification.

Another interesting concept is the forward-looking sidescan sonar system developed in COSMOS project [18]. On emission, the system provides a large forward looking angular aperture ($\approx 20^\circ$ in azimuth, $\approx 50^\circ$ in elevation). On reception, 32 along track sidescan beams are formed inside the emission aperture. Using a second antenna at reception, the system can also deliver bathymetric measurement. The system is then able to give a backscatter profile for each insonified pixel. In [5], this profile was used for the seafloor classification. This system actually provides equivalent information as the along-track swath of the multi-swath MBES system.

In the across-track system categories, ie. system that uses data collected on the across track swath, we consider the classical MBES system and SSS system. For classification purposes, high resolution SSS systems are commonly used. Seabed discrimination is obtained through textural analysis on side-scan mosaic. Different types of textural features have been proposed such as Haralick [64] and Wavelet-based [50] features. MBES systems deliver, for each insonified pixel, also the BS level but with the corresponding incident angle. Using the BS data only, classification method is similar to side-scan systems: textural features extracted from mosaic image are used as discrimination features [10, 61, 65]. The quality of the mosaic strongly depends on the calibration

process, as well as on the resolution of sounder. Such systems underestimate the dependence of the BS level upon the incidence angle. This dependence has been pointed out by a variety of studies including its relevance for classification purposes [3, 4, 37, 49], and for the estimation of geophysical parameters [7, 63, 66].

A second category of methods aims to fully exploit this angular dependence. It comes to infer angular-dependent statistical models for the BS level and to apply locally the appropriate model for each seafloor pixel [3, 4, 37]. The angular dependence is usually modeled as a BS profile, which describes BS levels as a function of incidence angles [5, 46, 49, 59]. In conventional MBES systems, it is necessary to make a homogeneity hypothesis along at least on part of the swath to estimate the BS profile. A classical alternative relies on locally evaluating the angular-dependent BS profiles for different seafloor types only for a few incident angles, which often greatly affect the discrimination power.

Overall, our analysis of along-track and across-track systems bring out two main types of features for seafloor characterization and classification:

- Point-wise statistical features (e.g., local mean and variance of the BS level), which locally describe the BS level and its variability at a given pixel. These features are typically suitable to characterize angular-dependent features.
- Textural features, which characterize the spatial correlation exhibited by the BS level in a given region, typically some neighborhood of a seafloor pixel. A variety of textural features may be considered such as cooccurrence-based and Wavelet-based features [50, 64], keypoint-based textural features [67], contrast-invariant gradient-based features [11] and spatial covariance features [12]. It may be noted that all these textural features assume an underlying regular image grid, which does not match the acquisition geometry of multi-swath systems. As stated above, the classical solution resorts to the creation of a mosaic for a regular pixel grid prior to the extraction of textural features, however at the expense of an information loss due to local averaging operations from the available angular and BS measurements.

In this study, we investigate both point-wise and textural features for MS-MBES. We decide to extract relevant features from the raw angular and BS data, not from the mosaic image. This method ensures to exploit the data at the highest resolution delivered by the system and to avoid distortion of the signal through interpolation.

6.3 Multi-swath MBES and survey data

6.3.1 Multi-swath MBES

The SEAPIX is a multi-swath MBES system based on a standard Mills-crossed geometry with two perpendicular linear antennas that can both transmit or receive which allows steering electronically the beams in the fore/aft and port/starboard directions. The main specifications of the system are given in Table 6.1.

The system architecture is very flexible and enables to select any insonification scenario. In between two successive emission, any acquisition parameters can be modified: Emission antenna, Beam emission steering angle, pulse type, power level. In this study, we focus on two insonification scheme, along-track and across-track swaths as follows:

Table 6.1 – Specification of SEAPIX system

Attributes	Values
Frequency	150kHz
Band	10kHz
Pulse	CW or FM (0.1ms to 20ms)
Beam	64 beams (equivalent angles from -60° to 60°)
Aperture (T/R)	$1.6^\circ \times 1.6^\circ$ (nadir) to $1.6^\circ \times 3.2^\circ$ (60°)

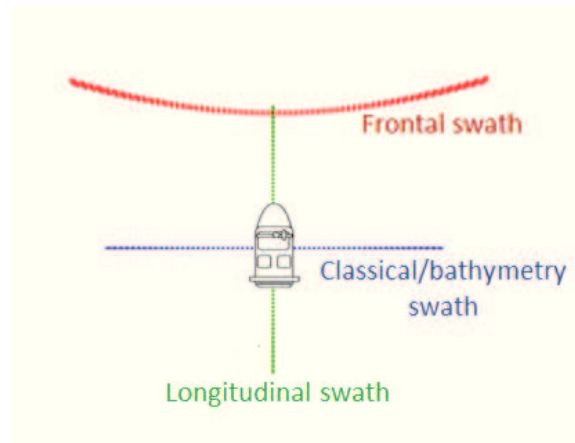


Figure 6.2 – SEAPIX operational modes: swath visualization for different functioning modes (blue swath-classical mode, red swath-forward looking mode, and green swath-longitudinal mode)

- Classical bathymetry mode (*AcT*): similar to classical MBES systems, the across-track swath in nadir (blue swath in Figure 6.2) is insonified by emitting sound wave from the along-track antenna, and receiving the echoes by the other (across-track) antenna. The beam-forming is performed on reception antenna to acquire the echoes from the various direction of arrival. For each reception beam, the seabed echo is detected using amplitude or phase detection. For each detection, the system calculates the georeferenced position, the incidence angle and the mean *BS*. Furthermore, the system can also extract the high resolution backscatter time series extracted around each seabed echo (called snippet).
- Longitudinal mode (*AlT*): by switching the roles of two antennas, along-track swath in nadir (green swath in Figure 6.2) is insonified. When the vessel is moving, the same pixel at nadir is insonified on multiple successive pings at different incident angles. Therefore, for each pixel at nadir the system collect the full *BS* profile.

Additionally, it is possible to alternate these two insonification modes during acquisition. Using this new scenario, the system can simultaneously acquire the two type of information on the seabed with a consistent georeferenced position and environment conditions.

As the considered acquisition modes share common acquisition hardware, the backscattering strength is computed using the same processing algorithm as follows:

1. Compensation based on the calibration of each antenna.
2. Compensation of the time varying gain (TVG).
3. Compensation of propagation losses.

4. Detection of the bathymetry in each beam and computation of its absolute geographical position.
5. Extraction of the high resolution backscatter signal inside -3dB beamwidth for each beam (snippet).
6. Reconstruction of backscatter profile of target strength along the insonified swath by interpolation of the snippet signals and the geographical position of each beam.
7. Normalization of the target strength by the insonified surface to obtain the backscattering strength level.

6.3.2 Survey Data

6.3.2.1 Acquisition campaign

The case-study area was selected in the bay of la Ciotat (Figure 6.3) based on the knowledge about the sediment distribution. The selected zone mainly consists of different types of posidonia (dense, medium, sparse) and sand. The definition of the different types of posidonia is based on its coverage per surface unit of 1m to distinguish among dense, medium, and sparse posidonia. The area of interest also comprises several regions of rock, sand ripples near the coast. A groundtruthing of the seafloor types was issued from underwater videos. These subareas were used as references to carry out a quantitative evaluation.

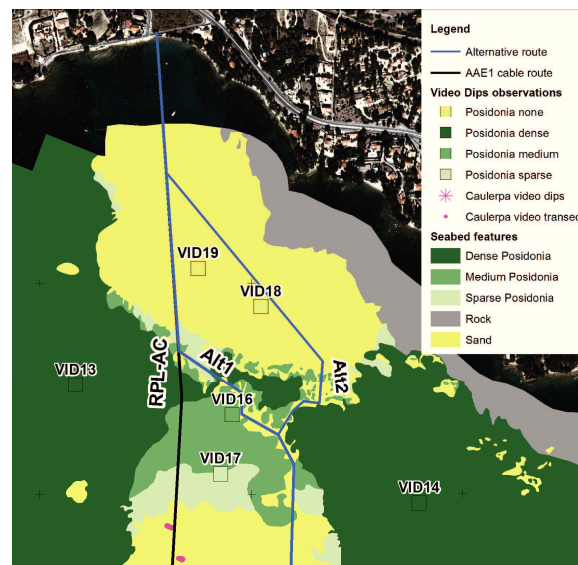


Figure 6.3 – Sediment distribution in the bay of la Ciotat France with several geographical positions of the recorded cameras

The survey data cover a $600\text{m} \times 1000\text{m}$ area. 17 parallel survey lines from North-West to South-East were acquired using both along-track and across-track modes with 50% spatial overlap. Vessel speed was controlled at 1.5m s^{-1} to obtain a reasonable along-track sampling with an approximate 1m resolution. In bathymetry mode, each survey line provides both angular and *BS* information for each pixel. With a spatial overlap of 50%, most pixels were insonified twice with two different incident angles for this mode.

After processing, the bathymetry mode delivers both a bathymetry map and a *BS* map. From the bathymetry map (Figure 6.4), we observe a variation of the water depth from North-West (10m) to South-East (30m). This slope was not accounted for in the post-processing.

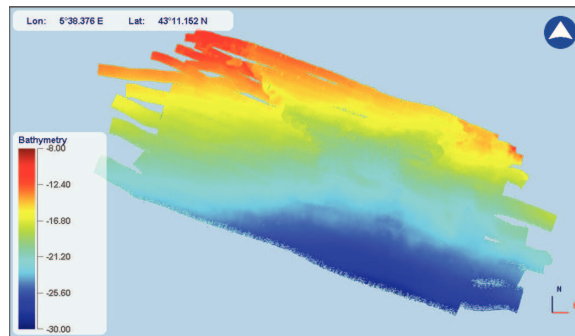


Figure 6.4 – Bathymetry map of the survey area in La Ciotat (France) in December 2015. The map is presented using Delph Roadmap software, under resolution of 1m.

The *BS* map (Figure 6.5) is constructed as a simple superposition of the data acquired from all survey lines. Both posidonia and sand areas are clearly visible. There is also a small region of sand ripples. Given the slight difference in *BS* level between medium posidonia and sparse posidonia, we eventually retained three main classes: dense posidonia, sparse posidonia and sand.



Figure 6.5 – High resolution Backscatterer mosaic of the survey conducted in La Ciotat (France) in December 2015. The visualization is shown by superposing each survey line. The map is presented via Delph Roadmap software, under resolution of 0.1m.

6.3.2.2 Data analysis

In a first stage of the analysis, we perform an evaluation of the consistency of the *BS* value measured between the two acquisition modes.

We estimate the signal-to-noise ratio (SNR) within the acquired datasets. The SNR is calculated from the ratio between the energy of the backscattered signal at the footprint-detected position and the energy of the signal in the water column.

An example is displayed in Figure 6.6(left) for the reference region of dense posidonia from the along-track dataset. The SNR decreases with greater incident angles and is lower on sand areas (SNR= -3dB at incident angle of 60°). This is expected since:

- the *BS* level decreases at longer range due to dispersion and absorption.
- the *BS* decreases at greater incident angles.

- Sand is harder sediment compared to posidonia and so the BS level decreases more rapidly with high incident angles.

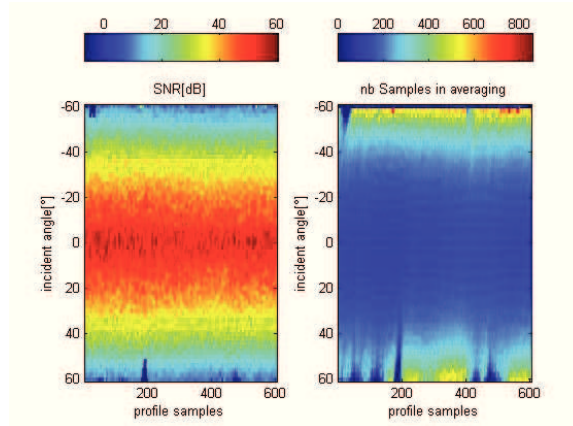


Figure 6.6 – Analysis of the BS data for the longitudinal mode in a dense posidonia area: Signal-to-Noise Ratio (SNR) values as a function of the incident angle (left), number of samples in a $5m$ – resolution seafloor pixel as a function of the incident angle for $\pm 1^\circ$ angular range (right).

Using a seafloor pixel grid of $5m$ – resolution, we also compute the average number of samples per seafloor pixel as illustrated in Figure 6.6. This information affects not only the quality of the mean BS level computed for a given incident angle, but also the standard deviation of these angular-dependent BS data. In Figure 6.6, we observe that several angular sectors involve no data. This is due to the yaw movement of the vessel vessel during the acquisition survey.

Given this preliminary analysis, we retain for the longitudinal mode an angular range between -40° to 40° . This choice leads to:

- A better SNR, about $16dB$ at highest incident angles;
- A homogeneous average number of data in each angular sector.

We also investigate the uncertainty in the geographical position on the backscatter data. The vessel was positioned using a GPS/RTK navigation with 10cm precision. Roll, pitch and heading were measured using a high grade INS. So the main source of uncertainty in positioning the BS data is the beam aperture width. Combining the SEAPIX system specifications in Table 6.1 and the maximum depth of 30m in the survey area, we have considered a resolution of

- 2m in diameter on across-track swath, which comes from the trade-off between the positioning uncertainty, and the number of samples in each $\pm 1^\circ$ angular range.
- 5m in diameter on along-track swath, which comes from the trade-off between the heading angle variation ($\pm 5^\circ$), and the number of samples in each $\pm 1^\circ$ angular range.

The study of the BS consistency between these two modes was reported in our previous publication [67]. The main results are shown in Figure 6.7 where the mean and standard deviation of the BS is displayed as a function of the incident angle for the bathymetry mode (blue line) and the longitudinal mode (red line). These analysis show that the system exhibits a good BS consistency measurement between the two modes. This is further emphasized by the analysis of intra-mode and inter-class distances (green, blue and brown lines Figure 6.8) vs. inter-mode distances (black line in Figure 6.8).

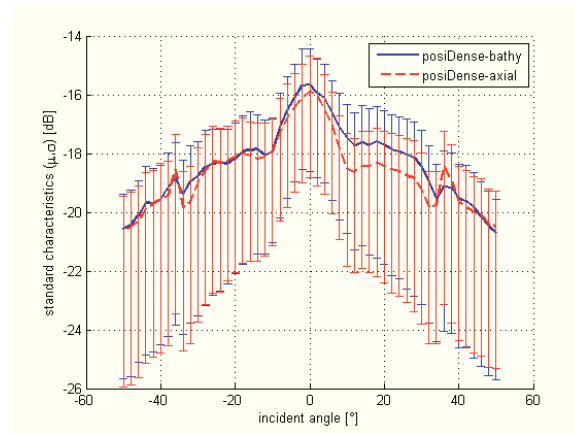


Figure 6.7 – Consistency between the data acquired from bathymetry mode (blue line) and longitudinal mode (red line). BS is reported to dB, and negative incident angle corresponds to vessel’s left/front (classical mode/longitudinal mode).

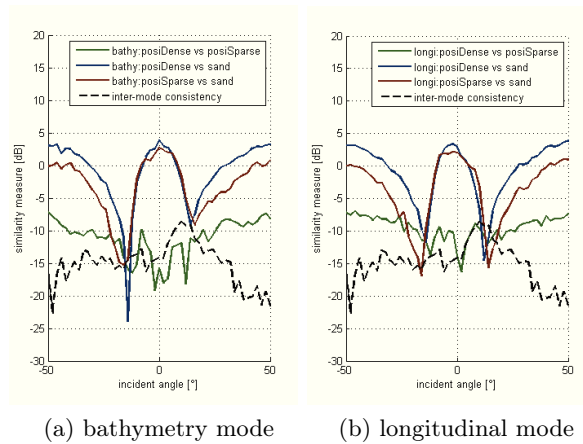


Figure 6.8 – Classification potential on the same operating modes (bathymetry mode in Figure 6.8a, and longitudinal mode in Figure 6.8b): similarity measure between each pair of sediment’s types: dense posidonia-sparse posidonia (green,-), dense posidonia-sand (blue,-), sparse posidonia-sand (brown,-). These measures are compared to the system consistency, which is the variation in BS of a same type of seafloor against the different operating mode. This consistency is expressed as the similarity measure averaged on 3 types of sediment above (black,-). The measure of similarity is computed using the Kullback-Leibler divergence for each interval of incident angle, and is displayed in dB.

6.4 Feature extraction

As discussed in Section 6.2, a variety of features has been proposed for seafloor type classification from backscatter data. Classical image-based features extracted from sonar mosaic are simple to compute but the spatially-irregular sampling associated with multi-swath acquisition geometry makes this method poorly relevant to investigate a joint analysis of across-track and along-track modes. We propose here features which can be extracted directly from irregularly-sampled point sets. Two types of features have been investigated:

- Point-wise statistical features (e.g., local mean and variance of the BS data);
- Textural features, namely Histograms of Oriented Gradient [58] and spatial covariance features [12]. We investigate these two types of textural features as they can be extended to irregular spatial sampling patterns, contrary for instance to other classical textural features such as cooccurrence statistics and Wavelet-based features [50, 64].

We detail in the following paragraphs how these different types of features are computed.

For both along-track and across-trackinsonification modes, we assume that each elementary backscatter information x is composed of a geographical position \mathbf{s}_x , an incident angle θ_x and a backscatter strength BS_x . We denote by p a pixel onto a reference seafloor grid \mathcal{G} . As highlighted in the previous section, the grid pixel size for the along-track mode, denoted by \mathcal{G}^{ALT} , is 5m, whereas the grid pixel size for the across-track mode, denoted by \mathcal{G}^{AcT} , is 2m. Let us denote by $\mathcal{N}_{p,r}^{ALT}$ (resp. $\mathcal{N}_{p,r}^{AcT}$) the set of elementary data associated with a given pixel p of the along-track (resp. across-track) seafloor grid \mathcal{G}^{ALT} (resp. \mathcal{G}^{AcT}) such as:

$$\mathcal{N}_{p,r}^{ALT} = \{x \text{ such that } \|\mathbf{s}_x - \mathbf{s}_p\| \leq r/2\} \quad (6.1)$$

with r a scalar value set to the resolution of the seafloor grid (i.e., 2m for the across-track mode). The same definition holds for the along-track mode with $r = 5\text{m}$. We may emphasize that the differences in the acquisition geometry of the along-track and across-track modes result in differences between the associated pixel-wise datasets. An along-track dataset at pixel p , $\{\mathbf{s}_x, \theta_x, BS_x, \forall x \in \mathcal{N}_{p,r}^{ALT}\}$, involves on average 12500 BS data covering the entire angular range from -60° to 60° . By contrast, a across-track dataset $\{\mathbf{s}_x, \theta_x, BS_x, \forall x \in \mathcal{N}_{p,r}^{AcT}\}$ results on average in 400 BS data corresponding only to two different angular sectors. In the subsequent, we drop the exponents ALT and AcT when referring to any of the two acquisition modes.

6.4.1 Point-wise statistical features

Following previous studies [3, 37, 68], we consider as point-wise statistical features the BS mean and variance denoted respectively by \mathbf{f}_p^m and \mathbf{f}_p^V for a given grid pixel p . For a given dataset $\{\mathbf{s}_x, \theta_x, BS_x, \forall x \in \mathcal{N}_{p,r}\}$, we compute angular-dependent mean and variance statistics as follows:

$$\mathbf{f}_p^m(\theta) = \frac{1}{\#(\mathcal{N}_{p,r,\theta})} \sum_{x \in \mathcal{N}_{p,r,\theta}} BS_x \quad (6.2)$$

$$\mathbf{f}_p^V(\theta) = \frac{1}{\#(\mathcal{N}_{p,r,\theta})} \sum_{x \in \mathcal{N}_{p,r,\theta}} (BS_x - \mathbf{f}_p^m(\theta))^2 \quad (6.3)$$

where $\#(\mathcal{N})$ is the number of data inside the neighbor region \mathcal{N} and $\mathcal{N}_{p,r,\theta}$ is a subset associated with mean angle θ :

$$\mathcal{N}_{p,r,\theta} = \{x : |\mathbf{s}_x - \mathbf{s}_p| < r/2, |\theta_x - \theta| < d\theta\} \quad (6.4)$$

with $d\theta$ an angular offset, typically set to 1° .

6.4.2 Histogram of Oriented Gradients

HOG feature is among the state-of-the-art image features for computer vision applications [11, 57, 58]. For our purpose, we have extended the extraction of HOG features to spatially-irregularly-sampled datasets. HOG feature basically relies on the computation of point-wise statistics for gradient vectors. Therefore, the key aspect here is the computation of point-wise gradients. Given

the very limited along-trackinsonified coverage of the longitudinal mode, no such local gradient measures can be defined for this mode. Hence, HOG features only apply to the dataset associated with the bathymetry mode.

To derive local gradients from the irregularly-sampled datasets, we have adopted the following method : for data x at position s_x , the gradient relates to a local linear first-order approximation of the backscatter map around position \mathbf{s}_x , such that gradient ∇x minimizes the following least-square criterion:

$$\nabla BS_x = \underset{\mathbf{g}}{\operatorname{argmin}} \left(\sum_{x_i \in \mathcal{N}_{x,r,\theta}} (\langle \Delta \mathbf{s}_{x_i}, \mathbf{g} \rangle - \Delta BS_{x_i})^2 \right) \quad (6.5)$$

where $\Delta \mathbf{s}_{x_i}$ is distance between the data sample x_i in the data x neighborhood $\mathcal{N}_{x,r,\theta}$ to the its position \mathbf{s}_x , ΔBS_{x_i} is the backscatter difference between the data sample x_i and the average backscatter level in the data neighborhood. By denoting $\Delta \mathbf{s}$ (resp. ΔBS) the ensemble of distance (resp. backscatter difference) of all data in the neighborhood, gradient ∇BS_x is given by:

$$\nabla BS_x = (\Delta \mathbf{s}^T \cdot \Delta \mathbf{s})^{-1} \cdot \Delta \mathbf{s}^T \cdot \Delta BS \quad (6.6)$$

This extraction is applied to measure the gradient datasets of acquisition data in the bathymetry mode $\nabla BS^{(AcT)}$. In this process, we suppose that all data in the neighborhood are from the same incident angle as the center x (θ_x).

Given the extracted gradient datasets $\nabla BS^{(AcT)}$, we follow [11] to extract rotation-invariant HOG features. We proceed according to the following 5 steps:

1. All gradients in the pixel's neighborhood $\mathcal{N}_{p,r,\theta}$ are rotated with respect to the main direction $\theta_{p,\theta}$ estimated as:

$$\theta_{p,\theta} = \angle \left(\sum_{x \in \mathcal{N}_{p,r,\theta}} \nabla x \right) \quad (6.7)$$

2. For each pixel, all data in the neighborhood is grouped into 4 cells on the top-left, top-right, bottom-left, bottom-right.
3. In each cell, the data is grouped again into 18 even sectors from 0° to 340° through its gradient direction.
4. For each sector $\mathcal{N}_{p,r,\theta}^{sec}$, we extract a representing value $\mathbf{f}_{sec,\theta}^{HOG}$ implying the variation in this direction from the data's BS changing and position.

$$\mathbf{f}_{sec,\theta}^{HOG} = \sum_{x \in \mathcal{N}_{p,r,\theta}^{sec}} w_{\mathbf{s}_x} \cdot |\nabla x| \quad (6.8)$$

where $w_{\mathbf{s}_x} = \exp(|\Delta \mathbf{s}_x|/r)$ is the weight applied on the distance from data x to the pixel's center.

5. Extracted feature is normalized for each cell to obtain a similar measure of directional influence.

6.4.3 Covariance feature

Covariance-based features are also among the state-of-the-art features for numerous computer vision applications, including texture recognition [69] and object recognition [12]. Interestingly, spatial covariance features naturally apply to irregularly-sampled datasets, as investigated in [69] for keypoint sets. We proceed in the same way for the raw backscatter datasets associated with each grid pixel. More precisely, we consider isotropic covariance features for K different radius values $\{\lambda_k\}_{1,\dots,K}$. We typically consider radius values $\lambda_k = k.d$ with $d = 0.5m$. The k^{th} covariance feature at pixel p is estimated as:

$$\mathbf{f}_p^{cov}(k, \theta) = \frac{1}{\#(\mathcal{N}_{p,\theta}(k))} \sum_{(x_1, x_2) \in \mathcal{N}_{p,\theta}(k)} (BS_{x_1} - \mathbf{f}_p^m(\theta))(BS_{x_2} - \mathbf{f}_p^m(\theta)) \quad (6.9)$$

$$\mathcal{N}_{p,\theta}(k) = \{(x_1, x_2) | x_1, x_2 \in \mathcal{N}_{p,r,\theta}, |\mathbf{s}_{x_1} - \mathbf{s}_{x_2}| \in [0, k.d]\} \quad (6.10)$$

$$(6.11)$$

As opposed to the HOG features, this covariance feature can be computed for the two acquisition modes as it relies on the computation of isotropic statistics over pair of points within a given spatial range.

6.5 Evaluation

6.5.1 Experimental setup

Using the ground-truth survey data described in Section 6.3.2, we performed a quantitative evaluation of the proposed features for the considered three-class classification problem. Our dataset is composed of three areas: a $200m \times 200m$ dense posidonia area, a $100m \times 100m$ sparse posidonia area and a $150m \times 200m$ sand area. For each region, we have extracted pixel-level features for each mode as follow:

Bathymetry mode (Across-track swath): The resolution r for the definition of pixel-level datasets is set to $2m$. We disregard incident angles between -5° to 5° (i.e., nadir observation) as the associated backscatter information is known to be weakly discriminative. For the computation of pixel-level gradients, we first apply a low-pass filter to each ping to reduce the resolution along the across-track axis to $1m$, to make it consistent with the spatial resolution of the along-track data. For the spatial covariance, we set the reference distance parameter to $d = 0.5m$ and parameter K to 4. The later allows us to evaluate both intra-ping statistics (k values of 1 and 2) and inter-ping statistics (k values of 3 and 4) given the mean inter-ping distance of $1m$. We have extracted a dataset of 67000 feature vectors for the dense posidonia region, 24000 for the sparse posidonia region and 16000 for the sand region.

Longitudinal mode (Along-track swath): In this mode, we consider for each pixel an angular range from -40° to 40° and seafloor grid resolution of $5m$, $r = 5m$. All features are computed using a 2° angular sector. Parameter K for the covariance features is set to 11 to match the reference distance $d = 0.5m$. We have extracted a dataset of 1200 features for the dense posidonia region, 300 for the sparse posidonia region, and 500 for the sand region.

Table 6.2 – Classification rate on the features extracted from bathymetry mode with RF

	\mathbf{f}^n	\mathbf{f}^V	\mathbf{f}^{HOG}	\mathbf{f}^{cov}	$PCA\mathbf{f}^{HOG}$
Nb. of Comp.	(1)	(1)	(72)	(4)	(59)
DP	93.13	92.18	99.56	92.30	99.14
SP	52.33	43.75	00.29	43.56	00.34
S	81.04	75.50	09.42	75.26	11.61
Overall*	82.19	78.86	64.93	78.86	64.29

*:weighted average of classification rate on all types of sediments

6.5.2 Seafloor classification performance

We evaluate the classification performance of the proposed features using a cross-validation procedure. We repeat 100 times a random split of the dataset into a training dataset (accounting for 75% of the data) and test base (accounting for the remaining 25%). Overall, we compute mean correct classification rates and their standard deviations. Following [70], we considered random forest (*RF*) as the reference classifiers. Among the state-of-the-art classifiers, *RF* classifiers provide simple and efficient means for fusion purposes between the two acquisition modes [70]. Experiments were carried out with random forests composed of 100 trees using the squared-root of the number of feature dimension as number of variables for each decision split and a bootstrap rate of 0.5.

6.5.2.1 Bathymetry mode

In this mode, for each pixel, the system gives an incident angle. Therefore, the incident angle should be considered as a feature $\mathbf{f}_p^{(IA)}$ along with the considerate features \mathbf{f}_p^c , and the analyzed features \mathbf{f}^e should have the form of $\mathbf{f}^e = [\mathbf{f}_p^{(IA)}, \mathbf{f}_p^c]$. To reduce the dimension of the feature $\mathbf{f}^{(HOG)}$ we apply a principle component analysis (PCA) reduction method: The first components corresponding to 90% of variance have been selected. The cross-validation test is displayed in Table 6.2.

Dense posidonia The classification works well for this class. Especially, its recognition rate is always better than the weighted average rate of all classes. This is due to the fact that the number of samples of dense posidonia in the validation database is much greater than the other classes. Therefore, the classifier is more adapted to this class.

Sparse posidonia This class has poorest result in the test and is confused to dense posidonia in most cases. This is consistent with the similarity measure (similarity measure - blue line in Figure 6.8).

Sand On this class, the classification rate obtained doesn't differ from the weighted average rate. In Section 6.3.2.2, the similarity measure criteria have shown that the data of this class is discriminant from the rest (red and green line in Figure 6.8). Therefore, even though the number of samples is low, the classifier is able to create a discriminant model for this class. The classification rate given by the feature \mathbf{f}^{HOG} is very poor. The features \mathbf{f}^{HOG} should be able to extract textural informations. But since the system resolution is too small, no textural information is present and this kind of feature is not discriminant. Classifier predicts to the class having the greater number of samples in the database: dense posidonia.

Table 6.3 – Cross-Validation test on the components of feature \mathbf{f}^{cov} extracted from bathymetry mode with RF

	Comp. 1	Comp. 2	Comp. 3	Comp. 4	\mathbf{f}^{cov}
DP	86.76	86.35	85.84	85.97	93.77
SP	25.03	21.535	19.82	21.09	34.64
S	63.88	61.40	54.27	57.76	74.14
Overall*	69.53	68.12	66.39	67.26	78.95

*:weighted average of classification rate on all types of sediments

Table 6.4 – Cross-Validation test on the combination of features extracted from bathymetry mode with RF.

\mathbf{f}^c	$[\mathbf{f}^m, \mathbf{f}^V]$	$[\mathbf{f}^m, \mathbf{f}^{HOG}]$	$[\mathbf{f}^m, \mathbf{f}^{cov}]$	PCA($[\mathbf{f}^m, \mathbf{f}^{HOG}]$)
Nb. of Comp.	(2)	(73)	(5)	(59)
DP	94.60	97.65	95.79	99.27
SP	58.44	39.45	59.05	04.22
S	82.65	71.39	82.53	51.80
Overall*	84.71	80.73	85.59	70.98

*:weighted average of classification rate on all types of sediments

Covariance feature We look at the feature \mathbf{f}^{cov} by analyzing the contribution of their components. The cross-validation result is displayed in Table 6.3 for each component as well as for the combination of them. It points out that the first two components give slightly better discriminant information than the others two. This could be explained by the fact that these first two components are computed from the data on the same ping and, therefore, are more consistent against navigation uncertainty. We also observed that the combination of the four components give a better result. In fact, these four components catch complementary information: the two first components catch information inside the same ping (intra-ping information) and the two other on successive pings (inter-ping information) which make their combination better.

Synthesis In order to select the best set of features for this mode, we go through the contribution of each feature onto the classification performance via Table 6.2. We find that the statistical features give better performance (84.77% for the feature \mathbf{f}^m , and 81.79% for the feature \mathbf{f}^V) than the textural features in our database. The PCA of this textural feature doesn't give a better performance. As explained before, the system resolution is not enough to reveal textural pattern that should be measured with *HOG*. As a result, we choose feature \mathbf{f}^m for the main discriminant feature for our database.

Additionally, we have analyzed if the combination of the features gives a better result, especially between the statistical features and the textural features. The test is applied on the combination of selected feature \mathbf{f}^m with the others, and the results are displayed in Table 6.4. We find a good improvement while combining these features, especially between feature \mathbf{f}^m and feature \mathbf{f}^{cov} . Even the contribution of textural features isn't important in our dataset; it still can be used to improve the classification rate. In conclusion, we select the combination between feature \mathbf{f}^m and feature \mathbf{f}^{cov} as the features for bathymetry mode.

Table 6.5 – Cross-Validation test on features extracted from longitudinal mode with RF

	\mathbf{f}^m	\mathbf{f}^V	\mathbf{f}^{cov}
DP	99.93	99.77	99.88
SP	95.77	90.79	68.51
S	100.00	100.00	100.00
Overall*	99.23	98.28	94.48

*:weighted average of classification rate on all types of sediments

Table 6.6 – Cross-Validation test on the combination of features extracted from longitudinal mode with RF

	$\mathbf{f}^m + \mathbf{f}^V$	$\mathbf{f}^m + \mathbf{f}^{cov}$	$\mathbf{f}^m + \mathbf{f}^V + \mathbf{f}^{cov}$
DP	99.92	99.91	99.93
SP	95.43	93.67	93.68
S	100.00	100.00	100.00
Overall*	99.16	98.86	98.87

*:weighted average of classification rate on all types of sediments

6.5.2.2 Longitudinal mode

In this mode, a pixel is represented by a set of features computed on different angular sector spanning an overall interval of -40° to 40° (feature profiles). The angular dependence is, therefore, taking account with the choice of the angular sectors, and is expressed through the relation between the sectors. The cross-validation test is realized first using each feature separately (Table 6.5) and then using combination of features (Table 6.6).

Dense posidonia We find better classification rate w.r.t other classes as in Section 6.5.2.1. Moreover, the very high rate obtained gives a proof of the importance of backscattering profile in the seafloor discrimination.

Sparse posidonia In this class, we get much better result with the backscatter profile, despite the small discrimination between dense posidonia and sparse posidonia. The statistical features still works better compare to covariance feature.

Sand As opposed to Section 6.5.2.1, this class gives the best result. It is understandable because its backscatter profile is very different from the posidonia’.

Synthesis The statistical feature profiles give better performance for this mode comparing to those from bathymetry mode. The result shows a near 100% classification rate with the feature profile \mathbf{f}^m . However, the combination between this feature profile with the others doesn’t improve the classification rate and especially the combination with the feature profile \mathbf{f}^{cov} . This could be explained via Random Forest classifier principle. Because this classifier selected randomly number of dimension in the considering features, the components of feature profile \mathbf{f}^{cov} have much more possibility to be chosen due to its large size (11 times more number of dimension than the others). Therefore, it has more influence in the combination of feature profiles.

We also test the dimension-reduction version of these feature profiles in Table 6.7. Each dimension of the profile is normalized (mean of 0, and variance of 1). The PCA is applied on the

Table 6.7 – Cross-Validation test on the the principle components analysis of features extracted from longitudinal mode with RF

	\mathbf{f}^m	\mathbf{f}^V	\mathbf{f}^{cov}	$\mathbf{f}^m + \mathbf{f}^V$	$\mathbf{f}^m + \mathbf{f}^{cov}$	$\mathbf{f}^m + \mathbf{f}^V + \mathbf{f}^{cov}$
*	(17)	(28)	(229)		(233)	(235)
DP	99.75	99.36	99.01	99.53	99.53	99.60
SP	94.18	88.70	77.34	97.14	92.35	91.77
S	100.00	100.00	99.44	99.96	99.80	99.84
Overall**	98.86	97.69	95.37	99.23	98.36	98.31

*:number of components using in classification

** :weighted average of classification rate on all types of sediments

normalized profile, and the number of components of 90% variance is selected for the test. The result shows a good compromise between the number of components and the classification rate. However, since the classification rate obtained using the feature \mathbf{f}^m is almost perfect and much more simple to calculate, we keep the feature \mathbf{f}^m as the best choice. Besides, we see again the influence of the feature \mathbf{f}^{cov} onto the classification rate.

In conclusion, we select the statistical feature \mathbf{f}^m , which gives

- Nearly 100% classification rate.
- Reasonable number of dimension (40).
- Simplicity in processing.

6.5.3 Seafloor segmentation

The cross-validation tests have shown that the best choices of features are:

- In the bathymetry mode: the combination of the statistical feature \mathbf{f}^m and the covariance feature \mathbf{f}^{cov} .
- In the longitudinal mode: the \mathbf{f}^m profile.

In this section, we will generate a preliminary classification map of the survey area using the selected features. The features are extracted separately for each acquisition mode and for each survey line. So, in bathymetry mode, only one incident angle is available for each pixel since line overlap is not taken into account. A classification results is computed on each survey line separately, and for each functioning mode. In bathymetry mode, the classification results are fused on overlapped survey line. We choose a simple VOTE method [71, 72]. The result is displayed in Figure 6.9 by superposing the result of longitudinal mode in nadir and of bathymetry mode in the rest.

The result shows a good matching between the backscatter mosaic image and the classification results with a good consistency between the two modes'. Figure 6.9a shows the classification of one line via random forest. The result matches with the bathymetry mode's mosaic for both modes, which confirms our choice of features. In Figure 6.9b, method VOTE combines the classification results on two overlapped survey lines. This fusion slightly improve the results by removing some mistakes in the classification done each separate line. Figure 6.9c displays the result on the whole acquisition zone via method VOTE. We find some differences between the classification result and the ground truth data at the bottom of the area (sparse posidonia .vs sand) and in the sand

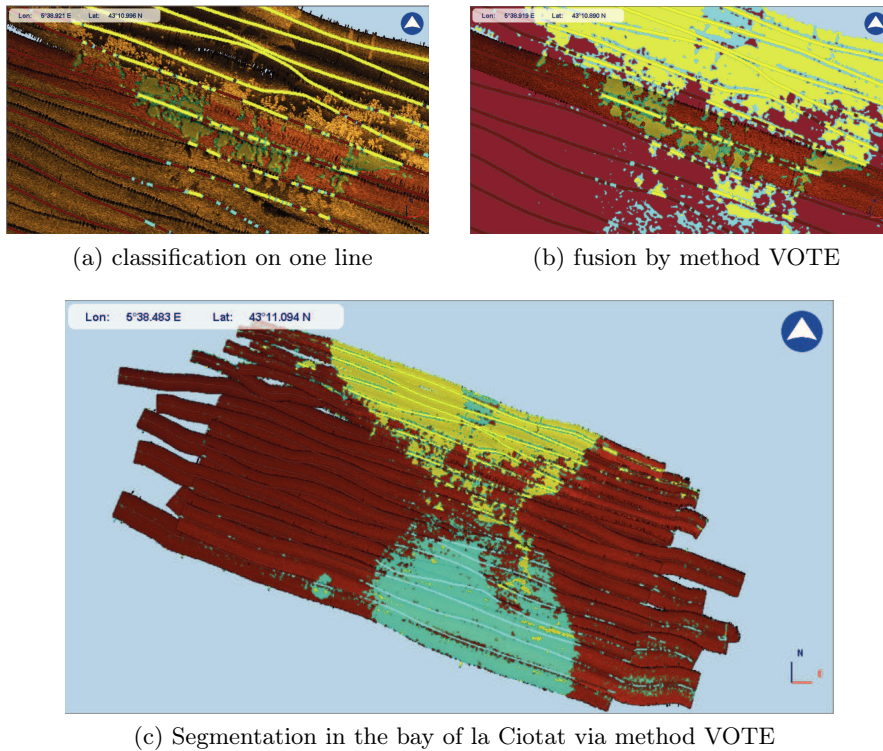


Figure 6.9 – Segmentation in the bay of la Ciotat, France: dense posidonia (brown), sparse posidonia (blue) and sand (yellow). Figure 6.9a shows the classification on one line by random forest while Figure 6.9b shows the result on the same zone by fusing the classification’s result from different lines via method VOTE. Figure 6.9c displays the result of method VOTE on the whole acquisition zone.

zone at the top (video 18: sand (longitudinal mode)/ sparse posidonia (bathymetry mode) .vs sand) of Figure 6.3. Indeed, these zones contain different types of sediment not included in the training dataset (sand with large ripple, *Caulerpa* abundance).

6.6 Conclusion and perspectives

In this study, we have explored the potential of a multi-swath MBES for seafloor classification. Among the entire possibleinsonification scenarios, we have focus our analysis on the scenario where the two orthogonal swath, along and across track swath, are alternatively emitted. These two modes give complementary seafloor backscattering strength measurements. On the conventional across track swath, the system delivers, for each pixel, the BS level for a very few incident angles but on a wide coverage. Furthermore, a full high resolution mosaic image can be constructed on which textural feature could be extracted. On the along-track swath, the system locally measures a full BS profile which is known to be a very effective discriminating feature, but only for pixels on the vessel trajectory. We have first checked that the BS levels are consistent between the two operating modes (bathymetry and longitudinal). Then, we have evaluated statistical and textural features by a cross validation test on a reference survey area. We have developed method to extract textural features (HOG) directly on the raw irregular sample space rather than on a regular mosaic image. This method ensures that the textural features extracted

are more robust to the interpolation process and navigation uncertainty. In our reference dataset, no evidence of textural pattern was found. This is mainly due to the medium emission frequency ($150kHz$) and the limited aperture angle ($\pm 50^\circ$) of the MBES system and seabed type. Nevertheless, our evaluation has clearly demonstrated that the best features are:

- Features from the along-track swath data and especially the mean BS .
- In across-track swath, the combination between the feature of mean BS \mathbf{f}^m and of spatial covariance \mathbf{f}^{cov} .
- In along-track swath, the profile of feature \mathbf{f}^m .

In along-track swath mode, the profile features offers a classification rate at nearly 100%. We check also that this feature is very stable. So it may be used further to extract seafloor geophysical coefficient using classical inversion models (Jackson [2]). In across-track swath, we have begun to explore a simple VOTE method to fuse classification results on overlapped survey line. Current researches are devoted to the development of intra-mode (over overlapped survey lines) and inter-mode fusion methodologies.

Fusion of MS MBES system data for seafloor classification

Released from 2010, SEAPIX is a multi-swath multi-beam echo sounder (MS-MBES) system. It offers different operating modes to acquire information not only from along-track swath (bathymetry mode), but from along-track swath (longitudinal mode) as well. Studies in Chapter 4 showed the consistency of different modes' data and their potential for seabed classification. After testing different types of features in Chapter 6, the combination of the mean backscattering strength f^m and of the spatial covariance was proven as the best choice for the data of the bathymetry mode in the terms of classification performance. For the longitudinal mode, the mean backscatter profile arised as the best feature. In this chapter, we address the exploitation and combination of these multi-mode features seabed classification and segmentation. We first focus on the classification based solely on each operating mode in order to evaluate the relative performance of each mode, as well as to benefit from the spatial redundancy due to the overlap between different swaths. The resulting approach is referred to as an intra-mode fusion. A second approach explores the combination of the two modes and is referred to as an inter-mode fusion.

7.1 Introduction

Seafloor classification is a popular topic in oceanography studies such as environment observation, industrial commercial, etc. [3–6, 8, 9]. In the context of fishery market, iXBLUE aims to develop the acquisition of habitat maps, which describes the distribution of the seafloor sediments. Such habitat maps are for interest for fishermen both for security issues (e.g., the detection of rocky areas for bottom-trawler) and for improved fishing search strategies.

In literature, seabed classification and mapping has been addressed using different types of acoustic systems as briefly reviewed in Chapter 2: especially, single-beam echo sounder (SBES), multi-beam echo sounder (MBES), side-scan sonar (SSS). In the first type of system, studies focused on the classification of time series acquired only on the vessel trajectory [17, 47]. By contrast, the two latter ones broadened the coverage zone and exploited backscattering strength (BS) data acquired for the insonified zone under the form of mosaic. The classification was generally based on some textural analysis in the mosaic [8–10] or on the angular dependence of the backscatter data with respect to the incident angle [5–7, 16, 23, 24, 59].

Since 2010, iXBLUE has been releasing its own MBES system. As detailed in Section 2.3, it was constructed based on two emission/reception antennas positioned in the Mills Cross structure. These antennas could not only exchange their roles, but also be used to form the beams in different directions including fore/aft, port/starboard, and known as a multi-swath MBES. As a result, this system is able to select the insonified swaths: nadir across-track swath, along-track swath, frontal across-track swath. It could provide not only information as a classical MBES

system, but also supplement information of the seafloor from different incident angles. Designed for fishery market, it aims to provide the best trade-off between hardware cost and performance level in seafloor backscatter imagery and characterization.

Chapter 6 analyzed the discriminative power of the different swaths. The along-track swath was shown to reach greater classification performance along the vessel trajectory, whereas the across-track swath provides a greater spatial coverage. We, therefore, propose here to combine multi-swath data. We aim to enhance seabed classification, while benefiting of the maximal spatial coverage. We develop the fusion of multi-swath data from one type of swath (intra-mode fusion) and from the two acquisition models (inter-mode fusion). As detailed below, the intra-mode fusion relies on a consensus method [73], whereas the inter-mode fusion is stated as a variational inverse problem.

The chapter is organized as follows. Section 7.2 states the considered issues. The fusion methods are described in Section 7.3. The application and evaluation of these methods onto real datasets is reported in Section 7.4.

7.2 Problem statement and related work

In this paper, we aim to exploit the new multi-swath MBES system SEAPIX in seafloor classification. We detail below the different issues to be dealt with. First, as a standard MBES system, SEAPIX can insonify the seafloor with a large spatial coverage (about 80m at a 30m depth for a typical 120° angular aperture). With an important overlap rate (50% in our case), there is a superposition between different acquisition lines. Hence, the first question to address is the fusion of spatially overlapping data.

The second issue to be dealt with is the fusion of the data from the longitudinal and bathymetry acquisition modes. The mean BS profile acquired within the longitudinal mode was showed to better discriminate seabed types than the information acquired in the bathymetry mode (the operating of standard MBES system) in Chapter 6. The limitation of the longitudinal mode is on its limited coverage range (the longitudinal (resp. bathymetry) mode offers a 5m (resp. 80m) swath with 12500 (resp. 400) samples on each pixel at a 30m depth). The combination of the data acquired by the longitudinal and bathymetry modes naturally arise as a promising solution. The difference in the acquisition geometry makes this inter-mode fusion challenging. Whereas seabed classification is in general carried out for some predefined seabed pixel grid for the bathymetry mode, typically the grid of the constructed mosaic, the longitudinal mode simply resorts to classification outputs onto the trajectory of the vessel projected onto the seabed. The latter does not require any predefined seabed pixel grid. As detailed in the next section, the proposed variational setting provides a generic framework to combine these two acquisition geometries.

Following the analysis reported in Chapter 6, we consider the following features for each acquisition mode:

- bathymetry mode: the mean incident angle, the mean BS level and the spatial covariance within each grid cell (features \mathbf{f}^m and \mathbf{f}^{cov} in Chapter 6);
- longitudinal mode: the mean angular-dependent BS profile within trajectory points (feature \mathbf{f}^m in Chapter 6).

Numerous seabed classification methods have been investigated in the literature for a standard MBES. They were categorized with respect to the type of information used for classification: BS level at some incident angle [16, 23, 24], BS profile [5–7, 59], or textural features [8, 10]. The

first category exploits the dependence of the *BS* level with respect to the incident angle by constructing angular-dependent models [9, 16, 23, 24]. The classification was realized from the evaluation of class-specific models for the incident angle from which a given pixel had been insonified. For instance, in [24], statistical models were considered, so that the classification can be stated within a Bayesian framework. A second category exploits *BS* profiles to take advantage of the angular dependence of the *BS* level over the entire angular range. The classification may rely on the *BS* profile itself [5, 6] as well as on derived heuristic or geo-physical parameters [7, 59]. The construction of this *BS* profile generally relied on a homogeneity hypothesis for the whole insonified swath [6, 7, 59]. Specific systems, for example forward-looking sonar system in COSMOS project [18], or SEAPIX system considered in this work, has also been designed to acquire such *BS* profiles from nadir backscatter data over successive time steps. A third category of approach considers textural features. They mostly resorted to texture-based features introduced in the computer vision literature, such as co-occurrence-based, Gabor or wavelet features [8, 51, 74, 75]. One may also categorize seabed classification with respect to the considered classification schemes. Whereas Bayesian frameworks have been among the most popular ones [6, 23], including naive Bayes classifiers as well as Markovian and variational schemes [4, 51, 76], machine learning strategies, such as SVM (Support Vector Machine) and random forest [9], have also been considered. Similarly to image segmentation issues, Bayesian models using regularization priors [3, 4] were in general leading to improved classification performance.

Data fusion arises as a critical issue in a variety of domain. In his review [77], F. Castanedo sorted data fusion issues into three principal categories (data association, state estimation, and decision fusion). Regarding seafloor classification, the fusion may be achieved at two levels: data fusion and decision fusion. In the first level, the fusion aims to build a unique dataset from different data sources. This process generally used data association methods to group the data in a pixel, and state estimation methods to remove redundant information, or to extract pixel-level features. The classification could then be achieved from this feature space [78–80]. In the second level, different classifications are issued from each data source and the fusion aims to fuse different classification outputs to build the final classification. This fusion generally takes into account the uncertainty associated with each data source. Therefore, these methods principally worked on associating the decisions, or their uncertainty on the sources' information, which belongs correspondingly to the level 3 (impact assessment/ threat refinement), and the level 2 (situation assessment/ situation refinement) and in the Joint Directors of Laboratories (JDL) data fusion model [81]. Voting procedures may be regarded as simple decision fusion schemes falling into this category, as considered in most of applications [82–85].

To better exploit the characteristics of each data source and decision uncertainties, different theories may be considered, including probability theory, belief theory and possibility theory [83]. In probability theory, target is hypothesized to belong to a unique class, and decision uncertainties are expressed via probability functions [86, 87]. The belief theory, however, extends this hypothesis by stating that a target could belong to several classes, and the uncertainties are introduced via mass functions [88–90]. The possibility theory generalizes the hypothesis that a target could belong to any class, and the belonging degrees are described via possibility functions [83]. Besides, different methods revolving on a weighted-based optimization [73, 91] were also introduced in order to combine with these techniques. In the context of seabed classification using data from different acoustic systems, one may cite [92], which addressed the fusion of SBES and SSS data. However, this study only considered nadir data, the nadir zone being the only zone where the two data sources were jointly available.

In our study, data fusion to build a unique dataset prior to applying a classification model does not appear relevant. With the overlap rate of 50% during the acquisition campaign, most

seafloor pixels were insonified twice under 2 arbitrary incident angles from the bathymetry mode. Fusing BS data from two arbitrary incident angles does not make sense. By contrast, we may achieve elementary classifications based on each BS information and then fuse them to deliver a pixel-level classification. For this intra-mode fusion, we rely on the inference of classification probabilities for individual backscatter data, formed by an incident angle and a mean BS level. Following [73], the fusion rule is stated as a weighing of classification probabilities over observed incident angles. We investigate both the optimization scheme proposed in [73] as well as a SVM-based formulation. Section 7.3.2 details this fusion scheme.

The inter-mode fusion involves a different issue. By nature, for a given area, only few seabed pixels comprise backscatter data from the longitudinal mode. For such pixels, the BS profile provides a classification with a much lower uncertainty than the bathymetry mode, lowering the interest of a fusion. Hence, the challenge of the inter-mode fusion is rather the ability to transfer low-uncertainty pixel-level classification outputs from the longitudinal mode to seabed pixels where only BS data from the bathymetry mode are available. The proposed fusion scheme relies on a variational level-set segmentation framework extended from [51, 93]. This approach is presented in Section 7.3.3.

7.3 Proposed approach

This section details the proposed intra-mode and inter-mode fusion schemes. They aim to generate the classification on the whole acquisition zone Ω , which is composed of different types of sediments Ω_j . Let us denote by p a pixel onto a reference seafloor grid \mathcal{G} . As in Chapter 6, the seafloor grid for the longitudinal mode, denoted \mathcal{G}^{AIT} , involves a 5m resolution, whereas the seafloor grid for bathymetry mode, denoted \mathcal{G}^{AcT} , involves a 2m resolution. The information extracted for a pixel p depends on the operating mode, and is denoted by x^{AcT} (resp. x^{AIT}) for bathymetry mode (resp. longitudinal mode). Besides the different feature extracted from these modes, the differences in their acquisition geometries also result in different numbers of pixel-level information. The dataset from the bathymetry mode involved for a given pixel information on only 2 incident angles while the longitudinal mode delivers a backscatter profile over the entire angular range of incident angles. We divide this angular range into the angular sectors of size 2° (corresponding to average aperture of SEAPIX system), and let us denote by ϑ the ensemble of these sectors ϑ_i , each is defined as

$$\vartheta_i = \{\theta \mid |\theta - \theta_i| \leq 1^\circ\} \quad (7.1)$$

where θ_i is even distributed from -60° to 60° . With a view to use common notations to the two modes, we introduce the following definition for data $x^{(AcT)}$ from the bathymetry mode:

$$x^{(AcT)} = \begin{cases} \mathbf{f}^{(AcT)} & \text{if } \exists \theta_i \\ NaN & \text{if } \nexists \theta_i \end{cases}$$

where i refers to angular sector index from which feature $\mathbf{f}^{(AcT)}$ was extracted, and θ_i the representing angle value of the angular sector.

7.3.1 Elementary classification models

This section presents the probabilistic models used to provide elementary pixel-level classifications. We exploit here 2 models: Bayesian and Random Forest (RF), which are capable of turning the acquired information into a probabilistic decision. While the first method stands for

a standard classifier, the latter one was verified as a state-of-the-art method which provided a performance result for the decision fusion [70]. Moreover, *RF* method was used to evaluate the selected features in Chapter 6, so it is expected to bring a better performance.

7.3.1.1 Probability approach

In a Bayesian framework, we exploit Gaussian mixture models to describe the angular-dependence *BS* data in logarithmic scale [37]. This model was verified to fit the MS-MBES's *BS* data in Chapter 4. Besides, it is also capable of representing the features of spatial covariance in the bathymetry mode.

Like [37], angular-dependence probabilistic model is constructed for each angular sector ϑ_i as a combination of Nf independent features.

$$\mathbb{P}_{\vartheta_i}(x^{(AcT)}|C) = \begin{cases} \prod_{k=1}^{Nf} \mathbb{P}_{\vartheta_i}(f_k^{(AcT)}|C) & \text{if } x^{(AcT)} \neq NaN \\ NaN & \text{if } x^{(AcT)} = NaN \end{cases}$$

We remind that we independently perform the classification on each acquisition line. Therefore, for the bathymetry mode, a seafloor pixel $p^{(AcT)}$ is insonified from only 1 incident angle belonging to the angular sector $\vartheta(x_p^{(AcT)})$. In this mode, the extracted features are the combination of mean \mathbf{f}^m and spatial covariance \mathbf{f}^{cov} (Section 7.2), that is to say $Nf = 5$. The probabilistic term (classification uncertainty) of the pixel p in the bathymetry mode is expressed as

$$\mathbb{P}_{\vartheta_i}(C_j|x_p) = \begin{cases} \frac{\mathbb{P}_{\vartheta_i}(x_p|C_j)}{\sum_k^{Nc} \mathbb{P}_{\vartheta_i}(x_p|C_k)} & \text{if } \mathbb{P}_{\vartheta_i}(x_p|C_j) \neq NaN \\ 1 & \text{if not} \end{cases}$$

$$\mathbb{P}^{(AcT)}(C_j|x_p^{(AcT)}) = \mathbb{P}_{\vartheta(x_p^{(AcT)})}(C_j|x_p^{(AcT)}) \quad (7.2)$$

where the value 1 means that there is no contribution from the angular sector ϑ_i .

In the case of the longitudinal mode, a seafloor pixel is scanned multiple times under different incident angles to form its angular *BS* profile \mathbf{f}^m (Section 7.2). The extracted feature is a combination of independent angular sectors, which is to say $Nf = 51$ corresponding to the number of angular sectors considered in the longitudinal mode. The probabilistic term (classification uncertainty) of the pixel p in this mode is expressed as

$$\mathbb{P}^{(AIT)}(C_j|x_p^{(AIT)}) = \frac{\mathbb{P}_{\vartheta_i}(x_p^{(AIT)}|C_j)}{\sum_k^{Nc} \mathbb{P}_{\vartheta_i}(x_p^{(AIT)}|C_k)} \quad (7.3)$$

where Nc is the number of considered classes. The class determination is based on the maximum likelihood (ML) rule

$$C = \underset{C}{\operatorname{argmax}} (\mathbb{P}(C|x_p)) \quad (7.4)$$

7.3.1.2 Random Forest approach

Known as a state-of-the-art machine-learning method, *RF* also proposes a good probabilistic interpretation as an input of decision fusion methods [70]. In the study in Chapter 6, this method was used to evaluate the proposed features. Therefore, in this step, we also exploit this method for seafloor classification. We remark that the input data needs some tuning to integrate the angular-dependence in the proposed features of the bathymetry mode. As proposed in Chapter 6, we combine this mode's proposed features $\mathbf{f}^{(AcT)}$ with its acquired incident angle $x_{RF}^{(AcT)} = [\theta_i, \mathbf{f}^{(AcT)}]$.

7.3.2 Intra-mode fusion

In this section, we present the proposed intra-mode fusion schemes. We first state several remarks about our acquisition data:

- In the bathymetry mode, our survey design resulted into an overlap rate of 50%. Subsequently, most of pixels in the seafloor were scanned twice from 2 different acquisition lines under mostly 2 different incident angles.
- In the longitudinal mode, the insonified zone was limited to the vessel's trajectory. This meant there was no superposition between different acquisition lines. Consequently, the intra-mode fusion does not apply.

Consequently, the intra-mode fusion strategy will be introduced only for the bathymetry mode. In the conventional approach [79, 86], the acquisition lines are used as the sources of information because they acquired the seafloor pixels multiple times. However, it is difficult to evaluate the credibility at the scale of the acquisition lines. In this study, we define the sources of information in a different manner. Based on the dependence of BS data onto the incident angle, the sources are defined as the incident-angle sectors. This definition guarantees data separation including intra-pixel data because each data was associated with a different incident angle. Besides, the classification uncertainty strongly depends on the incident angle, providing the means for defining the credibility of the different information sources.

We divide the range of incident angles $[-60^\circ, 60^\circ]$ into N_s equal angular sectors. Following [73], the fusion of these data sources is stated within a probabilistic setting under a logarithmic form:

$$\log(\mathbb{P}(C_j|x)) = \log(\mathbb{P}(C_j)) + \sum_{i=1}^{N_s} w_i \log\left(\frac{\mathbb{P}_{\vartheta_i}(C_j|x_i)}{\mathbb{P}(C_j)}\right) \quad (7.5)$$

where

- x is the information extracted from the acquisition data in a range of $[-60^\circ, 60^\circ]$. Its element x_i is the data x_p extracted from the angular sector ϑ_i . We may remind that for a given pixel only two incident angles are truly observed.
- C_j stands for class j .
- w_i is the weight/credibility applied on angular sector ϑ_i , which describes the contribution of this information associated with this sector to the final decision.

Given the definition of such class-specific classification likelihoods, the final decision comes to maximize this posterior likelihood:

$$C = \underset{C}{\operatorname{argmax}} (\log(\mathbb{P}(C|x))) \quad (7.6)$$

In this strategy, we will leave unclassified label to a pixel whose maximum posterior likelihood is not different from the second ones.

Given elementary classification models $\mathbb{P}_{\vartheta_i}(C_j|x_i)$ for each angular sector, the key issue is the calibration of the weights $\{w_i\}$. As detailed in the next two paragraphs, we consider two strategies, one based on [73] and a SVM-based formulation.

7.3.2.1 Consensus estimation

Following [73], the calibration of the weighing factors may be stated as the following minimization issue derived from criterion (7.5):

$$\mathbf{w} = \underset{\mathbf{w}}{\operatorname{argmin}} \left(\sum_{C_j} \frac{1}{\#(C_j)} \|\mathbf{x}^{(C_j)} \mathbf{w} + \mathbf{b}^{(C_j)} - \mathbf{y}^{(C_j)}\|^2 \right) \quad (7.7)$$

where

- \mathbf{x} is a data vector of size $[Nsp, Nc, Ns]$. Its element $\mathbf{x}_i^{(C_j)}(s) = \log(\mathbb{P}_{\vartheta_i}(C_j|x_i(s)))$ express the logarithm of the normalized probability of class C_j for sample s at angular sector of index i . If an angular sector is not observed, $\mathbf{x}_i^{(C_j)}(s)$ equals 0, *i.e.* it contributes nothing to the final decision.
- \mathbf{y} is a label vector of size $[Nsp, Nc]$. Element $\mathbf{y}^{(C_j)}(s)$ is equal to 0 if it is the true class (j), and -80 if not. The choice of -80 is meant for 0 in linear scale instead of $-\inf$.
- \mathbf{w} is a weighing vector of size $[N, 1]$, which describes the contribution of each source. This vector is positive to express the source contribution to the fusion scheme.
- $\mathbf{b}^{(C_j)}$ is a bias parameter for each class.

[94] exploits a gradient-based procedure to solve for the above minimization issue. It might be noted that in our formulation we normalize the criterion with respect to the number of samples within each class with a view to taking into account imbalanced class proportions. We detail the resulting gradient algorithm in Algorithm 1. As initialization, we consider constant weighting factors. During each iteration k , weight update $d\mathbf{w}^{(k)}$ and bias update $d\mathbf{b}^{(k)}$ are issued from the error $E^{(k)}$ between the fusion result $|\mathbf{x}\mathbf{w} + \mathbf{b}|$ and the desired fusion \mathbf{y} . Besides, in order to guarantee the positiveness of vector \mathbf{w} , the weight update $d\mathbf{w}^{(k)}$ is rescaled by a factor $\beta^{(k)}$ corresponding to 10% of current pondering vector \mathbf{w} . We enforce the non-negativeness of the weights from update coefficient $\beta^{(k)}$.

7.3.2.2 Support Vector Machine approach

As criterion (7.7) resembles a linear regression fit, we may consider a margin-based alternative as exploited by Support Vector Machine (SVM). SVM has been proven to be particularly robust and efficient for a variety of machine learning issues [95]. The proposed framework may be regarded as an extension of [91]. Formally, the considered fusion issue may restated as follows:

$$\text{Hyperplane: } f(\mathbf{x}) = \mathbf{x}\mathbf{w} + \mathbf{b} \quad (7.8)$$

$$\text{Decision: } \hat{y}_i = \operatorname{sgn}(f(x_i)) \quad (7.9)$$

$$\text{Where: } \sum_{i=1}^m \alpha_i y_i = 0 \text{ and } \mathbf{w} = \sum_{i=1}^m \alpha_i y_i x_i, \quad (7.10)$$

$$\{x_i, y_i\} \text{ is the set of support vectors lying in the margin.} \quad (7.11)$$

In this classification-based setting, we can directly derive a criterion based on class labels \mathbf{y} . We do not need to introduce a finite value for $\log 0 = -\inf$ as in the previous scheme. SVM was originally designed for a binary classification. The multi-class extension of this classifier can use one-vs-one (OVO) or one-vs-all (OVA) strategies. In the OVO strategy, a hyperplane is created to discriminate each pair of classes, whereas the OVA strategy trains one classifier to discriminate

Data: bathymetry mode's data: {incident angle i , log-likelihood of probability \mathbf{x} }

Result: weight estimated for different angular sector

initialization: $w_i^{(0)} = 1/N_s$;

while iteration k **do**

1. Class C_j error $E^{(k)}$ estimation for each sample s :

$$E_j^{(k)}(s) = \left| \mathbf{x}^{(C_j)}(s) \mathbf{w}^{(k-1)} + \mathbf{b}^{(C_j)} - \mathbf{y}^{(C_j)}(s) \right|$$

2. Weight update $\mathbf{dw}^{(k)}(i) = -\frac{2}{\#(C_j)} \sum_j \sum_s \mathbf{x}_i^{(C_j)}(s) E_j^{(k)}(s)$

3. Bias update: $\mathbf{db}^{(k)}(i) = -\frac{2}{\#(C_j)} \sum_s E_j^{(k)}(s)$

4. Update coefficient: $\beta^{(k)} = \frac{\alpha}{\|\mathbf{dw}^{(k)}(i)\|_0}$, $\alpha = 0.1$

5. Update: $\mathbf{w}^{(k)} = \mathbf{w}^{(k-1)} + \beta^{(k)} \mathbf{dw}^{(k)}$, $\mathbf{b}^{(k)} = \mathbf{b}^{(k-1)} + \beta^{(k)} \mathbf{db}^{(k)}$

6. Weight normalization: $w_i^{(k)} = \frac{w_i^{(k)}}{\sum_i w_i^{(k)}}$, $\mathbf{b}^{(k)} = \frac{\mathbf{b}^{(k)}}{\sum_i w_i^{(k)}}$

end

Algorithm 1: Hybrid algorithm of estimating weight for each angular sector.

each class from all the other ones. We select here an OVA strategy. Overall, the considered SVM-based algorithm is described in Algorithm 2. In this algorithm, the hyperplane was constructed so that the predicted class corresponds to -1 , which explains the negative sign in the algorithm. For each class j , the algorithm aims to identify weighing coefficients such that

$$f^{(j)}(\mathbf{x}^{(j)}) = \mathbf{x}^{(j)} \mathbf{w}^{(j)} + \mathbf{b}^{(j)} \geq 0 \geq f^{(k)}(\mathbf{x}^{(j)}) = \mathbf{x}^{(j)} \mathbf{w}^{(k)} + \mathbf{b}^{(k)}, \forall k \neq j \quad (7.12)$$

Data: data from the bathymetry: \mathbf{x} (provided as log-likelihood of class-related probabilities)

Result: weights estimated for the different angular sectors

initialization;

for class j **do**

Training a one vs all linear SVM model for class j : $SVM_j = \mathbf{w}\mathbf{x} + \mathbf{b}$;

$\mathbf{w}^{(j)} = -\mathbf{w}$;

$\mathbf{b}^{(j)} = -\mathbf{b}$;

end

Algorithm 2: SVM algorithm for estimating weight for each angular sector.

7.3.3 Inter-mode fusion

In Chapter 6, the great performance of the longitudinal mode along with its limited spatial coverage advocates for a fusion with the bathymetry mode, which provides a much greater spatial coverage though its classification performances are not as good.

This inter-mode fusion is stated as a variational issue. The variational method was introduced for image segmentation in different studies [93, 96], including for seabed mapping [76]. The

variational segmentation iteratively evolves the contours of the spatial regions associated with each class to minimize a predefined cost function J . Formally, this minimization leads to a PDE (Partial Differential Equation). Whereas earlier schemes relied on explicit parameterization of region contours “snake” [97], “B-snake” [98,99], level-set models exploit an implicit representation of a region as the zero level-set of a scalar function defined in the image plane.

More precisely, for a region Ω , denoting the interior zone by Ω_{int} , the exterior zone by Ω_{ext} and the contour Γ by, the level-set representation is stated as follows

$$\Omega_{int} = \{\mathbf{s} \in \Omega : \varphi(\mathbf{s}) > 0\} \quad (7.13)$$

$$\Omega_{ext} = \{\mathbf{s} \in \Omega : \varphi(\mathbf{s}) < 0\} \quad (7.14)$$

$$\Gamma = \{\mathbf{s} \in \Omega : \varphi(\mathbf{s}) = 0\} \quad (7.15)$$

By introducing the functions of Heaviside $H(\cdot)$ and Dirac $\delta(\cdot)$:

$$H(x) = \begin{cases} 1 & \text{if } x \leq 0 \\ 0 & \text{if } x < 0 \end{cases}, \delta(x) = \begin{cases} 1 & \text{if } x = 0 \\ 0 & \text{if not.} \end{cases}$$

we can derive the region associated with class j as well as its contour

$$\text{Class segmentation: } C_j(\mathbf{s}) = H(\varphi^j(\mathbf{s})) \quad (7.16)$$

$$\text{Class contour: } \Gamma^j(\mathbf{s}) = \delta(\varphi(\mathbf{s})) \quad (7.17)$$

To derive continuous and derivable cost functions, we consider the following approximations as in [100]

$$H_\alpha(x) = \begin{cases} \frac{1}{2} \left(1 + \frac{x}{\alpha} + \frac{1}{\pi} \sin\left(\frac{\pi x}{\alpha}\right)\right) & \text{if } |x| \leq \alpha \\ 1 & \text{if } x > \alpha \\ 0 & \text{if } x < -\alpha \end{cases}, \delta_\alpha(x) = \begin{cases} \frac{1}{2\alpha} \left(1 + \cos\left(\frac{\pi x}{\alpha}\right)\right) & \text{if } |x| \leq \alpha \\ 0 & \text{if } |x| > \alpha \end{cases}$$

It may be noted that this level-set representation is defined over the entire image plane and does not need to be restricted to a specific resolution grid attached to one of the two acquisition modes. This property is key to the joint exploitation of longitudinal and bathymetry data. Following [76,93], the considered variational cost function J involves three terms: a data-driven term which evaluates the consistency of the available inter-mode data for each segmented region, denoted by (Ω_j) , with respect to the expected model (\mathcal{M}_j) of each seafloor class j , a regularization term based on the contour length and partition term such that the resulting level-set-based segmentation truly results in a partition of the considered planar domain. Formally, the second and third terms are similar to [76]

$$J = J_1 + J_2 + J_3 \quad (7.18)$$

$$J_2 = \sum_j^{N_c} \gamma_j |\Gamma^{(j)}| = \sum_j^{N_c} \gamma_j \int_\Omega \delta_\alpha(\varphi^{(j)}(\mathbf{s})) ds \quad (7.19)$$

$$J_3 = \frac{\lambda}{2} \int_\Omega \left(\sum_j^{N_c} H_\alpha(\varphi^{(j)}(\mathbf{s})) - 1 \right)^2 ds \quad (7.20)$$

where \mathbf{s} is the position in the considered planar domain. We adapt the data-driven term to our inter-mode setting.

$$J_1 = J_1^{(AcT)} + J_1^{(AIT)} \quad (7.21)$$

$$J_1^{(AcT)} = w^{(AcT)} \sum_j^{Nc} SM\left(\Omega_j^{(AcT)}, \mathcal{M}_j^{(AcT)}\right) \quad (7.22)$$

$$J_1^{(AIT)} = w^{(AIT)} \sum_j^{Nc} SM\left(\Omega_j^{(AIT)}, \mathcal{M}_j^{(AIT)}\right) \quad (7.23)$$

where $SM(.,.)$ expresses the similarity between the segmented region and the expected ones. In [93], this measure was proposed as the likelihoods

$$SM(\Omega_j, \mathcal{M}_j) = \int_{\Omega_j} \mathcal{M}_j(x) d\mathbf{s}_x \quad (7.24)$$

where the likelihood model was applied $\mathcal{M}_j(x) = \log(\mathbb{P}(C_j|x))$. On the other hand, [76] proposed a region-level formulation, which is independent on the acquisition geometry of the observed data:

$$SM(\Omega_j, \mathcal{M}_j) = \#(\Omega_j) \left(\sum_i^{Nf} w_i KL\left(\Omega_j^{(i)}, \mathcal{M}_j^{(i)}\right) \right) \quad (7.25)$$

where $\Omega^{(i)}$ is an ensemble of feature i extracted from the region Ω and $\mathcal{M}^{(i)}$ the expected model of feature i . $KL(\Omega, \mathcal{M})$ is the Kullback-Leibler divergence [14] between the empirical model estimated from Ω and the expected ones \mathcal{M} . The probabilistic model is also applied in this case.

We implement this variational framework for the inter-mode fusion. We first recall that we aim to propagate the robust classification in the longitudinal mode into the whole acquisition zone via the bathymetry mode's data. Therefore, we find compatibility between our motivation and this method's engine. Besides, this method also helps to overcome the change between 2 different grid systems in these modes. As a result, the implementation of this method is presented in Algorithm 3 based on this idea. As initialization, we consider the level-set functions issued from the classification of along-track pixels from the longitudinal mode. This allows to exploit the best this mode's performance stated in Section 7.2. Whereas, the across-track data are used to expand the level-set functions based on its large coverage. This proposition is equivalent to set the longitudinal mode's weight $w^{(AIT)}$ to inf in the vessel's trajectory while the bathymetry mode is decisive for the other grid points. As such, our variational framework may be regarded as a propagation means between these operating modes.

We notice that in this proposition the initialization is restricted in the nadir zone, and the other grid points rest unclassified. It means the data, collected from the segmented zone, contain only information from nadir angles and lack of information from high incident angles. The similarity term proposed in (7.25), however, creates difficulties in demanding high-incident-angle information. Otherwise, the ones in (7.24) is not only adapted to this problematic, but also applicable to the models presented in Section 7.3.2. Therefore, we exploit the similarity term (7.24) in this study.

The minimization of the resulting variational cost evolves the level-set functions using a gradient descent:

$$\frac{\partial \varphi_1^{(j)}}{\partial t} = -\frac{J_1}{\Omega_j} = -\sum_i^{N_s} w_i \log(\mathbb{P}(C_j|x)) \delta_\alpha(\varphi^{(j)}) \left| \nabla \varphi^{(j)} \right| \quad (7.26)$$

$$\frac{\partial \varphi_2^{(j)}}{\partial t} = -\frac{J_2}{\Omega_j} = \gamma_j \nabla \cdot \nabla \varphi^{(j)} \delta_\alpha(\varphi^j) \quad (7.27)$$

$$\frac{\partial \varphi_3^{(j)}}{\partial t} = -\frac{J_3}{\Omega_j} = -\lambda \left(\sum_j H_\alpha(\varphi^{(j)}) - 1 \right) \delta_\alpha(\varphi^{(j)}) \quad (7.28)$$

where $g_{\sigma_i}(x) = \frac{1}{\sqrt{2\pi\sigma_i}} e^{-\frac{x^2}{2\sigma_i^2}}$ is the Gaussian kernel for smoothing the empirical density function of current feature. As stressed in [76], the initialization of the level-set functions $\varphi^{(0)}$ may greatly affect the quality of the final segmentation depending on the chosen data-driven term. Numerically, the evolution of the level set functions needs to satisfy a condition of its gradient $|\nabla \varphi| > 0$. The reinitilization of the level-set functions w.r.t. the current segmentation every 10 iterations enforces this constraint.

The first classification on longitudinal mode's data $Seg^{(0)}$ is used to initialize the level set function $\varphi^{(j)(0)}$ for each class j . Next, the level set evolution is estimated according to the contour proximity term $d\varphi_1^{(j)(k)}$ (resp. contour length term $d\varphi_2^{(j)(k)}$, class uniqueness term $d\varphi_3^{(j)(k)}$). The level set function is updated by taking into account all these terms. In this algorithm, we remark that there is a weighing set applied onto features w_i . This weighing corresponds to the angular dependence of the data x onto its incident angle. Therefore, we can exploit the estimation presented in Algorithm 1.

Data: bathymetry mode's data: {incident angle, backscatter strength}, longitudinal mode's data: backscatter profile

Result: Segmentation based on variational method

initialization: $Seg^{(0)}$: First classification in nadir with longitudinal mode;

while iteration k **do**

1. Re-initialization of level-set function φ each t iterations.

2. Estimation of level-set function evolutions: $d\varphi_1^{(j)(k)}$, $d\varphi_2^{(j)(k)}$, $d\varphi_3^{(j)(k)}$
using (7.26), (7.27), (7.28)

3. Updating of level-set function: $\varphi^{(j)(k)} = \varphi^{(j)(k-1)} + dt \left(d\varphi_1^{(j)(k)} + d\varphi_2^{(j)(k)} + d\varphi_3^{(j)(k)} \right)$.

end

Algorithm 3: Inter-mode fusion algorithm.

7.4 Results and Discussion

7.4.1 Considered dataset

We report experiments for a real dataset acquired in December 2015 in la Ciotat France, introduced in Section 3.4. During this survey, the multi-swath MBES system SEAPIX was exploited by activating alternatively the bathymetry and longitudinal modes. Therefore, all data were acquired for similar navigation conditions and multiple observations of a given seafloor area truly refer to the same seafloor class. As described in Section 3.4, we summarize the considered dual-mode data:

- In the bathymetry mode, the data along an acquisition line are mostly attached to the same incident angle. For a 2m resolution, we extracted the following pixel-level features: the mean incident angle, the mean BS level and the spatial covariance.
- In the longitudinal mode, the acquisition data were distributed only along the vessel trajectory, which was in the center of the acquisition lines. For a 5m resolution in the along-track direction, we extracted BS profiles for equally sampled angular sectors from -50° to 50° with a 2° angular resolution.

In this acquisition zone, several sites were groundtruthed from an in situ sampling: more precisely, a $200\text{m} \times 200\text{m}$ dense posidonia area, a $100\text{m} \times 100\text{m}$ sparse posidonia area and a $150\text{m} \times 200\text{m}$ sand area were identified. This dataset provides a ground truth for supervised learning as well as performance evaluation.

7.4.2 Single-mode classification results

We report in Figure 7.1 examples of single-mode classification maps using the classification models introduced in Section 7.3.1. Our goal is to fuse such single-mode classification maps to improve the spatial segmentation of the different seabed types. The classical method exploits the Gaussian mixture model, which was verified to best suit to the BS data in logarithmic scale and adapt well to spatial covariance feature. The classifier RF re-uses same parameters as in Chapter 6, which composed of 50 trees using the squared-root of the number of feature dimension as number of variables for each decision split and a bootstrap rate of 0.5.

In Figure 7.1a and 7.1b, we first display the studied region via first and second acquisition line mosaics (constructed from the bathymetry mode's data). They show a good continuity of the sand regions (dark gray level). We also observe a strong BS level in the nadir of the sand regions. We remark that sand involves a strong backscatter in vertical directions and weak one in high incident angles. This was verified in Section 4.1 while comparing the backscatter profile between sand and posidonias. Because the same calibration was applied in the acquisition lines, this process is more adapted to the dense posidonia than the others, especially the sand. As a result, we remove the data in nadir in the next study for the bathymetry data to reduce this influence.

Bathymetry mode: Figure 7.1c and 7.1d shows the classification results of the first line. The RF shows a better performance with less false predictions in the homogeneous regions. In Figure 7.1e and 7.1f, the superposition of both classified lines are displayed. The strong-color region highlights the overlap zone of these lines. In this region, the coherence of the classifications is shown in bold color while the conflict was presented in blur color. We observe that most conflicts happened on false predictions. This motivates our idea of the intra-mode fusion.

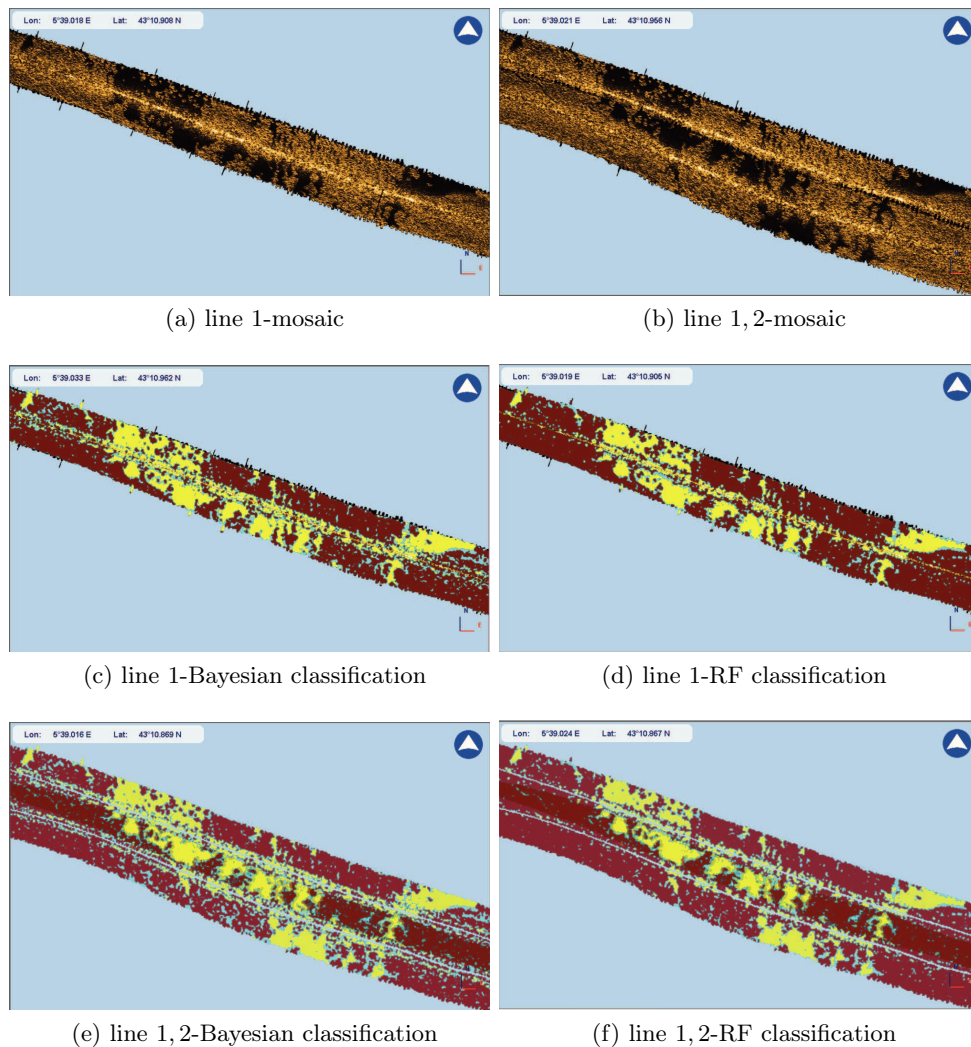


Figure 7.1 – Bathymetry mode classification visualization of the bay of la Ciotat composed of dense posidonia (brown), sparse posidonia (blue) and sand (yellow). The acquisition data was acquired with the MS-MBES SEAPIX in December 2015. Figure 7.1a and 7.1b display the mosaic of the first and second acquisition line. Figure 7.1c (resp. 7.1d) shows the classification of the first line with the classifier Bayesian (Gaussian mixture models) (resp. Random Forest). The superposition of classification results of both lines is found in Figure 7.1e (resp. 7.1f). The exploited features are the backscatter strength (logarithmic scale) and the spatial covariance (in different scales).

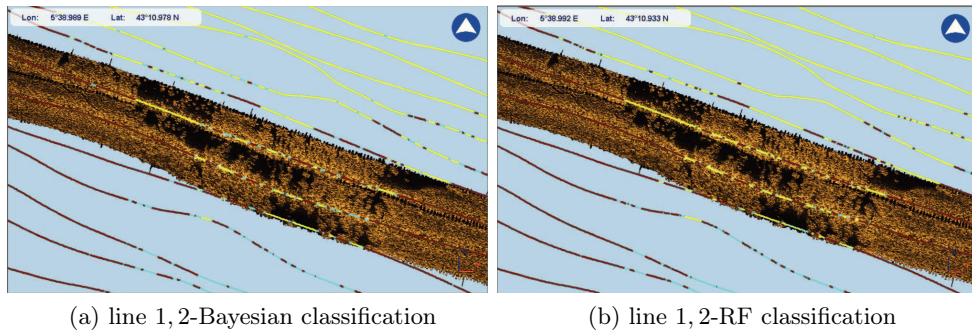


Figure 7.2 – Longitudinal mode classification visualization of the bay of la Ciotat composed of dense posidonia (brown), sparse posidonia (blue) and sand (yellow). The acquisition data was acquired with the MS-MBES SEAPIX in December 2015. Figure 7.2a (resp. 7.2b) shows the classification of the two first line with the classifier Bayesian (Gaussian mixture models) (resp. Random Forest). The classification results are displayed in the mosaic background introduced in Figure 7.1b. The exploited features are the profile of backscatter strength in logarithmic scale

Longitudinal mode: Figure 7.1 shows the classification results of the first and second lines with the longitudinal mode’s data. The results are quite equivalent between the two classifiers Bayesian and *RF*. Due to the good discrimination of this mode’s data ($> 90\%$ accuracy in Chapter 6), so the classification result depends less on the chosen classifiers. We display the classification results on the mosaic background, and observe a good continuity between two operating modes’ data. This continuity results from using alternatively these modes during the acquisition (Section 3.4), which guarantees the same seafloor was insonified. While the bathymetry mode is less functioning in nadir zone (Figure 7.1d), the longitudinal mode shows a better performance for along-track area.

In conclusion of this section, the classifier *RF* outperforms the naive Bayesian classifier. Hence a *RF* classifier will be chosen in the next studies. A preliminary result on the whole zone is displayed in Figure 7.3. The longitudinal mode’s is displayed in bold color on the vessel trajectory. The bathymetry mode’s is visualized via voting procedure between acquisition lines. In case of a class conflict, it is left unidentified, and is interpolated from its neighbors. The bathymetry mode’s result is displayed in light color on the whole zone except on the vessel trajectory. These results support the development of more advanced fusion schemes as explored in this chapter.

7.4.3 Intra-mode fusion

We first present our results using the intra-mode fusion (Section 7.3.2). We rely on the probabilistic outputs of the classification models illustrated in Figure 7.1.

Weight estimation We report the results associated with the consensus-based and SVM-based estimation of the weighing factors in model (7.7). In the SVM-based estimation, we applied the Karush-Kunn-Tucker conditions *kkt* to guarantee the algorithm convergence. For each class, this constraint is measured differently as false prediction proportion while applying equivalent weighing set. As illustrated in Figure 7.4, these weighing factors are clearly angular-dependent. We may remind that the estimated weights are non-negative weights for the consensus-based formulation,

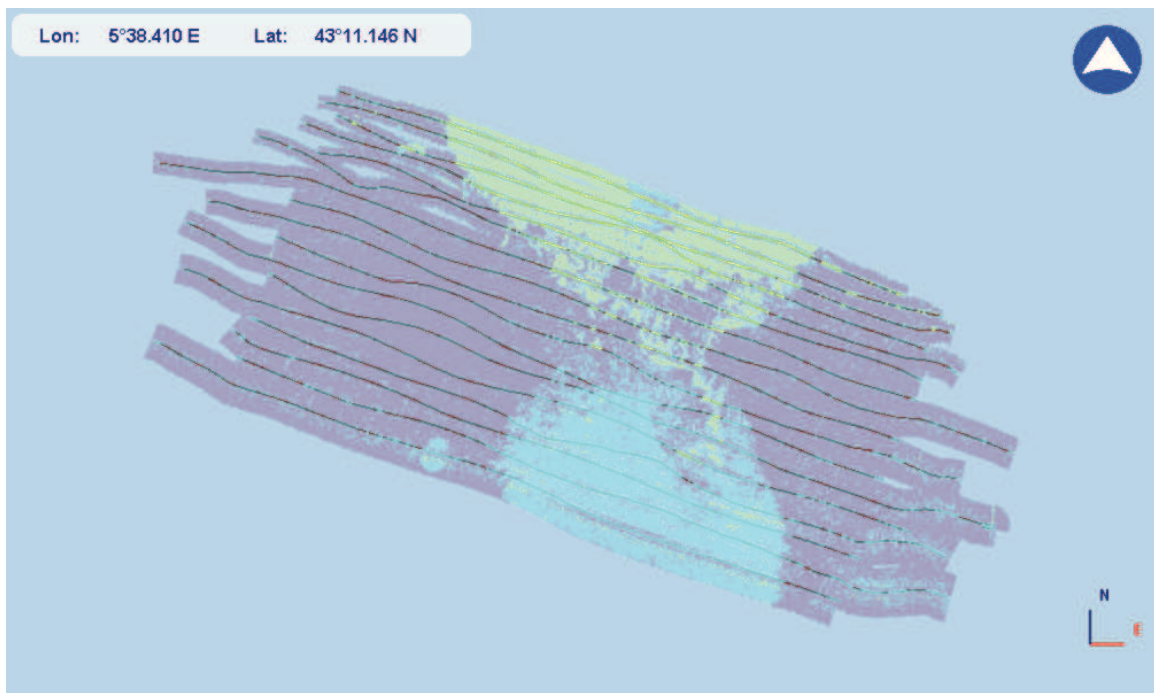
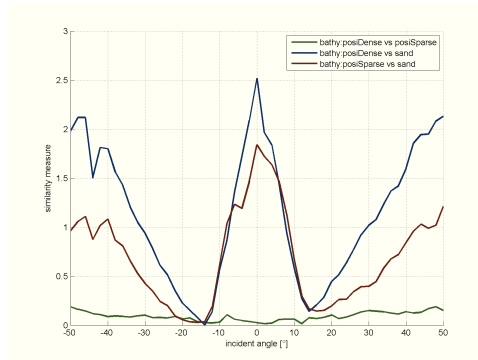
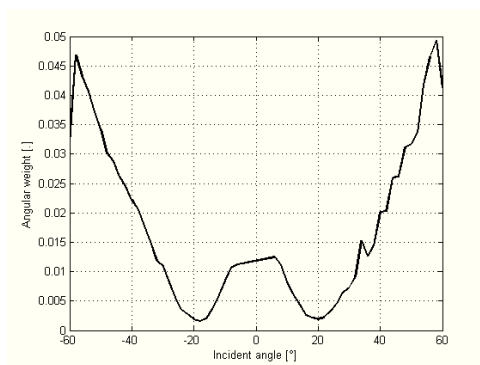


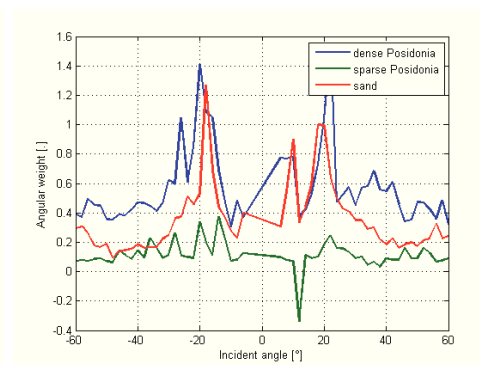
Figure 7.3 – Superposition of classified operating modes' data in the bay of la Ciotat composed of dense posidonia (brown), sparse posidonia (blue) and sand (yellow) via *RF*. The acquisition data was acquired with the MS-MBES SEAPIX in December 2015. The longitudinal mode's classification (bold color) is displayed on the vessel trajectory in the background of the bathymetry mode's classification (blurred color).



(a) Classification potential



(b) Consensus-based weight



(c) SVM-based weight

Figure 7.4 – Angular weighing set estimation for the data in la Ciotat, France, in December 2015. Figure 7.4a reports the classification potential between pairs of classes: dense posidonia - sparse posidonia (green), dense posidonia - sand (blue), sparse posidonia - sand (red). In the Figure 7.4b, the weighing set was estimated via the consensus method (Algorithm 1) for different probability measures (Bayesian and Random Forest). In the Figure 7.4c, this set was estimated via the SVM approach (Algorithm 2).

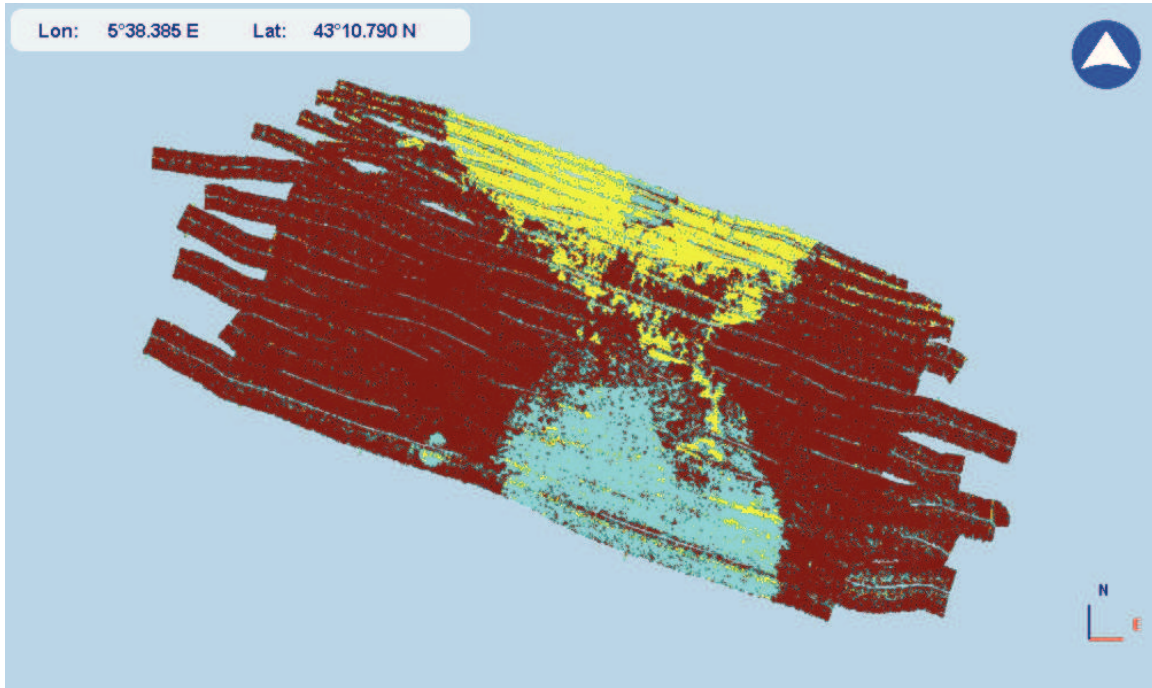
Table 7.1 – Comparison of classification performance between different weighing strategies: constant weight, consensus-based weight, and SVM-based-weight. We first evaluate the classification performances on 3 classes: dense posidonia (DP), sparse posidonia (SP) and sand (S). An overall rate, which is proportion of good predictions over the samples of all classes, is displayed to compare the performances of different strategies.

Classes	Constant weight	Consensus-based weight	SVM-based weight
DP	82.48	92.81	90.61
SP	80.43	74.11	73.82
S	90.39	84.70	93.81
Overall*	83.60	88.12	88.33

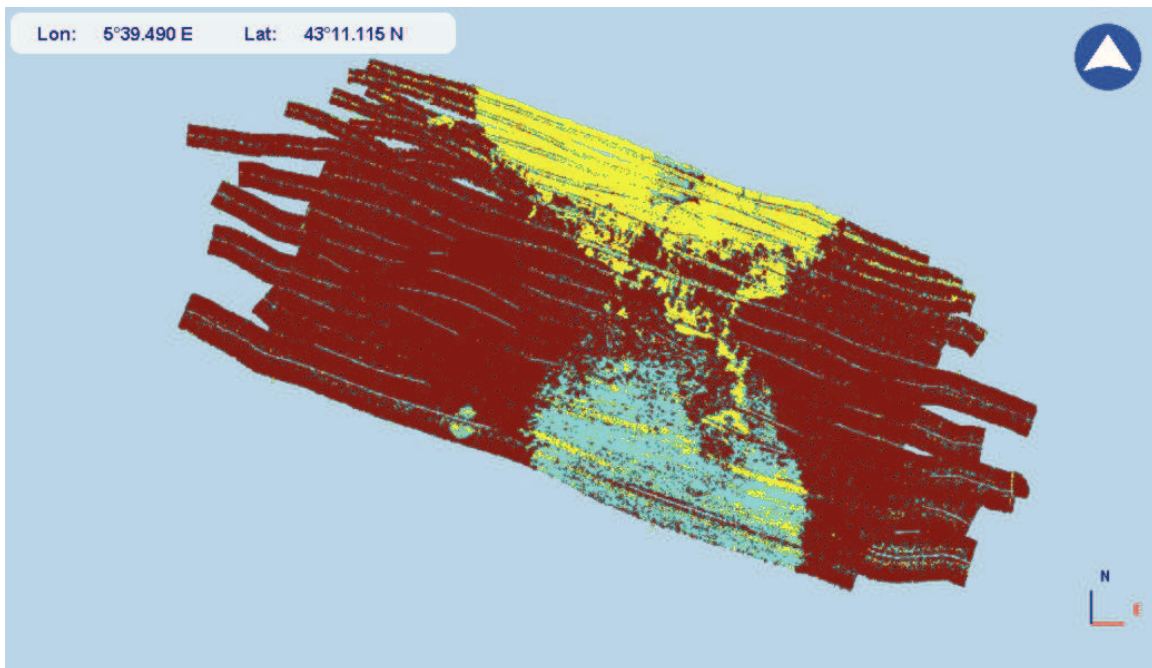
*:weighted average of classification rate on all types of sediments

which state the relative contribution of each angular sector in the fusion process. In other words, these weights may be interpreted as the discrimination level of each angular sector. The reported weights are in agreement with the discrimination potential illustrated in Figure 7.4a from Section 4.2. This analysis relies on the evaluation of the Kullback-Leibler divergence between each pair of sediments: dense .vs sparse posidonia (green), dense posidonia .vs sand (blue) and sparse posidonia .vs sand. The stronger the divergence is, the more discriminant these sediments are. We first find that there is not much difference between the two posidonia classes while they both are very different from the sand. Besides, we observe that these classes are more discriminated in the high incident angles, which corresponds to the estimated weight in Figure 7.4b. For the SVM-based formulation, most weights are also non-negative ones, though no such non-negativity constraint is imposed. The angular dependence of the SVM-based weights also appears noisier, which may also relate to the non-negativity constraint in the consensus-based formulation.

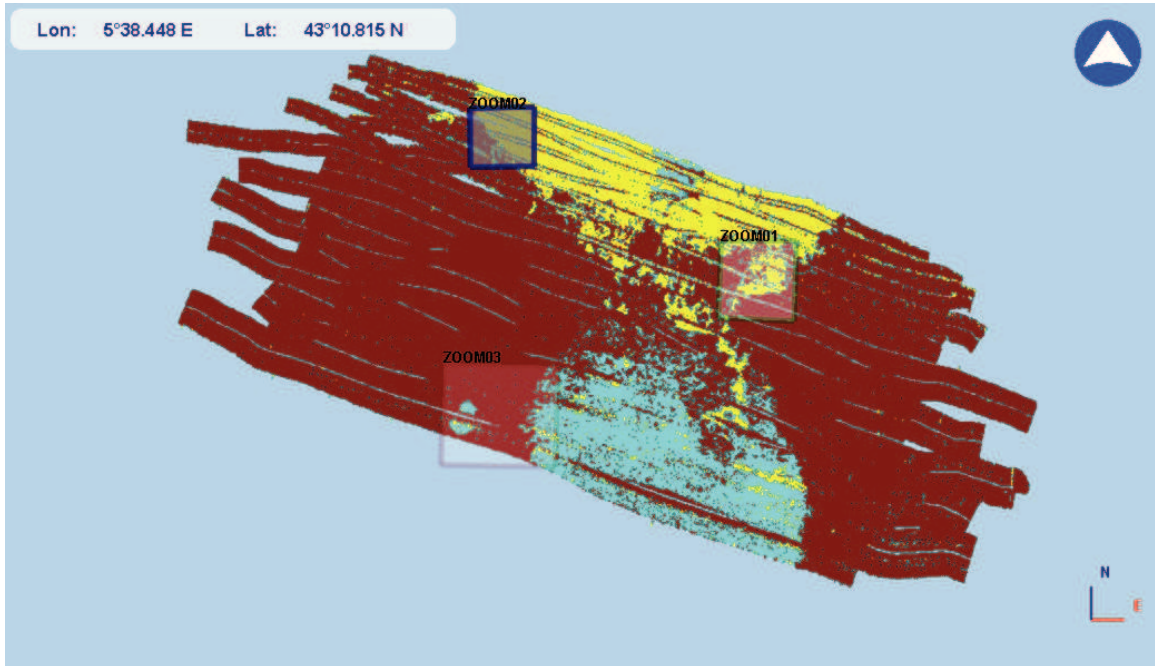
Evaluation We first evaluate the intra-mode fusion methods for the groundtruthed zones. We compute the global classification performance as the ratio of the number of correct prediction over the number of samples in the training zone. In Table 7.1, we compare the performance of the fusion schemes with respect to the conventional probability fusion (constant weighting). Overall, we obtain a clear gain of about 5% of correct classification using the fusion schemes. The SVM approach slightly outperforms the consensus-based one (88.33% vs. 88.12%).



(a) Constant weight



(b) SVM-based weight



(c) Consensus-based weight

Figure 7.5 – Visualization of the classifications with intra-mode fusion schemes on the bay of la Ciotat (France) composed of 3 main classes: dense posidonia (brown), sparse posidonia (blue) and sand (yellow). The acquisition data were acquired in December 2015 with the MS-MBES SEAPIX. Figure 7.5a displays the classical probability fusion (constant weight). Figure 7.5b and 7.5c present the classification with the proposed weighing schemes: SVM-based weight and consensus-based weight. In Figure 7.5c, 3 zooming regions (green, blue and red) are focused for more details in Figure 7.6, 7.7, 7.8.

The calibrated intra-mode fusion models are also applied on the whole acquisition zone. The fusion is realized for the bathymetry mode’s data except those in the nadir where the longitudinal mode’s classification will be displayed instead. The result are first evaluated from the coherence between the intra-mode fusion on the bathymetry mode and the classification on the longitudinal mode, which is displayed in Figure 7.5.

We focus on 3 zooming regions, illustrated as ZOOM01 (green), ZOOM02 (blue), ZOOM03 (red) in Figure 7.5c. Figure 7.6, 7.7, 7.8 displayed the analyzing details on these regions including mosaic, manual segmentation (ground truth), fusion by voting-scheme, probability, consensus-based weighing and SVM-based weighing. The proposed fusion schemes show a better homogeneity in the classification, and a good coherence to the mosaics. However, we observe less coherence between the fusion results and the groundtruths. We first remark that the groundtruths were realized on another datasets by geophysicists in seafloor classification. Even though the groundtruths mostly work on our mosaic, we also have some difficulties due to less coherence in geo-geographical positions. In ZOOM03 region, we find a complete confusion between the sparse posidonia (blue) and sand (yellow). This is actually caulerpa sand region, and we didn’t consider this sediment in our model. Despite of a type of sand, its backscatter profile is more similar to the sparse posidonia, which could be observed in the region mosaic (Figure 3.13). Next, we find confusion near to nadir of each acquisition line. This confusion happens mostly on the incident angles where the types of seafloor have a similar backscatter level (Figure 4.5b).

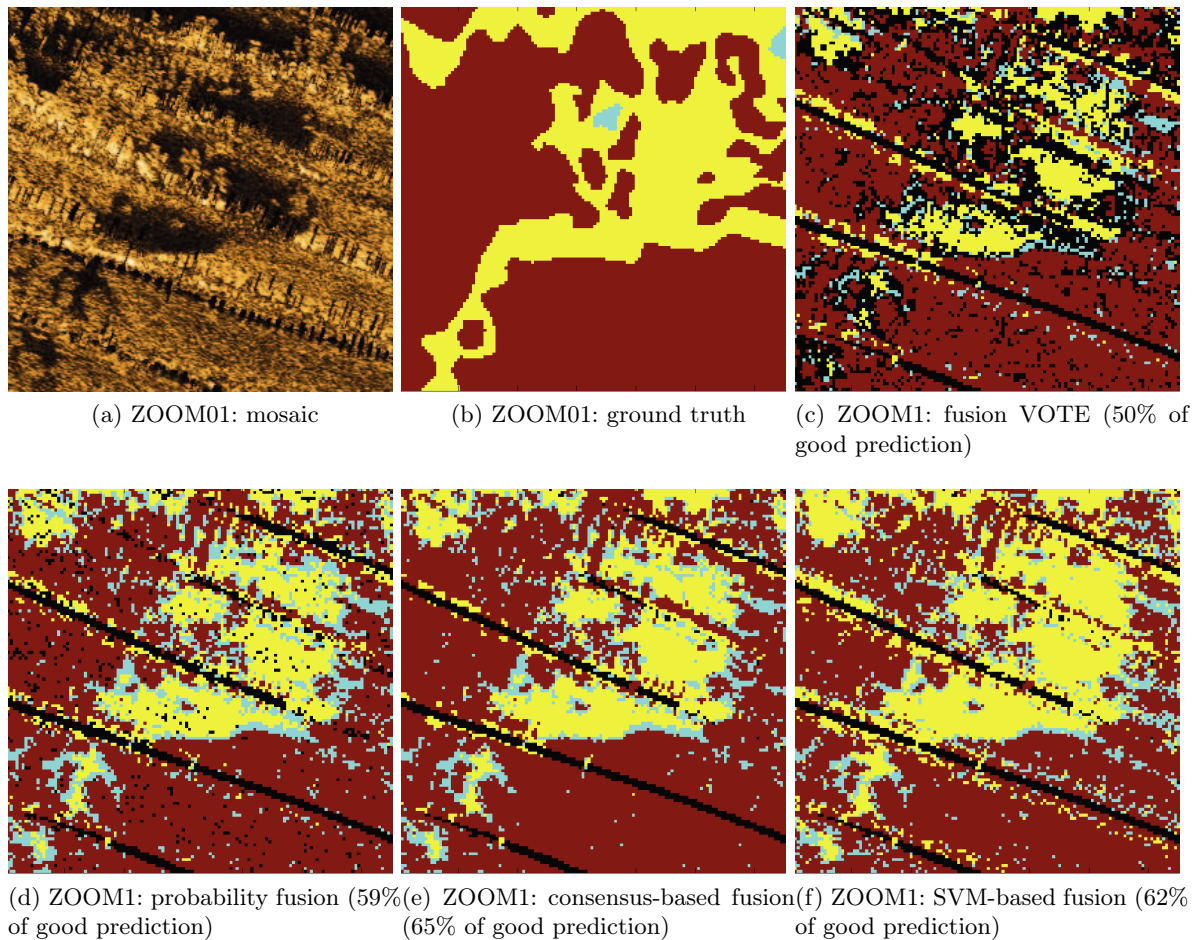


Figure 7.6 – Visualization of the classification with the intra-mode fusion schemes on the zooming region ZOOM01 (green box) in the acquisition zone (Figure 7.5c). This zone is composed of 3 main classes: dense posidonia (brown), sparse posidonia (blue), sand (yellow) and some unidentified areas (black). We first introduce the mosaics (Figure 7.6a) and the manual segmentations of acoustic experts (Figure 7.6b) on this regions. Next, we display the segmentation of this region via classical fusion methods: VOTE (Figure 7.6c) and probabilistic fusion (Figure 7.6d). We also reveal the overall classification rate of these methods. Finally, we present the visualization and the classification rate of the proposed weighing-based fusion methods: consensus-based (Figure 7.6e) and SVM-based (Figure 7.6f).

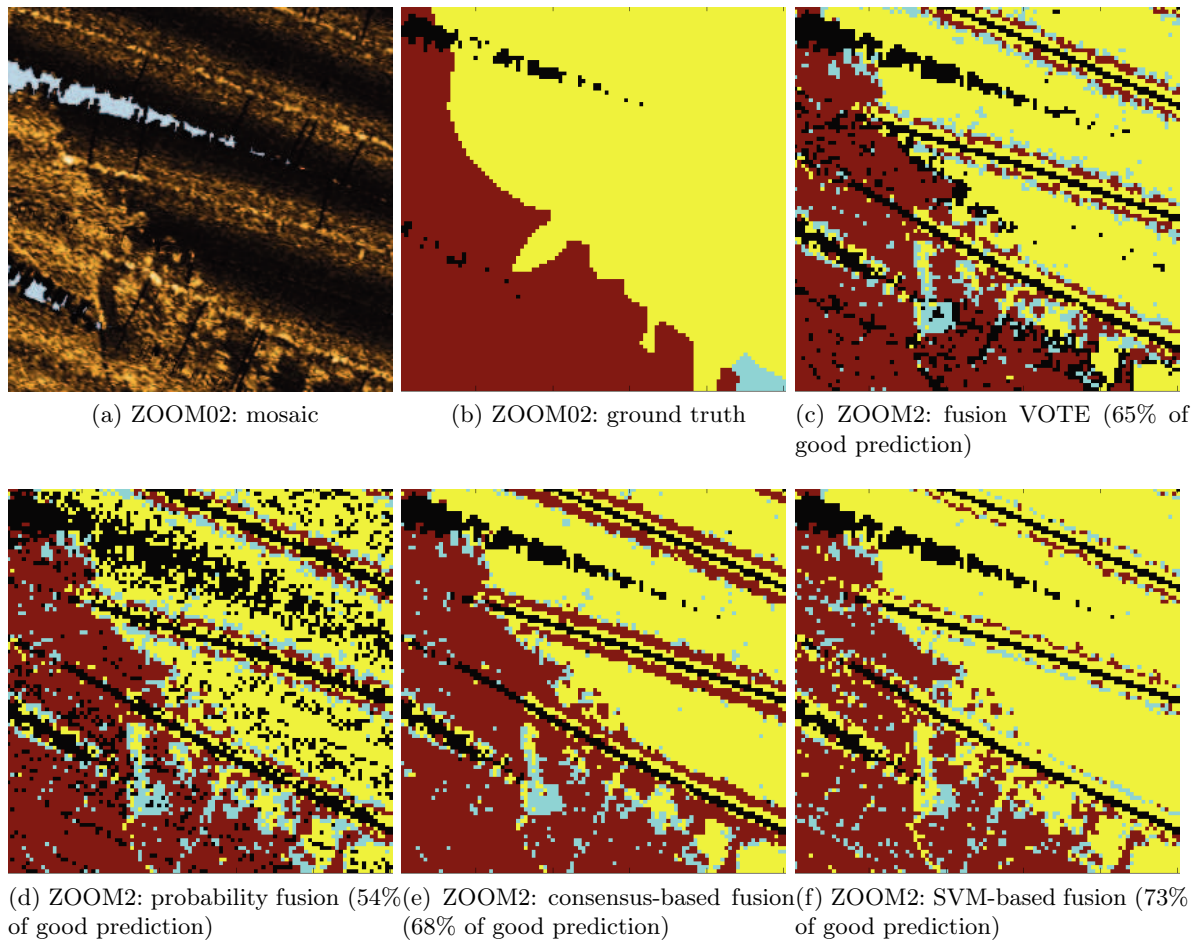


Figure 7.7 – Visualization of the classification with the intra-mode fusion schemes on the zooming region ZOOM02 (blue box) in the acquisition zone (Figure 7.5c). This zone is composed of 3 main classes: dense posidonia (brown), sparse posidonia (blue), sand (yellow) and some unidentified areas (black). We first introduce the mosaics (Figure 7.7a) and the manual segmentations of acoustic experts (Figure 7.7b) on this regions. Next, we display the segmentation of this region via classical fusion methods: VOTE (Figure 7.7c) and probabilistic fusion (Figure 7.7d). We also reveal the overall classification rate of these methods. Finally, we present the visualization and the classification rate of the proposed weighing-based fusion methods: consensus-based (Figure 7.7e) and SVM-based (Figure 7.7f).

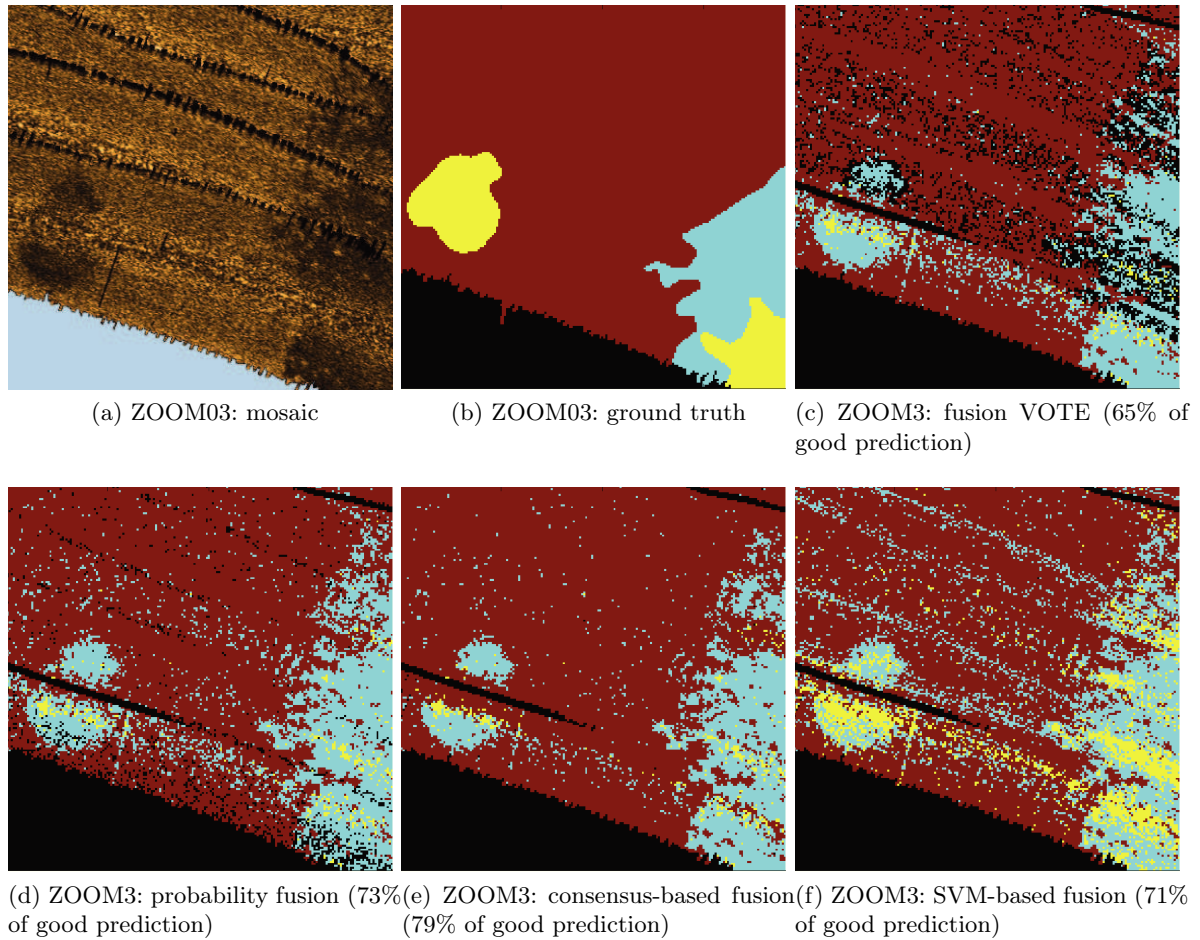


Figure 7.8 – Visualization of the classification with the intra-mode fusion schemes on the zooming region ZOOM03 (red box) in the acquisition zone (Figure 7.5c). This zone is composed of 3 main classes: dense posidonia (brown), sparse posidonia (blue), sand (yellow) and some unidentified areas (black). We first introduce the mosaics (Figure 7.8a) and the manual segmentations of acoustic experts (Figure 7.8b) on this regions. Next, we display the segmentation of this region via classical fusion methods: VOTE (Figure 7.8c) and probabilistic fusion (Figure 7.8d). We also reveal the overall classification rate of these methods. Finally, we present the visualization and the classification rate of the proposed weighing-based fusion methods: consensus-based (Figure 7.8e) and SVM-based (Figure 7.8f).

Table 7.2 – Comparison of the classification maps from different fusion schemes (constant weight, consensus-based weight and SVM-based weight) to the ground truth. The groundtruths are grouped into 3 main classes (dense posidonia - DP, sparse posidonia - SP and sand - S) and a class of other sediments. Map’s pixels are also classified into 3 main classes (DP, SP, S) and an unidentified class (U). Classification rates of interest is evaluated via colors: good rate (>80%) - green, medium rate (50%-80%) - orange, bad rate (<50%) - red.

	DP (664592)*	SP (491519) (36941)	S (131028)	<i>Others</i> (4906)
<i>Constant weight: 70%</i>				
DP	80.59	20.16	16.16	24.19
SP	9.86	64.82	40.69	43.03
S	1.86	10.70	32.55	21.67
U	7.68	4.31	10.60	11.11
<i>Consensus-based weight: 80%</i>				
DP	92.71	30.25	25.30	33.82
SP	5.87	58.29	36.16	42.01
S	1.40	11.37	38.41	24.05
U	0.03	0.08	0.13	0.12
<i>SVM-based weight: 74%</i>				
DP	80.57	19.85	14.00	20.73
SP	12.33	51.65	30.98	34.12
S	7.08	28.48	55.01	45.15
U	0.01	0.02	0.01	0.00

*:Number of pixels in class

The reported classifications are also compared to a reference classification set manually in Table 7.2. The seafloor involves 664592 pixels categorized into posidonia (dense DP, and sparse SP), sand (silt sand near to port $S^{(1)}$ and caulerpa sand $S^{(2)}$) and other (sand riddles, etc.). Bathymetry mode pixels are principally distributed on 2 sides of the vessel trajectories while the nadir zone is reserved for the longitudinal mode. They are classified into 3 main classes (dense posidonia-DP, sparse posidonia-SP) and sand-S), and an unidentified class-U. We first remark that there is a geographical position offset between the acquisition data and this classification reference. Indeed, this reference was realized from another acquisition campaign on the same regions.

The consensus-based weight shows a strong improvement in the classification result (80% .vs 74% in correct prediction rate) as well as in the homogeneity in segmentation. On the other hand, the SVM-based weight proposes a more balance in classification result while conserving a good prediction rate (74% .vs 70%). Besides, we observe again the confusion from the caulerpa sand to the sparse posidonia (resp. 40%, 36% and 31% of confusion in Table 7.2). Because 45% pixels of the sand class is caulerpa, it plays an important role in the low performance rate in the sand class (resp. 32%, 38%, 55% in Table 7.2).

To be more clear, we also reveal the classification rate comparing to the expert classification in the zooming results (Figure 7.6, 7.7, 7.8). We first find a great improvement in the classification rate with the proposed methods on these regions (ZOOM01: 59% .vs 65%, ZOOM02: 65% .vs 73%, ZOOM03: 73% .vs 79%). We remark that this classification rate is calculated via the number of good prediction all over classes. Therefore, we still get a good classification on the area ZOOM03 because of the important number of good predictions in the dense posidonia class.

Besides, the proposed pondering strategies reduce also the unidentified cases. Because the unidentified label results from the similar posteriori likelihoods between the classes, it proves the proposed strategies is good at maximizing the difference between calibrated posteriori likelihoods.

7.4.3.1 Inter-mode fusion

We here report the experiments carried out for the variational inter-mode fusion introduced in Section 7.3.3. At first, we considered the following parameter setting:

- The parameter α for effective region involves to the feature's resolution 2m in the bathymetry mode.
- The contour length's parameter $\gamma = 0$.
- The class unique parameter $\lambda = 0$.

This configuration signifies an information propagation from the longitudinal mode's classification via the bathymetry mode's data without any contour regularization. Figure 7.10a shows this approach can propagate low-uncertainty nadir information to neighboring areas connecting the nadir zone. Due to the confusion in the near-nadir incident angles between these zones (Chapter 4), it is difficult to overcome this issue in the intra-mode fusion (Figure 7.5). Besides, the classification result is more homogeneous compared to the intra-mode fusion with no spatial regularization. These phenomena origin from the propagation of level-set functions, which slightly connects neighbor pixels. We also observe in the sand zone, there is an unidentified region, which corresponds to the sand riddle region. The longitudinal mode's data state this sediment as a sand while the bathymetry mode's view it as a sparse posidonia in the high incident angles. As a result, the level-set function fails evolving in this region, and it was left unidentified. Besides these advantages, we observe on the bottom right a more important confusion between the sparse and dense posidonias compared to the intra-mode's fusion. Even though the longitudinal

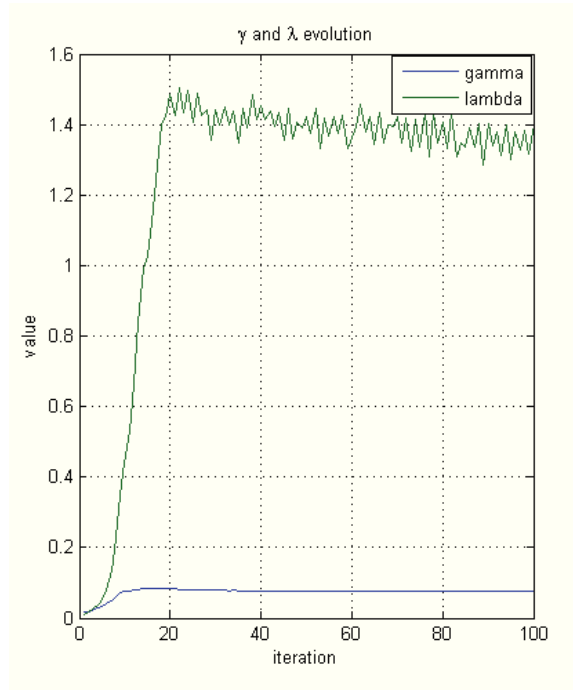


Figure 7.9 – Evolution of the regularization parameters in the inter-mode fusion scheme (λ - green, γ - blue).

mode proves its performance in the analysis/training zone, it doesn't describe all the cases in the acquisition zone. Consequently, we obtain a mis-classification via the longitudinal mode, and it results in an important confusion in this region.

$$\gamma^{(k)} = \text{median} \left(\frac{J_1}{J_2^{(k)}} \right), \lambda^{(k)} = \text{median} \left(\frac{J_1}{J_2^{(k)}} \right) \quad (7.29)$$

Next, we apply another parameter setting to activate the contour regularization option. The contour length parameter γ was set to 0.5 and the class uniqueness parameter λ to 1.3. These parameters were determined in (7.29) via an accelerated cross-validation setup where we accelerate the influence factor $dt = 100$ and the reinitialization loop $reinit = 1$. This strategy, for regularization parameters, means the influence of regularization process shouldn't be more important than the data-driven term. Figure 7.9 displays the evolution of these parameters as well as their convergence.

The application of this configuration shows a good result in Figure 7.10b. The segmentation is well adapted to the mosaic of the acquisition zone (Section 3.4). The mis-classification region was also reduced via the regularization with the bathymetry mode's information in the high incident angles. The result also shows the important influence in choosing the regularization parameters, where some small regions were removed due to their size. In Figure 7.11, 7.12, 7.13, we also give more details on previous 3 zooming regions (ZOOM01, ZOOM02, ZOOM03 in Section 7.4.3). In these regions, we show their mosaic and their ground truth, as well as the classification result on the longitudinal mode and the intra-mode fusion with consensus-based weight. Next, we display the classification with inter-mode fusion scheme with and without regularization. A great improvement is done in the nadir zone, where the conflict of backscatter level was found in the intra-mode fusion. However, the inter-mode fusion strategy doesn't solve the mis-classification

Table 7.3 – Comparison of the classification map from inter-mode fusion scheme to the ground truth. The groundtruths are grouped into 3 main classes (dense posidonia - DP, sparse posidonia - SP and sand - S) and a class of other sediments. Map’s pixels are also classified into 3 main classes (DP, SP, S) and an unidentified class (U). Classification rates of interest is evaluated via colors: good rate (>80%) - green, medium rate (50%-80%) - orange, bad rate (<50%) - red.

	DP (702234)*	SP (520963)	S (37774)	<i>Others</i> (137955)	<i>Others</i> (5318)
<i>Dual-mode fusion with regularization: 82%</i>					
DP	91.26	8.82	5.83	0.00	0.00
SP	6.50	73.90	44.04	0.00	0.00
S	1.13	13.76	48.10	76.78	76.78
U	1.11	3.52	2.04	23.22	23.22

*:Number of pixels in class

between the caulerpa sand and the sparse posidonia. This mis-classification is observed in both the bathymetry and longitudinal mode. Therefore, we need a better training base to deal with this issue.

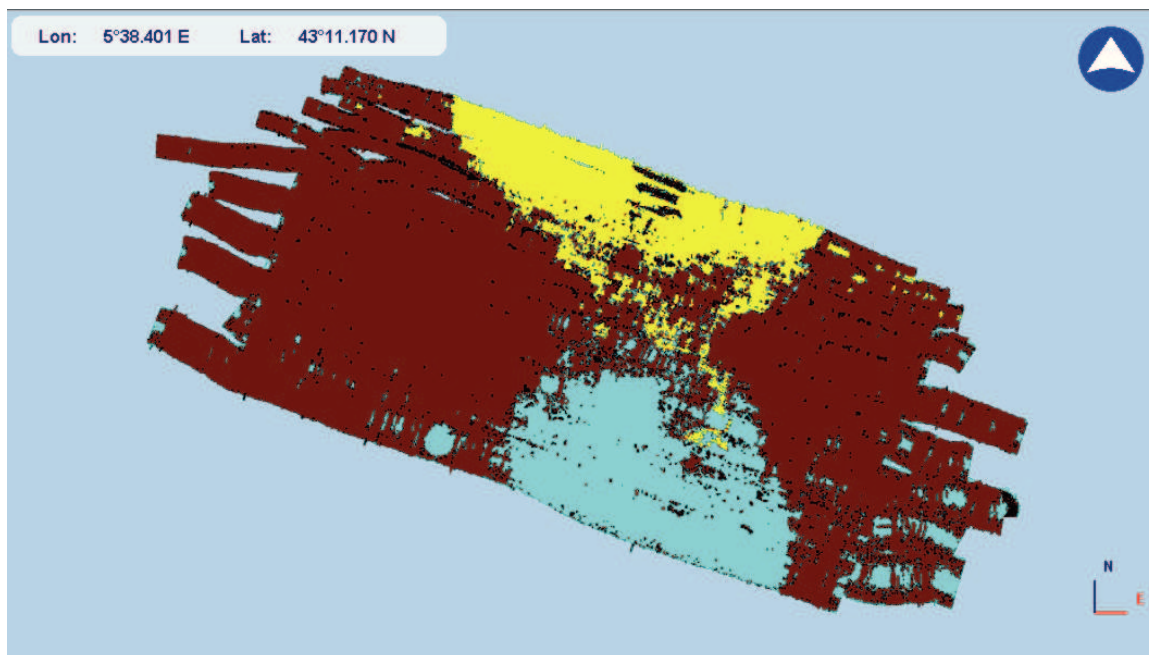
The reported classifications are also compared to a reference classification set manually in Table 7.3 as previously. The seafloor contains more pixels in this case (702234 vs. 664592) because the nadir zone is also taken into account. The result shows a strong improvement not only in the correct prediction rate (82%) but also in the homogeneity. The classification rate also increases for all classes. These details could also be found in the zooming areas (Figure 7.11, 7.12, 7.13).

7.5 Conclusion & Future works

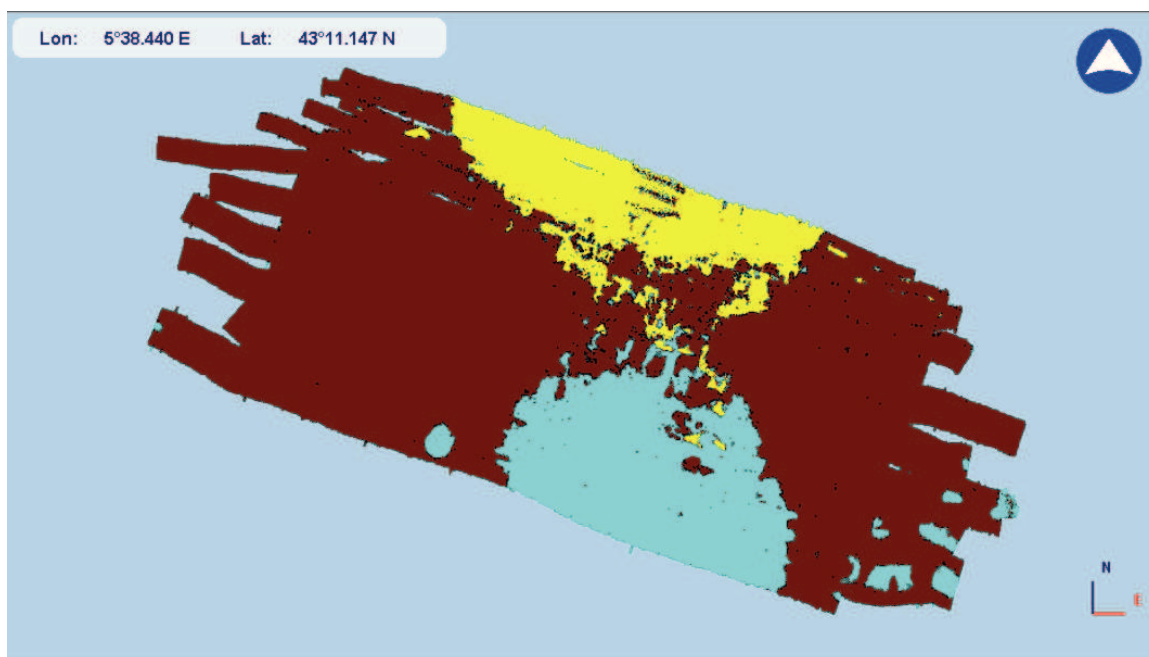
In this study, we address the fusion of multi-mode data from the multi-swath MBES SEAPIX for seafloor classification. This system was exploited with its two basic swaths: classical across-track swath and along-track swath. These swaths were alternatively insonified during the acquisition campaign via their corresponding operating modes: bathymetry mode and longitudinal mode. Our goal is to benefit from the complementarity of these two modes:

- In bathymetry mode, pixel information was limited in only one *BS* data in some incident angle, but it was acquired in a large area.
- In longitudinal mode, pixel-level information was much more complete, and could be extracted as a *BS* profile according to different incident angles. As a result, this mode provided a robust classification. However, this information was limited only on vessel trajectory. In addition, the sampling pattern over a given area typically leads to the acquisition of multiple *BS* information for a given seafloor pixel. These features advocate for fusion schemes to extract more robust seafloor classification maps as illustrated in Figure 7.10b.

We first addressed in the intra-mode fusion. We exploit only the across-track information which had been overlapped during the acquisition. In this study, each incident angle sector of 2° was considered as an independent source. The consensus model in logarithmic scale was exploited to combine different angular information by posing a weight into each information source. We proposed 2 estimation methods of the weighing factors of the angular sectors in the final decision: consensus-based estimation and SVM-based estimation. They both showed relevant results. Moreover, these methods also signified different approaches in the estimation.



(a) Non-regularization configuration



(b) Regularization configuration

Figure 7.10 – Visualization of classification map with the inter-mode fusion scheme on the bat of la Ciotat (France) composed of 3 main classes: dense posidonia (brown), sparse posidonia (blue), sand (yellow). The acquisition data were acquired in December 2015 with the MS-MBES SEAPIX. Figure 7.10a shows the classification with no regularization. Figure 7.10b gives the classification result applied regularization.

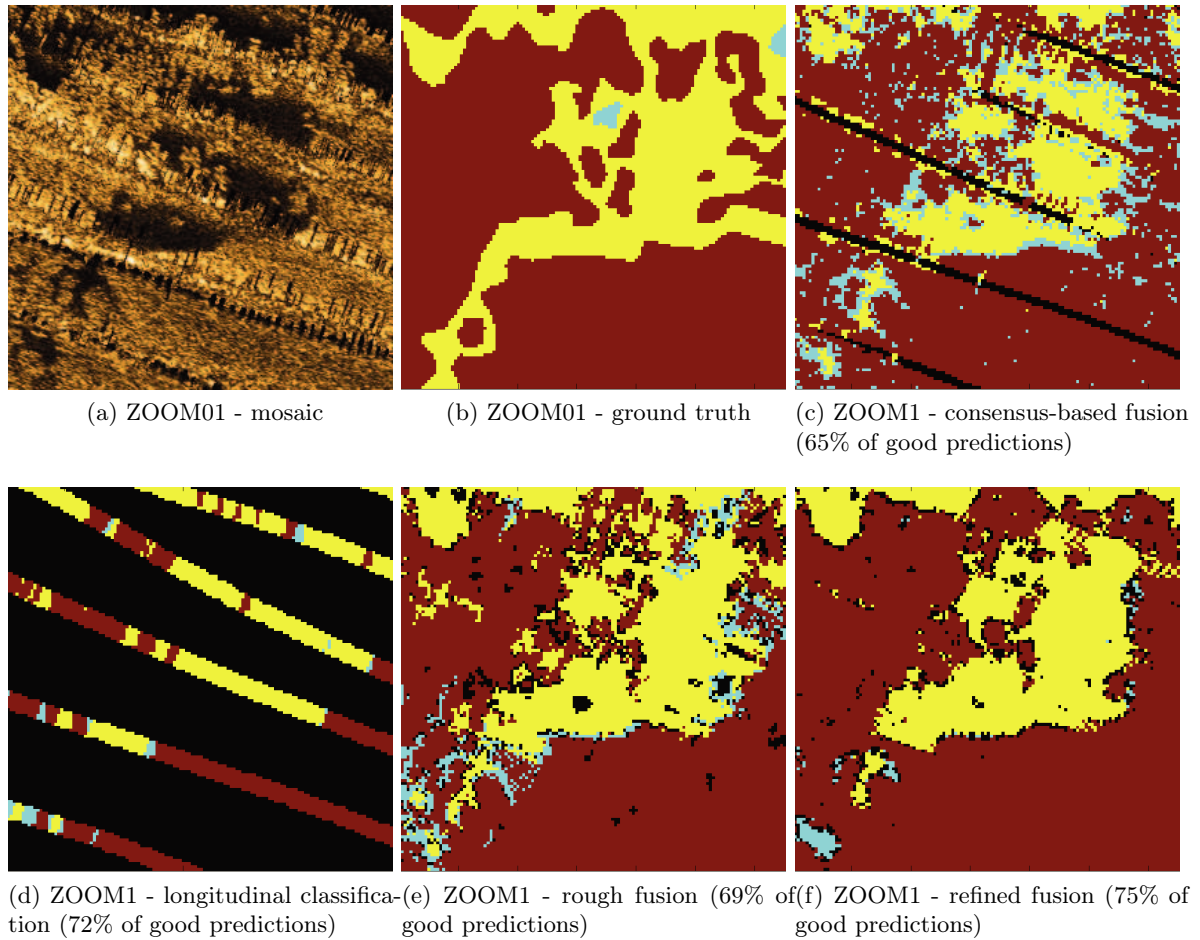


Figure 7.11 – Visualization of the segmentation via inter-mode fusion on the zooming regions ZOOM01 (green box) in the acquisition zone (Figure 7.5c). This zone is composed of 3 main classes: dense posidonia (brown), sparse posidonia (blue), sand (yellow) and some unidentified area (black). We first introduce the mosaics (Figure 7.11a) and the manual segmentations of acoustic experts (Figure 7.11b) on these regions. Next, we display the classification on these regions as well as the good prediction rate via intra-mode approaches: consensus-based fusion on bathymetry mode (Figure 7.11c) and classification *RF* on longitudinal mode (Figure 7.11d). Finally, we present the classification results and the good prediction rates via proposed inter-mode fusion method: rough fusion (Figure 7.11e) and refined fusion (Figure 7.11f).

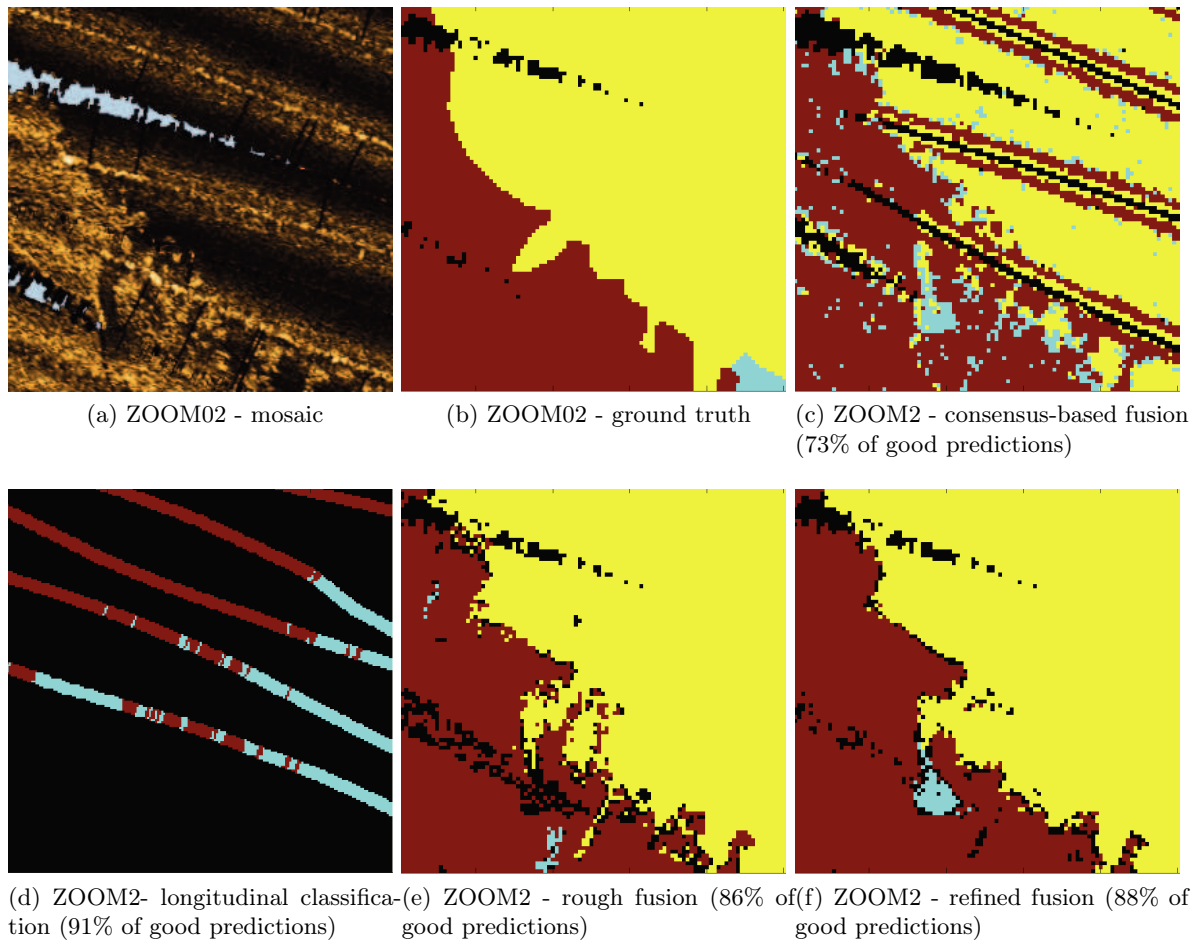


Figure 7.12 – Visualization of the segmentation via inter-mode fusion on the zooming regions ZOOM02 (blue box) in the acquisition zone (Figure 7.5c). This zone is composed of 3 main classes: dense posidonia (brown), sparse posidonia (blue), sand (yellow) and some unidentified area (black). We first introduce the mosaics (Figure 7.12a) and the manual segmentations of acoustic experts (Figure 7.12b) on these regions. Next, we display the classification on these regions as well as the good prediction rate via intra-mode approaches: consensus-based fusion on bathymetry mode (Figure 7.12c) and classification RF on longitudinal mode (Figure 7.12d). Finally, we present the classification results and the good prediction rates via proposed inter-mode fusion method: rough fusion (Figure 7.12e) and refined fusion (Figure 7.12f).

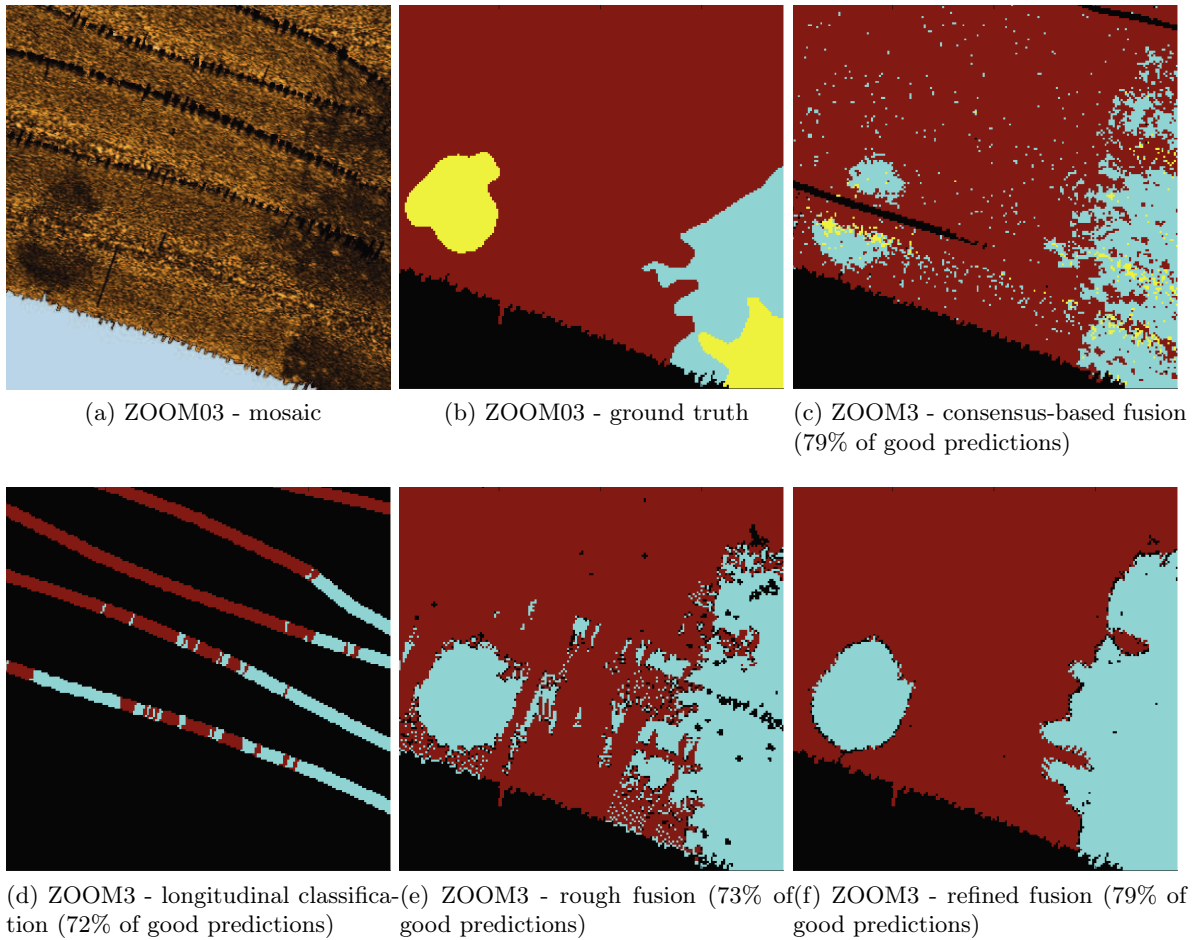


Figure 7.13 – Visualization of the segmentation via inter-mode fusion on the zooming regions ZOOM03 (red box) in the acquisition zone (Figure 7.5c). This zone is composed of 3 main classes: dense posidonia (brown), sparse posidonia (blue), sand (yellow) and some unidentified area (black). We first introduce the mosaics (Figure 7.13a) and the manual segmentations of acoustic experts (Figure 7.13b) on these regions. Next, we display the classification on these regions as well as the good prediction rate via intra-mode approaches: consensus-based fusion on bathymetry mode (Figure 7.13c) and classification RF on longitudinal mode (Figure 7.13d). Finally, we present the classification results and the good prediction rates via proposed inter-mode fusion method: rough fusion (Figure 7.13e) and refined fusion (Figure 7.13f).

The two methods differ in the considered weight calibration criterion. Overall, the SVM-based model reached slightly better classification on the cross-validation test while the consensus-based proved to be more relevant on the whole groundtruthed three-class dataset.

In the inter-mode fusion, a variational method was considered to combine information from different operating modes. This method evolves the segmented contour while guaranteeing a good similarity between the features of the segmented area and the reference class-specific features. Besides, the fact that this method worked on region instead of pixel allows overcoming the differences in the sampling pattern and acquisition resolution of the two modes. In the application of this method, we exploited the robust classification of longitudinal mode as an initialization and propagated this segmentation using bathymetry mode's information due to its large coverage. The result showed a strong improvement in the prediction rate as well as in the homogeneity of the segmented regions.

Conclusions and Perspectives

Aiming at providing a new acoustic system for the fishery market, a multi-swath multi-beam echo sounder (MBES) has been released since 2010 by iXBlue, namely SEAPIX. With a market price significantly lower than concurrent scientific echo sounders, SEAPIX is a flexible system which offers good performance in fish detection [1] as well as in seafloor bathymetry and backscatter measurements. Especially, this system proposes a multi-swath option, which allows the user to choose among different insonification swaths, each swath mode presenting its own advantage. The two following swaths are more particularly of interest:

- Across-track swath in the nadir direction is acquired with the bathymetry mode. Using this classical mode, the bathymetry profile and backscattering strength data are acquired with a large seafloor coverage across track the vessel.
- Along-track swath in the nadir direction is acquired with the longitudinal mode. This mode results in acquiring pixel-level full backscattering strength profile over a wide angular range for each seafloor pixels onto the vessel trajectory.

Whereas classic system typically offers either a highly-discriminative information (the *BS* profile issued once for each swath) or a large spatial coverage (the *BS* locally measured for each pixel in across-track swath), SEAPIX opens new avenues for jointly considering these two characteristics. Moreover, this system offers the *BS* profile from the along-track swath without homogeneity constraint. In this thesis, we aim to exploit this multi-swath functioning to improve seafloor classification and mapping.

In December 2015, we realized an acquisition campaign in la Ciotat (France). The SEAPIX system was taken in use with the multi-swath functioning to acquire real datasets with different operating modes (bathymetry, longitudinal, frontal). The acquisition zone involved three main types of sediments: two classes of posidonias (dense, sparse) and sand. We carried out a comprehensive analysis of the acquired data in order to

- Visualize the acquisition zone: In addition to the classic information such as bathymetry profile, we also realized a visualization module for different imagery types (side-scan, true-pix, snippet). We used the side-scan type to visualize the waterfall image of these datasets. On the other hand, we used the snippet-type to visualize the georeferenced backscatter map.
- Extract backscattering strength datasets: In this thesis, we exploited the two datasets associated with the bathymetry mode and the longitudinal mode. Besides the classic post processing, we also collected the raw data samples (containing geographical position, *BS* level and insonified incident angle). This leads to the creation of two pixel-level datasets:
 - Bathymetry mode dataset where a pixel contains the data samples that were mostly insonified from one incident angle.

- Longitudinal mode dataset where a pixel contains the data samples that were insonified for a large range of incident angles ($[-50^\circ, 50^\circ]$).

Because this is the first time the multi-swath function has been introduced, we used these datasets to evaluate the system consistency in acquiring information from different operating modes. In this evaluation, we defined three datasets, one from the bathymetry mode and two from the longitudinal mode (data-level, pixel-level). The data-level dataset for longitudinal mode is simply an ensemble of the swath profiles, which is similar to the bathymetry mode dataset and it provides a direct means to evaluate inter-mode consistency. On the other hand, the pixel-level dataset in longitudinal mode is an ensemble of seafloor pixel profiles which are formed by accumulating the data samples from different swaths. We analyzed these datasets according to two main procedures:

- The analysis of the data dispersion for these datasets over the considered angular range with a 2° angular resolution. The result showed a good consistency between the bathymetry mode dataset and longitudinal data-level dataset. Moreover, the pixel-level dataset demonstrated its advantage in offering an equivalent *BS* level with a much lower angular data dispersion.
- The evaluation of the similarity between the bathymetry mode dataset and longitudinal data-level dataset. The similarity measure relied on inter-class and intra-class similarities. The complementary analysis also supported the consistency of the system. It also points out the potential of the system for the discrimination of the considered seabed types especially for the high incident angles.

From this evaluation, we also verified that the backscattering data from these different datasets over a given angular sector could be well-modeled by Gaussian mixture models in logarithmic scale.

From the review of the state-of-the-art in seabed classification, we first applied to our bathymetry mode dataset three types of approaches:

- Level-based methods: By building a model for each angular range, the classification applied to seafloor pixels characterized by an incident angle and a *BS* level.
- Profile-based methods: under the assumption that the seafloor is homogeneous over the whole swath, the classification applied to a *BS* profile over the acquired angular range.
- Texture-based methods: the classification relied on textural features extracted from the mosaic image built for the acquisition zone.

The reported results supported the following conclusions:

- The level-based methods only distinguished well the sand class from the two posidonia ones. Dense and sparse posidonia classes were difficult to distinguish due to their similarity of the underlying distribution of the *BS* level. Besides, there was also a confusion in the near nadir interval $[10^\circ, 20^\circ]$.
- The profile-based methods worked well for the discrimination of the three seabed classes, including between the two posidonia classes.
- The texture-based methods were inappropriate for discrimination purposes, suggesting the absence of fine-scale textural information in the reconstructed seafloor mosaics.

Overall, these experiments supported to select level-based methods on high incident angles for the bathymetry mode dataset. By contrast, due to its sampling pattern, profile-based methods appear to be the most relevant ones for the longitudinal mode dataset. Based on these conclusions, we further explored different feature extraction schemes. Besides, pixel-level mean and variance characteristics, we also adapted higher-order state-of-the-art features used in computer vision to the considered *BS* data, namely HOG (Histogram Of Gradients) and spatial covariance. Rather than computing such features from a mosaic, which was proven poorly informative, we extracted such features directly from the raw *BS* data. From cross-validation experiments, we determined for each mode the best feature combination using random forest classifiers:

- Bathymetry mode: the combination of the mean and spatial covariance.
- Longitudinal mode: the profile of the mean backscattering strength.

It may be noted that the proposed HOG-like feature did not reach a high discrimination level. This may relate to the absence of significant fine-scale information in the processed dataset, which may in turn point out limitations of SEAPIX system with respect to higher-resolution MBES.

As mentioned earlier, a key characteristic of SEAPIX system is the choice let to the user for switching from one acquisition mode to another one during a survey. We then considered an operational setting where for a given seabed area, we may be provided with *BS* data from both the bathymetry and longitudinal modes along different acquisition lines. Our objective was to address a fusion strategy so that one could benefit the complementary features of these two modes, namely the discrimination potential and the spatial coverage. Fusion strategies at two different levels were explored:

- Intra-mode fusion: In the bathymetry mode, the sampling design led to an approximate overlap rate of 50%, such that a given seafloor pixel was insonified twice from 2 different acquisition lines. Using as inputs elementary pixel-level classification likelihoods for each acquisition line, we stated this intra-mode fusion within a consensus framework. It resulted in learning the relative weights given to each angular sector in the final decision. Different weighing and learning criterion were considered. Overall, the consensus-based and SVM-based both led to relevant results with a gain of about 5% in terms of correct classification rate.
- Inter-mode fusion: this fusion mode aimed to exploit the discrimination efficiency of the bathymetry mode dataset in high incident angles and high-discrimination performance of the longitudinal pixel-level profiles in the nadir regions. The inter-mode fusion is stated in a variational level-set segmentation framework with a view to propagating the high-confidence classification in the nadir regions. A good classification performance was reported with a relative gain of about 2% compared with the sole use of bathymetry mode. The variational regularization also results in spatially-smoother segmentation maps.

During the thesis, we also observed several perspectives for future works. First, besides of the presented basic operating modes, SEAPIX also offers a frontal mode, which may replace the bathymetry mode data in under-vessel regions thanks to their higher incident angles. We observed, in Figure 3.10, a good example where the information was better viewed via this operating mode in nadir regions. Additionally, SEAPIX also offers scanning mode. In that mode, the vessel stay at a fix position and the sounder scans the seafloor by steering the emission in fore/aft and port/starboard directions in the range -40° to 40° . This mode allows an analysis of the seafloor *BS* strength distribution dependency upon azimuth angles. This mode may be

of a key interest in case of highly-structured seafloor classes such as sand riddles, where the heading angle greatly affects the backscatter data. It may be stressed that the proposed feature extraction and fusion schemes should apply to the two additional modes. It may also be noted that the variational inter-mode fusion may be easily extended to the fusion from three modes or more. This would mainly rely on introducing additional data-driven terms corresponding to new modes. In the framework of this thesis, the data were acquired using the CW modulation. In Section 4.3, it was shown that using a FM modulation, consistent backscatter strength values are obtained. For the same resolution, The FM mode enables to get a higher propagation range. It appears, then, promising to explore the class-dependent impact of this modulation and its potential for classification purposes.

Regarding the geophysical characterization of the seafloor from SEAPIX data, we only addressed in this thesis seabed classification and segmentation issues. The characteristics of the longitudinal mode, which extracts a robust pixel-level backscattering profile with no swath-level homogeneity hypothesis, strongly suggest to explore its potential for the inversion of geophysical parameters from the backscattering profiles. In this respect, it will be particularly interesting to perform qualitative and quantitative comparison with single-beam echo sounders, which involve similar seabed sampling patterns.

A last perspective relates to the optimization of the multi-mode sampling strategy for the mapping of a given zone of interest. From the reported experiments, the "optimal" sampling strategy should obviously be seafloor-class-dependent. Predefined sampling strategies for classic seabed types as well as the real-time adaption of the sampling strategy, with respect to characteristics of the seafloor, would be both of interest of the operational use of the proposed framework.

Bibliography

- [1] Frederic Mosca, Guillaume Matte, Olivier Lerda, Florent Naud, Didier Charlot, Maxence Rioblanco, and Christophe Corbières. Scientific potential of a new 3d multibeam echosounder in fisheries and ecosystem research. *Fisheries Research*, 2015.
- [2] Darrell R Jackson, Dale P Winebrenner, and Akira Ishimaru. Application of the composite roughness model to high-frequency bottom backscattering. *The Journal of the Acoustical Society of America*, 79(5):1410–1422, 1986.
- [3] Gilles Le Chenadec, Jean-Marc Boucher, and Xavier Lurton. Angular dependence of-distributed sonar data. *Geoscience and Remote Sensing, IEEE Transactions on*, 45(5):1224–1235, 2007.
- [4] S Dugelay. Deep seafloor characterization with multibeam echosounders using image segmentation and angular acoustic variations. In *OCEANS’96. MTS/IEEE. Prospects for the 21st Century. Conference Proceedings*, volume 3, pages 1545–1550. IEEE, 1996.
- [5] Stelio Haniotis, Pierre Cervenka, Carlos Negreira, and Jacques Marchal. Seafloor segmentation using angular backscatter responses obtained at sea with a forward-looking sonar system. *Applied Acoustics*, 89:306–319, 2015.
- [6] Knut Landmark, Anne H Schistad Solberg, Andreas Austeng, and Roy Edgar Hansen. Bayesian seabed classification using angle-dependent backscatter data from multibeam echo sounders. *IEEE Journal of Oceanic Engineering*, 39(4):724–739, 2014.
- [7] Luciano Fonseca and Larry Mayer. Remote estimation of surficial seafloor properties through the application angular range analysis to multibeam sonar data. *Marine Geophysical Researches*, 28(2):119–126, 2007.
- [8] AN Tasseti, S Malaspina, E Punzo, G Fabi, and A Mancini. Using multibeam echosounder datafor a gis-ready seafloor characterization in the adriatic sea. In *OCEANS 2015-Genova*, pages 1–8. IEEE, 2015.
- [9] David Stephens and Markus Diesing. A comparison of supervised classification methods for the prediction of substrate type using multibeam acoustic and legacy grain-size data. *PloS one*, 9(4):e93950, 2014.
- [10] Ph Blondel and O Gómez Sichi. Textural analyses of multibeam sonar imagery from stanton banks, northern ireland continental shelf. *Applied Acoustics*, 70(10):1288–1297, 2009.
- [11] David G Lowe. Distinctive image features from scale-invariant keypoints. *International journal of computer vision*, 60(2):91–110, 2004.

-
- [12] Oncel Tuzel, Fatih Porikli, and Peter Meer. Region covariance: A fast descriptor for detection and classification. In *European conference on computer vision*, pages 589–600. Springer, 2006.
- [13] Navneet Dalal and Bill Triggs. Histograms of oriented gradients for human detection. In *2005 IEEE Computer Society Conference on Computer Vision and Pattern Recognition (CVPR'05)*, volume 1, pages 886–893. IEEE, 2005.
- [14] Solomon Kullback. *Information theory and statistics*. Courier Corporation, 1997.
- [15] Daniel D Sternlicht and Christian P de Moustier. Remote sensing of sediment characteristics by optimized echo-envelope matching. *The Journal of the Acoustical Society of America*, 114(5):2727–2743, 2003.
- [16] AliReza Amiri-Simkooei, Mirjam Snellen, and Dick G Simons. Riverbed sediment classification using multi-beam echo-sounder backscatter data. *The Journal of the Acoustical Society of America*, 126(4):1724–1738, 2009.
- [17] E Pouliquen and X Lurton. Identification de la nature du fond de la mer à l’aide de signaux d’écho-sondeurs. *Le Journal de Physique IV*, 2(C1):C1–941, 1992.
- [18] Pierre Cervenka and Jacques Marchal. Imaging with a new multi-look front-scan sonar system. *Acta Acustica united with Acustica*, 90(1):38–48, 2004.
- [19] Darrell Jackson and Michael Richardson. *High-frequency seafloor acoustics*. Springer Science & Business Media, 2007.
- [20] APL-UW High-Frequency Ocean Environmental. Acoustic models handbook. *Applied Physics Laboratory, University of Washington, APL-UW TR*, 9407, 1994.
- [21] Robert J Urick. The noise background of the sea: ambient noise level. *Principles of Underwater Sound (ed. RJ Urick)*, pages 202–236, 1983.
- [22] LAURENT HELLEQUIN. *Analyse statistique et spectrale des signaux de sondeurs multi-faisceaux em950 application a l’identification des fonds sous marins*. PhD thesis, Rennes 1, 1998.
- [23] Dick G Simons and Mirjam Snellen. A bayesian approach to seafloor classification using multi-beam echo-sounder backscatter data. *Applied Acoustics*, 70(10):1258–1268, 2009.
- [24] G Le Chenadec and Jean-Marc Boucher. Sonar image segmentation using the angular dependence of backscattering distributions. In *Oceans 2005-Europe*, volume 1, pages 147–152. IEEE, 2005.
- [25] David Middleton. New physical-statistical methods and models for clutter and reverberation: The ka-distribution and related probability structures. *IEEE Journal of Oceanic Engineering*, 24(3):261–284, 1999.
- [26] Timothy C Gallaudet and Christian P de Moustier. High-frequency volume and boundary acoustic backscatter fluctuations in shallow water. *The Journal of the Acoustical Society of America*, 114(2):707–725, 2003.
- [27] Eo Jakeman and PN Pusey. A model for non-rayleigh sea echo. *IEEE Transactions on antennas and propagation*, 24(6):806–814, 1976.

- [28] Mark V Trevorrow. Statistics of fluctuations in high-frequency low-grazing-angle backscatter from a rocky sea bed. *IEEE Journal of Oceanic Engineering*, 29(2):236–245, 2004.
- [29] Avant projet, projet: Optipeche smf. Technical report, sep 2007.
- [30] RE Francois and GR Garrison. Sound absorption based on ocean measurements: Part i: Pure water and magnesium sulfate contributions. *The Journal of the Acoustical Society of America*, 72(3):896–907, 1982.
- [31] RE Francois and GR Garrison. Sound absorption based on ocean measurements. part ii: Boric acid contribution and equation for total absorption. *The Journal of the Acoustical Society of America*, 72(6):1879–1890, 1982.
- [32] Xavier Lurton, Geoffroy Lamarche, Craig Brown, Vanessa Lucieer, Glen Rice, Alexandre Schimel, and Tom Weber. Backscatter measurements by seafloor-mapping sonars - guidelines and recommendations. Technical report, 05 2015.
- [33] R2Sonic. Sonic 2024/2022 broadband multibeam echosounders:operation manual v5.0. *Revision 001*, 2014.
- [34] Philippe Alain. New tools in multisensor gis integration and visualization. In *Information Fusion and Geographic Information Systems*, pages 145–153. Springer, 2011.
- [35] Andrej N Kolmogorov. *Sulla determinazione empirica di una legge di distribuzione*. na, 1933.
- [36] Nikolai V Smirnov. Estimate of deviation between empirical distribution functions in two independent samples. *Bulletin Moscow University*, 2(2):3–16, 1939.
- [37] Mirjam Snellen, Dimitrios Eleftherakis, AliReza Amiri-Simkooei, Ronald L Koomans, and Dick G Simons. An inter-comparison of sediment classification methods based on multi-beam echo-sounder backscatter and sediment natural radioactivity data. *The Journal of the Acoustical Society of America*, 134(2):959–970, 2013.
- [38] Nicholas J Redding. Estimating the parameters of the k distribution in the intensity domain. Technical report, 1999.
- [39] Gideon Schwarz et al. Estimating the dimension of a model. *The annals of statistics*, 6(2):461–464, 1978.
- [40] Eric Langford. Quartiles in elementary statistics. *Journal of Statistics Education*, 14(3):1–27, 2006.
- [41] Jan Puzicha, Thomas Hofmann, and Joachim M Buhmann. Non-parametric similarity measures for unsupervised texture segmentation and image retrieval. In *Computer Vision and Pattern Recognition, 1997. Proceedings., 1997 IEEE Computer Society Conference on*, pages 267–272. IEEE, 1997.
- [42] A Efren and Elif Tuna. On some properties of goodness of fit measures based on statistical entropy, 2013.
- [43] John Reidar Mathiassen, Amund Skavhaug, and Ketil Bø. Texture similarity measure using kullback-leibler divergence between gamma distributions. In *European conference on computer vision*, pages 133–147. Springer, 2002.

-
- [44] Harold Jeffreys. An invariant form for the prior probability in estimation problems. *Proceedings of the royal society of London. Series A, mathematical and physical sciences*, pages 453–461, 1946.
- [45] JK Chung, PL Kannappan, CT Ng, and PK Sahoo. Measures of distance between probability distributions. *Journal of mathematical analysis and applications*, 138(1):280–292, 1989.
- [46] K. Landmark, A. H. Schistad Solberg, A. Austeng, and R. E. Hansen. Bayesian seabed classification using angle-dependent backscatter data from multibeam echo sounders. *IEEE Journal of Oceanic Engineering*, 39(4):724–739, Oct 2014.
- [47] Ali R Amiri-Simkooei, Mirjam Snellen, and Dick G Simons. Principal component analysis of single-beam echo-sounder signal features for seafloor classification. *IEEE Journal of Oceanic Engineering*, 36(2):259–272, 2011.
- [48] Paul A van Walree, Jaroslaw Tegowski, Cees Laban, and Dick G Simons. Acoustic seafloor discrimination with echo shape parameters: A comparison with the ground truth. *Continental Shelf Research*, 25(18):2273–2293, 2005.
- [49] LJ Hamilton. Acoustic seabed segmentation for echosounders through direct statistical clustering of seabed echoes. *Continental Shelf Research*, 31(19):2000–2011, 2011.
- [50] Turgay Celik and Tardi Tjahjadi. A novel method for sidescan sonar image segmentation. *IEEE Journal of Oceanic Engineering*, 36(2):186–194, 2011.
- [51] Imen Karoui, Ronan Fablet, Jean-Marc Boucher, and Jean-Marie Augustin. Seabed segmentation using optimized statistics of sonar textures. *IEEE Transactions on geoscience and remote sensing*, 47(6):1621–1631, 2009.
- [52] Alireza Amiri-Simkooei, Mirjam Snellen, and Dick G Simons. Using the mbes for classification of riverbed sediments. In *Proceedings of the 9th European Conference on Underwater Acoustics: ECUA 2008, 29 June-4 July 2008, Paris, France*. Société Française d’Acoustique, 2008.
- [53] G Canepa, L Pautet, and E Pouliquen. Manual of boris-ssa: Bottom response from inhomogeneities and surface using small slope approximation. *NATO Undersea Research Centre, Memorandum M-0152*, 2005.
- [54] Gilles Le Chenadec, J-M Boucher, X Lourton, and J-M Augustin. Angular dependence of statistical distributions for backscattered signals: modelling and application to multibeam echosounder data. In *OCEANS 2003. Proceedings*, volume 2, pages 897–903. IEEE, 2003.
- [55] Cécile Berron. *Potentialités de l’inversion géoacoustique de données multicapteurs de sonars cartographiques pour la caractérisation des fonds marins*. PhD thesis, Brest, 2008.
- [56] Leo Breiman. Random forests. *Machine learning*, 45(1):5–32, 2001.
- [57] William T Freeman, Ken-ichi Tanaka, Jun Ohta, and Kazuo Kyuma. Computer vision for computer games. In *Automatic Face and Gesture Recognition, 1996., Proceedings of the Second International Conference on*, pages 100–105. IEEE, 1996.

- [58] William T Freeman and Michal Roth. Orientation histograms for hand gesture recognition. In *International workshop on automatic face and gesture recognition*, volume 12, pages 296–301, 1995.
- [59] J Hughes Clarke. Toward remote seafloor classification using the angular response of acoustic backscattering: a case study from multiple overlapping gloria data. *IEEE Journal of Oceanic Engineering*, 19(1):112–127, 1994.
- [60] Craig J Brown, Brian J Todd, Vladimir E Kostylev, and Richard A Pickrill. Image-based classification of multibeam sonar backscatter data for objective surficial sediment mapping of georges bank, canada. *Continental Shelf Research*, 31(2):S110–S119, 2011.
- [61] Suresh Subramaniam, Herb Barad, Andrew B Martinez, and B Bourgeois. Seafloor characterization using texture. In *Southeastcon'93, Proceedings., IEEE*, pages 8–p. IEEE, 1993.
- [62] Christian De Moustier and Haruyoshi Matsumoto. Seafloor acoustic remote sensing with multibeam echo-sounders and bathymetric sidescan sonar systems. *Marine Geophysical Researches*, 15(1):27–42, 1993.
- [63] Frank W Bentrem, John Sample, Maria T Kalcic, and Michael E Duncan. High-frequency acoustic sediment classification in shallow water. In *OCEANS'02 MTS/IEEE*, volume 1, pages 7–11. IEEE, 2002.
- [64] Ph Blondel and LM Parson. Quantitative characterisation of geological processes using sidescan sonar imagery. 1998.
- [65] JM Augustin, R Le Suave, X Lurton, M Voisset, S Dugelay, and C Satra. Contribution of the multibeam acoustic imagery to the exploration of the sea-bottom. *Marine Geophysical Researches*, 18(2-4):459–486, 1996.
- [66] Luciano Fonseca, Craig Brown, Brian Calder, Larry Mayer, and Yuri Rzhanov. Angular range analysis of acoustic themes from stanton banks ireland: A link between visual interpretation and multibeam echosounder angular signatures. *Applied Acoustics*, 70(10):1298–1304, 2009.
- [67] Trung-Kien Nguyen, Didier Charlot, Jean-Marc Boucher, Gilles Le Chenadec, and Ronan Fablet. Seabed classification using a steerable multibeam echo sounder. In *OCEANS 2016 MTS/IEEE Monterey*, pages 1–4. IEEE, 2016.
- [68] Xavier Lurton and Jean-Marie Augustin. A measurement quality factor for swath bathymetry sounders. *Oceanic Engineering, IEEE Journal of*, 35(4):852–862, 2010.
- [69] Huu-Giao Nguyen, Ronan Fablet, and Jean-Marc Boucher. Visual textures as realizations of multivariate log-gaussian cox processes. In *Computer Vision and Pattern Recognition (CVPR), 2011 IEEE Conference on*, pages 2945–2952. IEEE, 2011.
- [70] Björn Waske and Sebastian van der Linden. Classifying multilevel imagery from sar and optical sensors by decision fusion. *IEEE Transactions on Geoscience and Remote Sensing*, 46(5):1457–1466, 2008.
- [71] Lei Xu, Adam Krzyzak, and Ching Y Suen. Methods of combining multiple classifiers and their applications to handwriting recognition. *IEEE transactions on systems, man, and cybernetics*, 22(3):418–435, 1992.

-
- [72] Arnaud Martin. Comparative study of information fusion methods for sonar images classification. In *2005 7th International Conference on Information Fusion*, volume 2, pages 7–pp. IEEE, 2005.
- [73] Jon Atli Benediktsson and Philip H Swain. Consensus theoretic classification methods. *IEEE transactions on Systems, Man, and Cybernetics*, 22(4):688–704, 1992.
- [74] Suresh Subramaniam, Herb Barad, Andrew B Martinez, and B Bourgeois. Seafloor characterization using texture. In *Southeastcon'93, Proceedings., IEEE*, pages 8–p. IEEE, 1993.
- [75] Jean-Marie Augustin. Developing and deploying sonar and echosounder data analysis software.
- [76] Imen Karoui. *Segmentation par méthodes markoviennes et variationnelles des images texturées: application à la caractérisation sonar des fonds marins*. PhD thesis, Télécom Bretagne, 2007.
- [77] Federico Castanedo. A review of data fusion techniques. *The Scientific World Journal*, 2013, 2013.
- [78] T Aridgides, M Fernández, and G Dobeck. Side-scan sonar imagery fusion for sea mine detection and classification in very shallow water. In *Proc. of SPIE*, volume 4394, pages 1123–1134, 2001.
- [79] U Hoelscher-Hoebing and D Kraus. Unsupervised image segmentation and image fusion for multi-beam/multi-aspect sidescan sonar images. In *OCEANS'98 Conference Proceedings*, volume 1, pages 571–576. IEEE, 1998.
- [80] Naveen Kumar, Urbashi Mitra, and Shrikanth S Narayanan. Robust object classification in underwater sidescan sonar images by using reliability-aware fusion of shadow features. *IEEE Journal of Oceanic Engineering*, 40(3):592–606, 2015.
- [81] David L Hall and James Llinas. An introduction to multisensor data fusion. *Proceedings of the IEEE*, 85(1):6–23, 1997.
- [82] Louisa Lam and SY Suen. Application of majority voting to pattern recognition: an analysis of its behavior and performance. *IEEE Transactions on Systems, Man, and Cybernetics-Part A: Systems and Humans*, 27(5):553–568, 1997.
- [83] Arnaud Martin. Comparative study of information fusion methods for sonar images classification. In *Information Fusion, 2005 8th International Conference on*, volume 2, pages 7–pp. IEEE, 2005.
- [84] Lei Xu, Adam Krzyzak, and Ching Y Suen. Methods of combining multiple classifiers and their applications to handwriting recognition. *IEEE transactions on systems, man, and cybernetics*, 22(3):418–435, 1992.
- [85] Scott Reed, Ioseba Tena Ruiz, Chris Capus, and Yvan Petillot. The fusion of large scale classified side-scan sonar image mosaics. *IEEE transactions on image processing*, 15(7):2049–2060, 2006.
- [86] David P Williams. Bayesian data fusion of multiview synthetic aperture sonar imagery for seabed classification. *IEEE Transactions on Image Processing*, 18(6):1239–1254, 2009.

- [87] Tom Aridgides, M Fernandez, and G Dobeck. Fusion of adaptive algorithms for the classification of sea mines using high resolution side scan sonar in very shallow water. In *OCEANS, 2001. MTS/IEEE Conference and Exhibition*, volume 1, pages 135–142. IEEE, 2001.
- [88] Cédric Rominger and Arnaud Martin. Recalage et fusion d’images sonar multivues: utilisation du conflit. *Revue Nationale des Technologies de l’Information*, (21):231–246, 2011.
- [89] H Laanaya, A Martin, D Aboutajdine, and A Khenchaf. Classification des sédiments marins par fusion de classifieurs binaires svm. *Caractérisation du milieu marin, Brest, France*, 2006.
- [90] Hicham Laanaya, Arnaud Martin, Ali Khenchaf, and Driss Aboutajdine. Post-classification d’images texturées par fusion crédibiliste. *Fouille de données complexes dans un processus d’extraction des connaissances*, page 37, 2008.
- [91] Bjorn Waske, Gunter Menz, and Jon Atli Benediktsson. Fusion of support vector machines for classifying sar and multispectral imagery from agricultural areas. In *Geoscience and Remote Sensing Symposium, 2007. IGARSS 2007. IEEE International*, pages 4842–4845. IEEE, 2007.
- [92] David Kernéis. *Amélioration de la classification automatique des fonds marins par la fusion multicapteurs acoustiques*. PhD thesis, Télécom Bretagne, 2007.
- [93] Christophe Samson. *Contribution à la classification d’images satellitaires par approche variationnelle et équations aux dérivées partielles*. PhD thesis, Université Nice Sophia Antipolis, 2000.
- [94] Jon Atli Benediktsson, Johannes R Sveinsson, and Philip H Swain. Hybrid consensus theoretic classification. *IEEE Transactions on geoscience and remote sensing*, 35(4):833–843, 1997.
- [95] Bernhard Schölkopf and Alexander J Smola. *Learning with kernels: support vector machines, regularization, optimization, and beyond*. MIT press, 2002.
- [96] James A Sethian. Level set methods, evolving interfaces in geometry, fluid mechanics computer vision, and materials sciences. *Cambridge Monographs on Applied and Computational Mathematics*, 3, 1996.
- [97] Michael Kass, Andrew Witkin, and Demetri Terzopoulos. Snakes: Active contour models. *International journal of computer vision*, 1(4):321–331, 1988.
- [98] Sylvie Menet, Philippe Saint-Marc, and Gerard Medioni. Active contour models: Overview, implementation and applications. In *Systems, Man and Cybernetics, 1990. Conference Proceedings., IEEE International Conference on*, pages 194–199. IEEE, 1990.
- [99] Laurent D Cohen. On active contour models and balloons. *CVGIP: Image understanding*, 53(2):211–218, 1991.
- [100] Tony F Chan and Luminita A Vese. Active contours without edges. *IEEE Transactions on image processing*, 10(2):266–277, 2001.

Cette thèse, co-dirigée par Jean-Marc Boucher et Ronan Fablet (IMT Atlantique) et co-encadrée par Didier Charlot (iXBlue), Gilles Le Chenadec et Michel Legris (ENSTA Bretagne), a été réalisée dans le cadre d'une convention CIFRE au sein de la société iXBlue.

iXblue développe et commercialise un sondeur multifaisceaux (MBES) SEAPIX principalement dédié au marché de la pêche. Ce système a été développé pour offrir le meilleur compromis entre performances de détection et son coût de revient. Outre les caractéristiques classiques d'un MBES, il propose la particularité unique de pouvoir insonifier des fauchées différentes sous le navire par dépointage électronique du faisceau d'émission de bâbord à tribord et d'avant en arrière. Le travail de thèse a pour objectif d'étudier l'apport de ces nouvelles capacités multi-fauchées dans l'analyse et la classification des fonds marins.

La première partie du travail a consisté à réaliser une analyse détaillée de la chaîne de mesure. Cette étude a permis d'évaluer la consistance des niveaux de rétrodiffusion entre les différents modes d'insonification. La deuxième partie s'est intéressée à la recherche des caractéristiques discriminantes du signal rétrodiffusé en tenant compte de la géométrie d'acquisition de chaque mode d'insonification. La dernière étape du travail a porté sur des méthodes de fusion des données acquises. Cette étude s'est réalisée en deux approches; la première considère des données venant du même mode d'insonification (intra-mode) et la seconde venant de modes différents (inter-mode), pour la cartographie des fonds marins. Les résultats expérimentaux obtenus mettent en évidence l'intérêt de la chaîne de traitement proposée et d'une architecture multi-mode sur les jeux de données réelles traitées.

Mots clefs : Système multifaisceaux, MBES multi-fauchée, rétrodiffusion, Classification des fonds marins, Descripteur, Fusion d'information

This thesis, co-directed by Jean-Marc Boucher and Ronan Fablet (IMT Atlantique) and co-supervised by Didier Charlot (iXBlue), Gilles Le Chenadec and Michel Legris (ENSTA Bretagne), was realized in the context of a convention CIFRE with the company iXBlue.

iXblue develops and commercializes a multibeam echosounder (MBES) SEAPIX primarily dedicated to the fishery market. The system is optimized to offer the best compromise between performances capabilities and cost. In addition to the classical characteristics of an MBES, it offers the unique feature of scanning the seafloor (and the water column volume) by electronic beamform multiple the emission swaths from port to starboard, as well as from forward to backward. The objective of the thesis is to study the contribution of these new multi-swath capacities in the analysis and classification of the seafloor.

The first part of the work consisted in carrying out a detailed analysis of the measurement chain. This study evaluated the consistency in acquiring the backscattering strength from different insonification modes. The second part investigated the discriminant characteristics of the backscattered signal while taking into account the acquisition geometry of each insonification mode. The last stage of the work involved to methods of fusing the acquired data. This study was carried out in two approaches; the first considers data from the same insonification mode (intra-mode) and the second from different modes (inter-mode), for the seafloor classification. The obtained experimental results highlight the interest of the proposed processing chain and a multi-mode architecture on the real datasets.

Keywords: Multibeam echosounder, Multiswath MBES, Backscattering strength, Seafloor classification, Point-wise feature, Information fusion